TIME-DEPENDENT SEISMIC HAZARD ASSESSMENT IN THE MINING REGIONS OF THE GAUTENG PROVINCE, SOUTH AFRICA.

Brian Sibonelo Zulu
School of Geoscience, University of Witwatersrand

A Dissertation submitted to the Faculty of Science, University of Witwatersrand, Johannesburg, in fulfilment of the requirements for the degree of Master of Science.

Johannesburg, February 2018

DECLARATION

I declare that this Dissertation is my own, unaided work. It is being submitted for the Degree of Master of Science at the University of the Witwatersrand, Johannesburg. It has not been submitted before for any degree or examination at any other University.

(Signature of candidate)

1st Day of June 2018 in Silverton, Pretoria

ABSTRACT

A time-dependent probabilistic assessment of the seismic hazard along the densely populated northern rim of the Witwatersrand Basin of the Gauteng Province, South Africa, is described. Seismicity in this region is mainly induced by deep gold mining and flooding of worked-out mines. Seismic hazard assessment in the gold mining regions has not been incorporated in global projects such as the Global Seismic Hazard Assessment Program (GSHAP), although the seismicity related to the gold mining activities accounts for about 90 % of the seismicity of South Africa. Time-dependent seismic hazard estimates are given in terms of peak ground acceleration and 5 % damped response spectra at periods of 0.1 s, 0.5 s, 1.0 s and 2.0 s for 10 % probability of exceedance in 50 years (475 year return period) for two different periods; namely, Period A (1970 - 2004) and Period B (2005 - 2015). Seismic hazard estimates are higher in Period A (mining period) owing to higher activity rates than in Period B (flooding period). The highest estimated PGA value was approximately 0.250 g for a return period of 475 years in the western part of the region in Period A, while the corresponding estimated PGA value was 0.206 g for a return period of 475 years in the same region in Period B. The spectral acceleration values also decreased from Period A to Period B. It was observed that the Far West Rand seismic zone contributes the most to the hazard in the study region, followed by the West Rand seismic zone and then the East Rand seismic zone. The Central Rand seismic zone is the least active seismic zone and contributes the least to the hazard of the study region. The hazard estimates are higher in the western parts of Johannesburg where mining remains active compared to the eastern parts of Johannesburg where flooding takes place.

Acknowledgements

I would like to send my special thanks to the following people and organisations:

- The Council for Geoscience for funding this work under the Microzonation Project and all the resources I used,
- My supervisors, Dr. Vunganai Midzi and Prof. Raymond Durrheim for their guidance and insightful reviews of this dissertation,
- The Microzonation Project Manager, Mrs Michelle Grobbelaar for funding this work under her project,
- Mr. Brassnavy Manzunzu for assisting with GIS images,
- Mr. Denver Birch for the review of this work,
- And lastly my fiancée, Miss Lwandisiwe Nyikinya for all kinds of support throughout my studies.

CONTENTS

LIST OF FIGURES

LIST OF TABLES

1. INTRODUCTION

Seismic hazard is defined as the probable level of ground shaking associated with recurrence of earthquakes (Giardini et al., 1999). Seismic hazard assessments are divided into two main approaches, deterministic seismic hazard assessment (DSHA) and probabilistic seismic hazard assessment (PSHA). The deterministic seismic hazard approach is normally used in regions where active tectonic features such as faults are well mapped and understood. The main idea is to determine the maximum expected magnitude (M_{max}) or the maximum credible earthquake motion at the site of interest (Baker, 2008). The maximum expected magnitude is defined as the reasonable maximum expected magnitude for any given seismic source zone based on its assessment, therefore this is the expected upper bound of all possible future earthquakes (Reiter, 1990, 80-81). Probabilistic seismic hazard analysis (PSHA) estimates the probability that different levels of earthquake-caused ground-motions will be exceeded at least once at a given location in a given future time period at the site of interest (Budnitz et al., 1997). The PSHA results are presented as estimated probabilities for each year or estimated annual frequencies. The PSHA method is generally viewed as comprising of all possible future earthquake events and ground motions with a finite probability of occurrence (Baker, 2008).

PSHA is conducted in the gold mining region on the northern rim of the Witwatersrand basin extending from the Far West Rand to the East Rand (Figure 1 and Figure 3). The PSHA method is widely used in studies of critical structures such as dams, nuclear power plants and tall buildings, but not much similar work has been done in the mining regions of South Africa. Induced seismicity can cause more damage than natural seismicity in regions of low to moderate seismicity, for example the M_L 4.8 on 12 May 2018 which occurred at Timpson, Texas (Atkinson et al., 2015). Peak ground acceleration (PGA) in excess of 0.2 g has been observed in the copper mining region in Poland and gold mining region in South Africa (Lasocki, 2005; Zulu and Manzunzu, 2015). Petersen et al. (2016) noted that the high natural hazard levels in California were similar to those of induced earthquakes in Colorado, Kansas, New Mexico, Oklahoma and Texas. Petersen et al. (2014) observed that the inclusion of induced seismicity generally increases seismic hazard estimates. This is likely true for the region under investigation here, given that several damaging mining-related events have occurred within the mining regions, for example, the M_L 5.3 mining-related event in Stilfontein, which occurred on 9 March 2005, and the M_L 5.5 Orkney mining-related event of 5 August 2014 (Midzi et al., 2015; Saunders et al*.,* 2008). An example of the damage caused by the 2005 Stilfontein mining-related event is shown in Figure 2. These mining-related events pose a danger to buildings and human life. Seismicity in Gauteng is dominated by mining-related events due to gold mining.

Following the M_L 5.3 mining-related event in Stilfontein, which occurred on 9 March 2005, a committee was formed to investigate the risks posed by large seismic events to mines, miners and public at large, including infrastructure in the gold mining regions (Durrheim et al., 2007). There were many questions, findings, discussions and recommendations raised during those meetings. These include the effects of mine flooding, rising water levels and major geological structures on seismicity; and the likelihood of damaging seismicity in the future. Some of the key recommendations were: to establish continuous monitoring networks or cluster networks within each mining region that will continue operating even after mines close; and also to expand the South African National

Seismograph Network (SANSN) (Durrheim et al., 2007). The SANSN was improved since 2005 and cluster networks are now operational. It is therefore important to assess the impact of mine flooding on seismic hazard and seismicity within the mining regions.

Gold was first discovered in the Central Rand, Johannesburg in 1886, East Rand in 1914, West Rand and Klerksdorp in 1937, Orange Free State in 1946 and Kinross in 1955 (Durrheim, 2010). The Witwatersrand basin still remains one of the major producers of gold, although there has been a decline in the production in the last couple of decades due to political instability, depreciation of the gold price (1981-2002), depletion of reserves, increasing production costs and other competing emerging markets. The peak production of gold occurred in 1970 when about 1,000 tons of gold was produced (Riemer and Durrheim, 2012). The production decreased in 1985 to about 620 tons, and a further decrease in production to 320 tons in 2003 (Riemer and Durrheim, 2012) and down to about 150 tons in 2015 (Lehotla, 2015). Mining-related seismicity activity is generally roughly proportional to the amount of rock mined, and thus has also shown a general decrease.

Mining-related seismicity was encountered in the early 1900s when extensive stopes reached depths of several hundred meters (Vieira et al., 2001). The first seismograph to monitor this seismicity was installed in 1910 at Union Observatory in Johannesburg and the second was installed in the village of Ophirton (Durrheim, 2010). Gold mining activities in South Africa are now as deep as 4 km, which has resulted in mining-related events occurring at depths of up to about 5 km (Durrheim, 2010). Regional seismic hazard assessments (Giardini et al., 1999) did not consider mine-related seismicity, although this accounts for 90 % of seismicity in South Africa (McGarr, 1976; Singh and Hattingh, 2009; Wood, 1913). The Global Seismic Hazard Assessment Program (GSHAP), which started in 1992, also did not consider the temporally-varying of mining-related events and it's impact on the seismic hazard (Giardini et al., 1999). The time-dependency of the catalogue and it's impact on the recurrence parameter, hence on the seismic hazard of the region is an important part of this study.

Mine-related seismic events are earthquakes that occur on either fresh ruptures or pre-existing faults, but are thought to be induced or triggered by stress changes created by mining activities. Mine-related seismic events can occasionally reach magnitudes up to M_L 5.5 (Midzi et al., 2015). Events with magnitudes up to M_L 5.5 are recorded by the cluster networks, which are well described in Chapter 3. Rockbursts are often also associated with seismic events ≥ M_L 0.5 (Durrheim, 1999). The rockbursts are a subset of mining-induced and mining-triggered events, therefore, are part of the mine-related seismic events. A rockburst is defined as a sudden and violent disruption of rock or disturbance of excavation walls in mines, which is caused by or accompanied by, a shock or tremor of sufficient magnitude to cause obvious damage to excavations and support, or widespread simultaneous falls of rock (Rockburst Commission of the International Society for Rock Mechanics, (as cited in Durrheim, 1999)). The seismic events of $M_L \geq 3.0$ are shown in Figure 3. There are two classifications of rockbursts, *i.e*. either in terms of the source mechanism or in terms of the damage mechanism. The main source mechanism categories are face-parallel bursts, pillar bursts, pillar foundation failures, slip on

geological structures and strain bursts. The damage mechanism categories are near-field rockbursts, violent shakedown bursts and shakedown bursts (Durrheim, 1999).

This study focuses on mining-related events that occur within the gold mining regions of the Gauteng Province, and thus includes both mining-induced and mining-triggered earthquakes. Induced events can be viewed as the events resulting from an unnatural activity that causes stresses to change on a fault causing it to slip or in an intact rock mass causing it to fail. McGarr et al. (2002) define an event as 'induced' when most of the driving force is provided by mining activities, and 'triggered' when the event is caused by small fractional changes in the background seismicity or stress. It is very difficult to differentiate mining-induced events, mining-triggered events, and mining explosions because the seismograph networks were deployed at a regional scale and stations are far from the mines. Explosions and blasting events are events of small magnitudes, typically less than M_L 1, hence they are seismic events less than the magnitude of completeness. Therefore, these events were not used in calculating the recurrence parameters. Tectonic earthquakes outside the mining regions are not considered. The mining region considered in this study is on the northern rim of the Witwatersrand basin of the Gauteng region around Johannesburg, as shown in Figure 3.

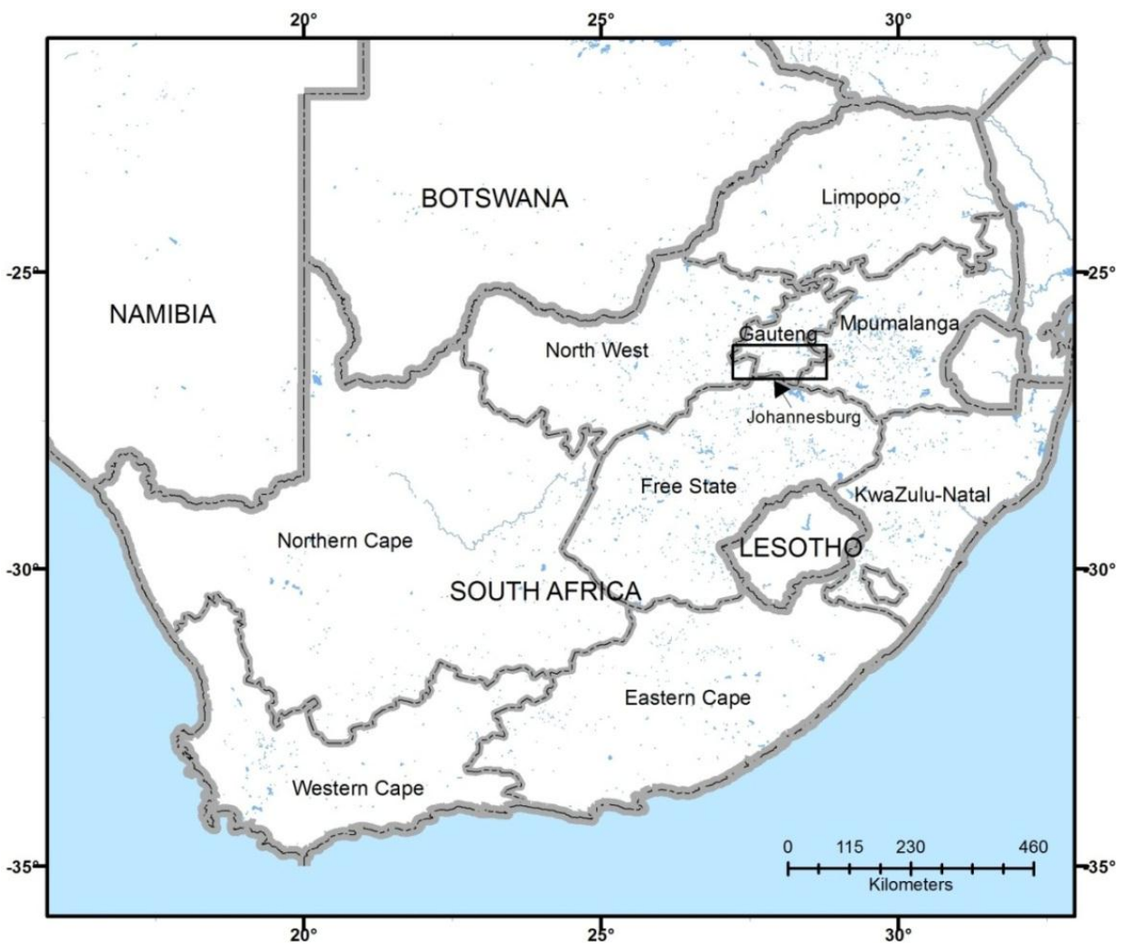

Figure 1. Locality map of the study area shown by a black rectangle.

Figure 2. Structural damage observed during the Stilfontein March 2005 earthquake (Saunders et al*.*, 2008).

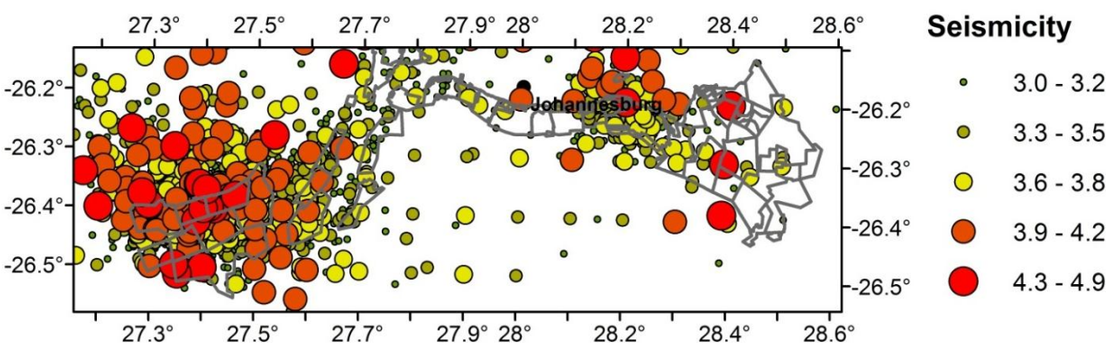

Figure 3. Seismicity for the northern rim of the Witwatersrand basin with the grey lines representing the mining boundaries.

1.1 Aim and Objectives

The main aim of this study is to conduct a time-dependent probabilistic assessment of the seismic hazard in the part of the Witwatersrand Basin that is in the Gauteng Province, South Africa, which is mainly due to seismicity in the gold mining regions. The time-dependent probabilistic seismic hazard analysis is a modification of the classical approach by introducing a time factor. Seismic hazard estimates will be given in terms of PGA and 5 % damped response spectra at periods of 0.1 s, 0.5 s, 1.0 s and 2.0 s for 10 % probability of exceedance in 50 years (475 year return period). The main objectives are:

- Compile a catalogue of earthquakes within a 100 km radius of Johannesburg. Homogenise all magnitudes to moment magnitude (M_w) and assess the completeness levels of the catalogue.
- Using the completeness levels of the catalogue, divide the catalogue into different time periods.
- Demarcate seismic zones for the identified time periods, assess recurrence parameters and the maximum expected magnitude (M_{max}).
- Select appropriate Ground Motion Prediction Equations (GMPEs). Test the selected GMPEs with observed data.
- Assess uncertainties associated with the seismic source model and ground motion model to be implemented in the hazard calculation using the logic tree technique.
- Run numerous hazard sensitivity calculations for all input parameters.
- Compile the final input parameters for calculations.
- Compute and assess seismic hazard for the different time periods.

1.2 Study Region

One of the aims of this study was to compile a homogenised catalogue of earthquakes covering the gold mines in the Gauteng Province for the northern rim of the Witwatersrand region. The earthquake catalogue of the study region is bounded by coordinates 27.1° to 28.6° Longitude and -26.0° to -26.6° Latitude as shown in Figure 3. The mining regions in this study cover the area from the Far West Rand to the East Rand. Most of the mines have ceased operating and have been flooded by water. Standard practice in most seismic hazard studies is to compile a catalogue of earthquakes within a radius of 300 km (International Atomic Energy Agency, 2010). Most ground-motion prediction equations are calibrated for distances of between 100 and 300 km radius. The maximum expected earthquake in each seismic zone is expected to be felt at a distance of at least 100 km. A 100 km radius was chosen for this study because the sources are gold mines within 100 km from Johannesburg. Induced events have a high-frequency content (Nakatani et al., 2008; Plenkers et al., 2010) and high-frequency seismic events attenuate faster than low-frequency events (McGarr and Fletcher, 2005; Padhy and Subhadra, 2010); thus, a 100 km radius was deemed to be appropriate for mining-related events.

2. METHODOLOGY OF PROBABILISTIC SEISMIC HAZARD ANALYSIS AND TIME-DEPENDENT HAZARD ANALYSIS

The mathematical formulation used in most PSHAs assumes that the occurrence of earthquakes can be represented as a Poisson process (Kijko, 2011). The mathematical definition of a Poisson process is a discrete probability distribution that expresses the probability of a given number of events occurring in a fixed interval of time and or space assuming these events occur with a known average rate and independently of the time since the last event (Ross, 2014). The probability is given by:

$$P(N = n) = \frac{(v.t)^n}{n!} e^{-vt} \ , \tag{2.1}$$

where *t* is the interval time, *n* is the number of events in *t*, *v* is the annual number of events, hence:

$$v = \sum_{i=1}^{ny} \frac{n_i}{ny} \ , \tag{2.2}$$

where *ny* is the number of years each with n_i events (Baker, 2008). The Poisson process assumes that the occurrence of earthquakes is randomly distributed. It is worth pointing out that the occurrence of mining-related seismicity does not necessarily follow a Poisson distribution because these events do not occur randomly in time and space, because they are related to the mining activities, but the same procedure is commonly used in PSHA studies for mines (Atkinson et al., 2015). Under this assumption, the probability that a ground-motion parameter, *Z,* will exceed a specified value, *z*, at least once in time period, *t*, at a specific site of interest is given by:

$$P(Z > z|t) = 1 - e^{-v(z)t} \leq v(z)t \tag{2.3}$$

where *v(z)* is the mean frequency during a specific time period, *t*, for which the level of the ground-motion parameter, *Z*, exceeds the value, *z*, at the site of interest from all possible earthquakes from all sources in the region of interest (Budnitz et al., 1997; Cornell, 1968). Equation (2.3) is only valid given that *v(z)* is the appropriate mean value for time period, *t*. In this study, the hazard results are reported in terms of the frequency of exceedance, *v(z).* The return period is defined by Thenhaus and Campbell (2003):

$$R(z) = \frac{1}{v(z)} = \frac{-t}{\ln(1-P[Z>z])} \tag{2.4}$$

Equation (2.4) is used to calculate the return period for a probability of exceedance for a specific number of years of a structure of interest. The commonly used return period is calculated for 10 % probability of exceedance in 50 years:

$$R(z) = \frac{-50}{\ln(1-0.1])} = 475 \text{ years}, \quad (2.5)$$

which corresponds to a return period of 475 years. The frequency of exceedance, *v(z)*, is a function of the frequency of earthquake occurrence, the stochasticity of size and location of all possible future earthquakes, and the stochasticity in the level of ground-motion they may produce at the specific site of interest (Cornell, 1968; McGuire, 1976). It is computed by the expression:

$$v(z) = \sum \alpha_n(M_{min}) \int f(m)[\int f(r|m).P(Z > z|m,r)\,.dr]\,.dm, \quad (2.6)$$

where $\alpha_n(M_{min})$ is the annual frequency of all possible earthquakes occurring on source *n* above a minimum magnitude threshold of engineering significance M_{min}; $f(m)$ is the probability density of any earthquake size between the minimum magnitude threshold of engineering significance M_{min} and a maximum earthquake the source can produce M_{max}; it is not the probability density of the maximum events; $f(r|m)$ is the probability density function for distance to an earthquake of variable magnitude *m* occurring on a specific source *n*; and $P(Z>z|m,r)$ is the probability that, given an earthquake of magnitude *m* at distance *r* from the specific site of interest, the peak ground-motion will exceed the level *z* at least once (Cornell, 1968; McGuire, 1976). The annual frequency of earthquake occurrence, $\alpha_n(M_{min})$, and the probability density of the size distribution of the earthquakes, $f(m)$, were both determined by the earthquake recurrence relationships. The distribution for the distance between the earthquake rupture and the site of interest is generally determined by the geometry of the seismic sources. The earthquake ruptures are distributed equally over a regular grid of a region described as a seismic zone (Pagani et al., 2014). The conditional probability of exceedance, $P(Z>z|m,r)$, was determined using the ground-motion attenuation relationships. The attenuation relationships define the level of ground-motion in terms of a log-normal distribution in terms of magnitude, source-to-site distance, fault mechanism, and site conditions as described by equation (Campbell, 2003b):

$$\ln Z = c_1 + c_2 M - c_3 \ln R - c_4 r + c_5 F + c_6 S + \text{Ɛ}, \quad (2.7)$$

where *M* is magnitude, *R* is a distance, *r* is a site-source distance, *F* is a source rupture mechanism, *S* is a site factor and Ɛ is a aleatory error term with zero mean and *R* given by:

$$R = \begin{cases} r + c_7 \exp(c_8 M) \\ \sqrt{r^2 + [c_7 + \exp(c_8 M)]} \end{cases} \quad (2.8)$$

where c_1 to c_8 are regression coefficients.

The processes of mining-related seismicity and time-variation of mining-related seismicity allows the modification of the classical approach. The modified approach has been applied at a very local level inside a copper mine in Poland (Lasocki, 2005). The method is modified by evaluating the past characteristics for the mine seismicity and then forecasting the future seismicity of the mine in time.

This methodology allows the mine operators to make an informed decisions about the anthropogenic events which may cause damage (Bommer et al., 2015).The difference between the anthropogenic events and the natural seismicity is significant in both space and time owing to the complexity of mining (Lasocki, 2008). The anthropogenic events are quasi-stationary and their occurrence process is non-Poissonian (Lasocki, 2008). This methodology of seismic hazard assessment be can avoided at a regional level since it commonly applied at a very local scale. A standard procedure can be applied at a regional level (Atkinson et al., 2015; Bommer et al., 2015).

The application to mining-related seismicity requires some modification to the classical approach of PSHA as described by Convertito et al. (2012). Because of the variation of production rate, due to factors such as the political instability, depreciation of the gold price (1981-2002), depletion of reserves, increasing production costs and other competing emerging markets, level of mining, risk, mining strikes *etc,* the earthquake occurrence is not stationary in time. Hence, parameters such $\alpha_n(M_{min})$ and the *b*-value of the Gutenberg-Richter (GR) relationship vary with time, and the hazard integral is modified as follows:

$$v(z) = \sum \alpha_n(M_{min}) \int \int f(m)[\int f(r|m).P(Z > z|m,r)\,.dr]\,dm\,dt \qquad (2.9)$$

where *t* ranges between (*T*, *T*+Δ*t*), which was investigated. The maximum expected magnitude (M_{max}) must be selected considering the limitation on the upper bound due to the size of the seismogenic volume. Thus, a lower and upper truncated formulation of *f(m)* is used rather than the classic approach and the other recurrence parameters vary with time such as the *b*-value and *a*-value (Convertito et al*.,* 2012). This is the methodology used in this study.

3. EARTHQUAKE CATALOGUE

3.1 Sources of earthquake data

3.1.1 Global seismic networks

Records of most events all over the world are compiled by organisations such as the Advanced National Seismic System (ANSS), the Comprehensive nuclear-Test-Ban Treaty Organisation (CTBTO), the International Seismological Centre (ISC) and the National Earthquake Information Centre (NEIC).

The ISC is based in the UK and was founded in 1964 with the responsibility of collecting and analysing phase data of earthquakes from around the world. In their analysis efforts, the ISC recalculates earthquake source parameters using the seismological data collected from different seismological agencies and presents the information in a seismological bulletin, which is available online. The Comprehensive Nuclear-Test-Ban Treaty Organisation (CTBTO) was established in 1996 to monitor worldwide nuclear testing using seismometers, hydro-acoustic, infrasound and radionuclide technologies and is now based in Vienna, Austria. The CTBTO is an international organisation responsible for detecting nuclear tests performed anywhere on the Earth, including tests performed underground, underwater and in the atmosphere. The CTBTO has approximately 50 primary seismic stations across the globe and more than 100 auxiliary seismic stations. The Advanced National Seismic System (ANSS) is based in the USA and provides earthquake information, such as the magnitude and location, as fast as possible and as accurately as possible through global networks. The National Earthquake Information Centre (NEIC) is also based in the USA and provides seismic source parameter solutions for mainly larger events of $M_L \geq 3.0$ and also some smaller events, especially in the USA.

3.1.2 National seismic networks and history of seismic monitoring in South Africa

Mining-related seismicity was first encountered in the early 1900s in Johannesburg, soon after gold was discovered in 1886 when extensive stopes reached depths of several hundred meters (Durrheim, 2010; Riemer and Durrheim, 2012). The history of earthquake monitoring in South Africa can be divided into five stages:

- The first stage extends until 1899 and corresponds to the time span when there were no instrumental recordings at all.
- The second stage began in 1899 when a Milne seismograph was installed in Cape Town (Strasser and Mangongolo, 2012). This seismograph was later upgraded to a Milne-Shaw instrument in 1920 and then stopped working in 1931. In 1935, the University of Cape Town resumed the operation of this seismograph until 1947, with another horizontal Milne-Shaw seismograph. In 1949, the Bernard Price Institute (BPI) at the University of the Witwatersrand took over the operation of the Milne-Shaw seismological instruments until 1968. It corresponds to the early instrumental period when isolated seismic

stations were deployed at a regional level. In addition to the Cape Town instrument, a seismograph was installed at the Union Observatory in Johannesburg in 1910 (Gane et al., 1946; Saunders et al., 2008) and another seismograph was installed in the village of Ophirton and later moved to Boksburg in 1913 (Durrheim, 2010). The first surface seismograph network was deployed in the Witwatersrand Basin in 1939 by the BPI (Durrheim, 2010). This seismograph network was composed of four seismic stations (Gane et al., 1946).

- The third stage began in 1939 when a network of four seismic stations was deployed by the Geological Survey of South Africa (GSSA) which is now the Council for Geoscience (CGS). These four stations were located in Pretoria, Pietermaritzburg, Grahamstown and Kimberley, and were later supplemented by the fifth station in Windhoek. The Pretoria and Windhoek stations were integrated into the World-Wide Standard Seismographic Network (WWSSN) in the early 1960s. There were also six seismic stations deployed in the municipality of Johannesburg, at the Bernard Price Institute, Forest Hill School, the Union Observatory, Dr. Schonland's residence in Parkview, Rossmore Junior High School and Regent Park School (Gane et al., 1946).
- The fourth stage started in 1971, after the most damaging earthquake ever recorded in South Africa, the Ceres-Tulbagh earthquake of M_L 6.3 on 29 September 1969. The South African National Seismograph Network (SANSN) was then established with seven seismographs in 1971 which expanded to 27 stations by 1997 (Saunders et al., 2008) (Figure 4). From 1971, reliable instrumentally-determined source parameters are available for most events during this stage. The number of SANSN seismic stations was stable from 1998 to present.
- The fifth stage started in May 2010 when the Strategic Water Management Project (SWMP) network was established (Table 1 and Figure 5). The network is operated by the Council for Geoscience mainly to monitor seismicity related to mine flooding which started in 2005 in the Central and East Rand using accelerometers (with a frequency range of DC up to 200 Hz) that enable strong ground-motions to be recorded. Subsequently, the Japan International Cooperation Agency (JICA) network (Table 2 and Figure 5) and Mine Health and Safety Project (MHSP) networks were deployed in July 2012 and are used to monitor mining-related seismicity in the mining regions of the Far West Rand and Klerksdorp mining districts respectively (Table 3 and Figure 5). The networks are also referred as the CGS cluster networks.

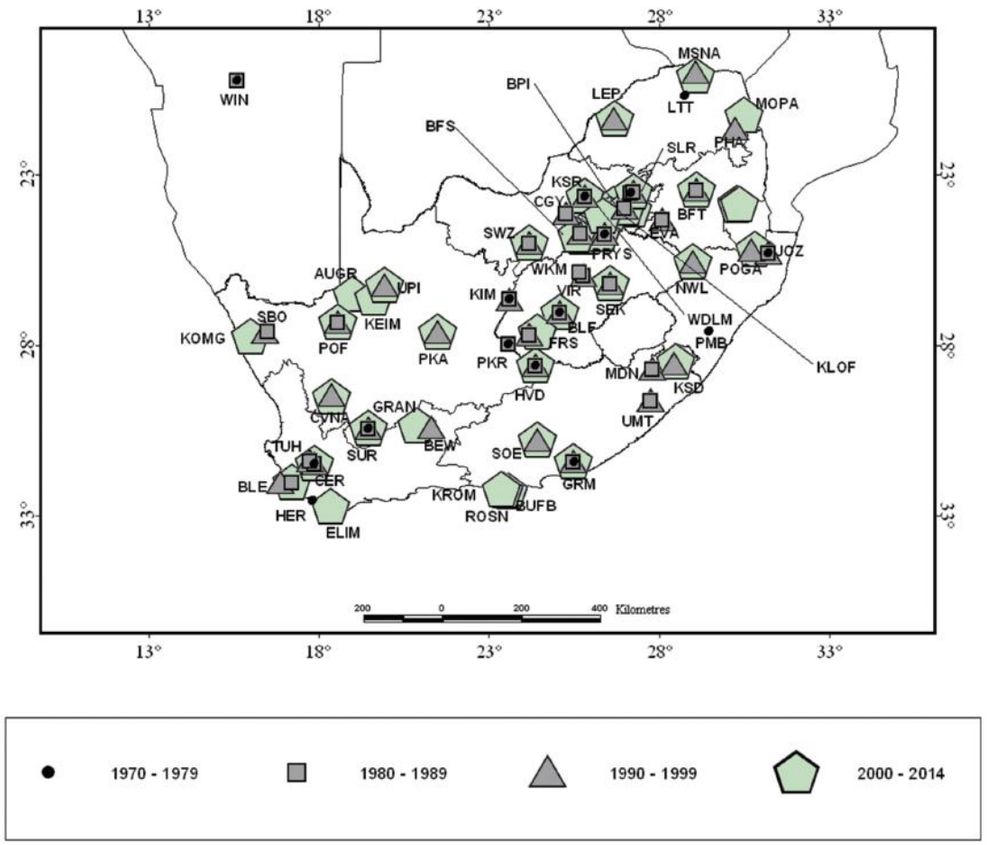

Figure 4. The South African National Seismograph Network (SANSN) and Cluster Networks from 1970 to 2014 (Saunders et al., 2016).

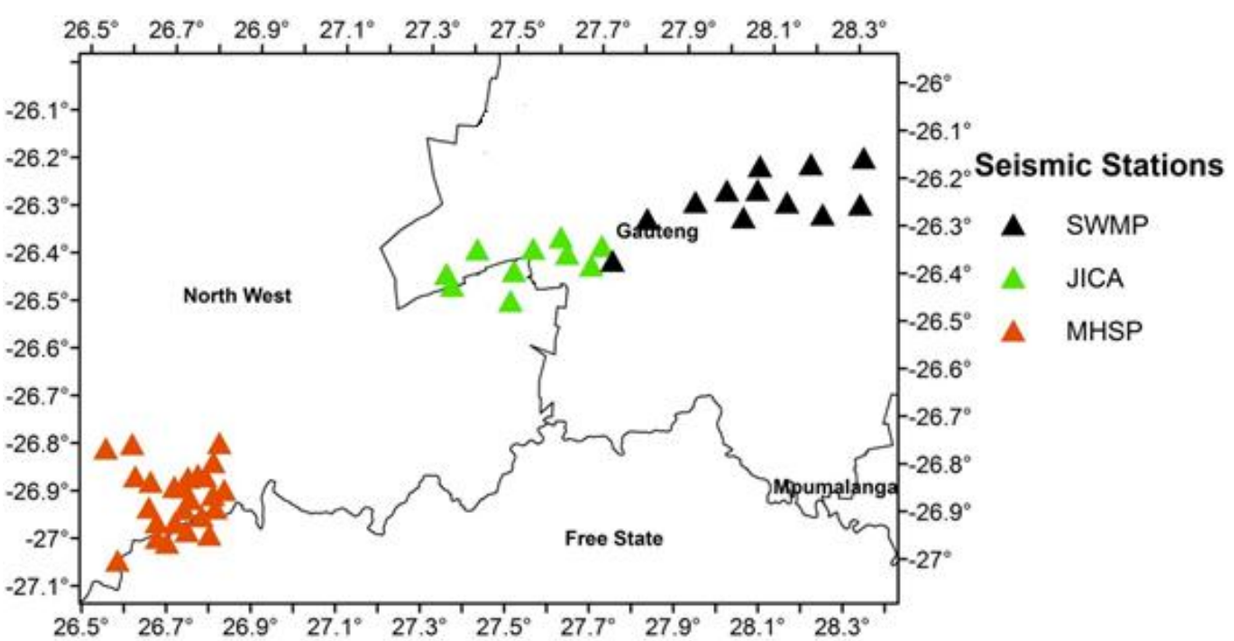

Figure 5. Location of seismic monitoring stations operated by CGS as from 2012.

Table 1. Strategic Water Management Project (SWMP) stations operational table.

Station Code	Year	Month	Lat	Lon
ALBD	2010	05	-26.2580	28.1402
BNON	2010	05	-26.1590	28.3170
CNVL	2010	05	-26.2572	28.3127
CTDP	2010	05	-26.2336	28.0701
GOUD	2010	05	-26.1759	28.1936
HDEW	2010	05	-26.0946	27.8961
OBSV	2010	05	-26.1835	28.0742
ORMO	2010	05	-26.2368	27.9982
RDWR	2010	05	-26.2922	28.0391
SPCM	2010	05	-26.2810	28.2246
UNJO	2010	05	-26.2626	27.9249
WILL	2010	05	-26.2000	28.3184

Table 2. Japan International Cooperation Agency (JICA) stations operational table.

Station Code	Year	Month	Lat	Lon
BLYV	2012	03	-26.4276	27.3447
CORB	2012	03	-26.3703	27.5469
DRF5	2012	03	-26.4183	27.5034
ELND	2012	03	-26.4525	27.3583
EZUL	2012	03	-26.3609	27.7082
FOCH	2012	03	-26.4809	27.4968
KEVO	2012	03	-26.3744	27.4156
KLF3	2012	03	-26.3790	27.6270
LEBN	2012	03	-26.3447	27.6111
SDEP	2012	03	-26.4020	27.6846

Table 3. Mine Health and Safety Project (MHSP) stations operational table.

Station Code	Year	Month	Lat	Lon
AG5	2012	07	-26.9125	26.7517
AGGR	2012	07	-26.9630	26.7171
AGHS	2012	07	-26.9338	26.7372
BFSD	2012	07	-26.8648	26.7861
BSP	2012	07	-26.9033	26.8060
FBF	2012	07	-26.7940	26.8184
KDGC	2012	07	-26.8781	26.6579
KPNG	2012	07	-26.9801	26.7455
KMDR	2012	07	-26.8096	26.5504
MOAB	2012	07	-26.9869	26.7990
MWC	2012	07	-26.8340	26.8050
OGC	2012	07	-26.9958	26.6756
PNMR	2012	07	-26.7999	26.6125
RCAS	2012	07	-26.8676	26.6213
SJ5	2012	07	-26.8614	26.7692
SJ6	2012	07	-26.8678	26.7461
SJ7	2012	07	-26.8886	26.7328
SJ8	2012	07	-26.8878	26.7142
SJ10	2012	07	-26.8922	26.8323
SJ12	2012	07	-26.9311	26.8125
TLEK	2012	07	-26.9634	26.6743
VMBD	2012	07	-26.9323	26.6548
VRCP	2012	07	-27.0057	26.6993
VRVW	2012	07	-26.9483	26.7800
WDF	2012	07	-27.0451	26.5830

3.2 Catalogue compilation

3.2.1 Merging collected data

SEISAN is a seismic analysis software used to process and analyse earthquake catalogues (Ottemöller et al., 2014). Different catalogues from different sources (ISC, CTBTO, ANSS, NEIC, SANSN and CGS cluster networks) were merged using programs in SEISAN, to produce a catalogue with duplicates.

3.2.2 Removal of duplicate events

Duplicate events were removed following the process described below. The SEISAN program was firstly used because it has the ability to check the duplicate events by comparing the origin time of the earthquake and location although its reliability is not perfect, then duplicates were then manually identified as suggested by Hussein et al. (2008). Earthquakes which are assumed to be duplicated were then treated using the following criteria:

- All events from the different networks were first retained in an initial catalogue,
- Events were compared in terms of location (error within 5 km or 0.05 degrees), magnitude (error ≤ 0.3) and origin time (error ≤ 60 s). If these three parameters were very close to each other, then those events were assumed to be duplicates; if not, then those events were kept in the catalogue,
- Events reported with M_W were given first preference,
- Events from the CGS cluster networks were given first preference, followed by events recorded by the SANSN,
- The events located with a higher number of stations were considered to be better constrained and were kept in the catalogue,
- Events with a higher decimal accuracy in location were considered to be more reliable and were kept in the catalogue.

The actual process of removing duplicates following the criteria described above was conducted manually to ensure control over the process. The merged catalogue resulted in a total of 33,536 seismic events after duplicates were removed. It is with confidence that the majority of duplicates were removed and any remaining duplicates would not significantly influence the results. A total of 3,140 duplicates were removed.

3.3 Homogenisation of the Earthquake Catalogue

The merging of earthquake data from different sources produced a non-homogenised earthquake catalogue owing to the different magnitude scales that were used. In South Africa alone, four different local magnitude (M_L) scales have been used to estimate the sizes of the local earthquakes. Other magnitude scales such as the body wave magnitude (m_b), surface wave magnitude (M_S) and moment magnitude (M_W) have been used for moderate to large earthquakes. The other international agencies such as ANSS, CTBTO, ISC and NEIC also used different magnitude to estimate the sizes of moderate to large earthquakes in South Africa. Combining the data from these agencies resulted in a non-homogenised or heterogeneous earthquake catalogue which needed to be homogenised.

It is standard in PSHA studies that a homogenised catalogue is used. The moment magnitude scale is used in PSHA studies because it does not saturate (Hanks and Kanamori, 1979). The moment magnitude scale was used in this study because all ground-motion prediction equations considered use the moment magnitude. Then, all the other magnitude scales were then converted to moment magnitude scale as follows:

- Events reported with M_W were kept in the catalogue.
- Events reported with any other scale were converted to M_W using the magnitude scale conversion formulae described below.

The different local magnitude scales used at the CGS were first homogenised to a single local magnitude scale and then converted to moment magnitude as described below.

3.3.1 Evolution of M_L

The seismicity of South Africa can be divided into two stages. The first stage refers to the period when there was no instrumental recording and early instrumental recording (pre-1939). The second stage refers to when there was instrumental recording (1939 onwards). These stages can be referred to as historical seismicity and instrumental seismicity. During these stages, four M_L scales were used in South Africa at different times, as described below.

3.3.2 Historical Seismicity

Historical seismicity is seismicity that was not recorded by a seismograph but described by people or documented in journals, newspapers and diaries, hence, their locations and magnitudes are not considered accurate. The sizes of these seismic events were estimated using intensity data (Fernández and Guzman, 1979). The historic catalogue of South Africa was compiled by Fernández and

Guzman (1979) and later updated by Brandt et al. (2005) (Albini et al., 2014). They converted the maximum observed Modified Mercalli intensity to estimate the local magnitude (equation 3.1):

$$M_L = \frac{2}{3} I_{\max} + 1.0. \tag{3.1}$$

where I_{max} is the maximum observed intensity according to the Modified Mercalli Intensity scale of 1956. There are few such events in the study region and they are excluded in the final catalogue due to a very high error in the location accuracy, which may lead to incorrect assessment of recurrence parameters for the purpose of this study. The catalogue of this study covers seismicity from 1970, during which there were early instrumental recordings.

3.3.3 Instrumental seismicity

Instrumental seismicity is seismicity that was recorded by seismographs operated by the CGS and the other agencies mentioned above. The recorded seismograms are then analysed to compute the location (latitude, longitude and depth), date of the event, time of the event, size of the event and other parameters from the frequency and amplitude content of ground-motions (Vaccari et al., 2005). The list of these parameters is called an earthquake catalogue (Woessner et al., 2010). The first magnitude scale was proposed by Richter (1935).

The local magnitude is as devised by Richter (1935) for the region of California. The evaluation of local magnitude for local events in South Africa was done using the maximum amplitude of the vertical short period component in the S-L wave complex (Richter, 1935). These amplitudes are then converted to local magnitude values using the magnitude-distance attenuation curves of the frequency response of the SANSN (Fernández, 1973; Fernández, 1977).

Three local magnitude scales were used during the instrumental seismicity stage. These three scales reflect the evolution of the Richter scale. The first scale used was the Richter scale (1935) (equation 3.2). The second scale used was developed by Hutton and Boore (1987) (equation 3.4), whilst the third scale was developed by Saunders et al. (2012) (equation 3.5).

The definition of Richter (1935) for earthquakes in Southern California is given as follows:

$$M_L = log_{10}A_1 - log_{10}A_0, \tag{3.2}$$

where A_1 is the maximum trace amplitude in millimetres recorded by the Wood-Anderson (horizontal) torsion seismograph at an epicentral distance of 100 km. A_0 is the trace amplitude of the "standard" earthquake at the same epicentral distance. This scale was calibrated by the recording of earthquakes in a range of 30 to 600 km. This scale was used by the CGS between 1971 and March 1997.

Richter's local magnitude scale was first modified in 1979 using numerous observations of seismic events in the 0 - 350 km epicentral distance range. The local magnitude obtained was (equation 3.3):

$$M_L = 1.26 + 0.84log_{10}R_{epi} + log_{10}\left(\frac{A_V}{T}\right) + S.C., \quad (3.3)$$

where R_{epi} is the epicentral distance in kilometres, A_V is the maximum vertical amplitude of ground-motion expressed in micrometres and T is the period in seconds, *S.C.* is a station correction factor evaluated from observations (Fernández and Guzmann, 1980). This scale was derived but never used.

Brandt (1997) found that the relation of Hutton and Boore (1987) was the best scale to be used at that time since as it compared well with the modified Richter relation. This relation (equation 3.4) was found by the straightforward regression analysis of 7,355 measurements of ground-motion amplitude from 814 earthquakes to derive station and distance corrections:

$$M_L = log_{10}A_1 + 1.110\log\left(\frac{R_{hpo}}{100}\right) + 0.00189\left(R_{hpo} - 100\right), \quad (3.4)$$

where A_1 is the same as defined in equation (3.2) and R_{hpo} is the hypocentral distance in kilometres. This scale was used from April 1997 to up the end of 2011.

A new relation to determine the local magnitude was developed by Saunders et al. (2012) using 263 earthquakes recorded at a range of epicentral distances of 10 - 1,000 km by the SANSN. The relation is:

$$M_L = log_{10}(A_1) + 1.149log_{10}\left(R_{epi}\right) + 0.00063R_{epi} + 2.04 - S, \quad (3.5)$$

where A_1 is the same as defined in equation (3.2), R_{epi} is the epicentral distance in kilometres and S is the station correction term. This scale was used from 2012 to present.

3.3.4 Homogenisation of M_L

There are three M_L scales which have been used from the 20th century to present as described in the section above. These three M_L scales needed to be homogenised into a single M_L equivalent to the scale developed by Saunders et al. (2012). It is important to

homogenise all these magnitude scales so they report the same equivalent local magnitude type. Where phase and amplitude data are available, events were relocated using the latest local magnitude scale (Saunders et al., 2012).

However, 11 seismic events in the catalogue recorded pre-1971, do not have phase and amplitude data available as the magnitude of most of these seismic events were derived from intensities. In this case, a decision was made to assume that this early local magnitude scale was equivalent to the Saunders et al. (2012) scale. The 11 seismic events recorded pre-1971 in the catalogue in all four source zones out of a total of 33,536 seismic events, these seismic events should not be significant to the outcome of this work.

The seismic events recorded between 1971 when the SANSN was established and March 1997 were calculated using the local magnitude scale calibrated for Southern California by Richter (1935). Saunders et al. (2010) recalculated the magnitude of 200 earthquakes previously calculated using the local magnitude by Richter (1935). Using a straight forward regression technique, he obtained a relation between the Hutton and Boore (1987) and Richter (1935) magnitude scales (equation 3.6):

$$M_L(Hutton\ and\ Boore) = 1.010 M_L(Richter) + 0.118, \quad (3.6)$$

also shown in Figure 6. Using this relation the magnitude values of all events recorded between January 1971 and March 1997 were converted to the equivalent Hutton and Boore (1987) values.

The seismic events recorded between April 1997 and December 2011 were calculated using the local magnitude scale calibrated for Southern California by Hutton and Boore (1987). A significant amount of phase data was available to recalculate the magnitude values of the seismic events during this period, hence it was possible to compare or correlate the magnitude scale derived by Hutton and Boore (1987) and the magnitude scale derived by Saunders et al. (2012) (Figure 7). A total of 425 earthquakes were recalculated using the local magnitude scale by Saunders et al. (2012) from 1997 to 2010. The magnitude values ranged from 0.3 to 4.0. A maximum sample of 10 earthquakes was chosen for each magnitude bin. The relationship found between the Saunders et al. (2012) and Hutton and Boore (1987) magnitude scales is given in equation 3.7:

$$M_L(Saunders) = 0.9444 M_L(Hutton\ and\ Boore) + 0.0932\ \pm 0.14, \quad (3.7)$$

by combining equation (3.6) and equation (3.7) we found the relationship between Saunders et al. (2012) and Richter (1935), given in equation 3.8:

$$M_L(Saunders) = 0.9538 M_L(Richter) + 0.2046\ \pm 0.14, \quad (3.8)$$

therefore, equation (3.7) and equation (3.8) were used to convert two previously used M_L scales into the single local magnitude scale of Saunders et al. (2012).

3.3.5 Magnitude conversions to M_w

In this study, we followed an approach similar to that of Hussein et al. (2008) to obtain linear statistical regression relations between different magnitude types (m_b and M_L) using earthquake data. The linear regression was adopted because there were sufficient data to implement it. A total of 242 seismic events were recorded and reported with both m_b and M_L as shown in Figure 8. The linear regression of these seismic events resulted in the following:

$$M_L = 0.515m_b + 1.64 \pm 0.8. \quad (3.9)$$

Thereafter, the relation (equation 3.10) derived by Brandt and Saunders (2015) was used to convert M_L to M_W. They used a general orthogonal regression between M_W and M_L using 23 earthquakes recorded by the SANSN for the magnitude range $3.6 \leq M_L \leq 4.4$ and to obtain the relationship given below:

$$M_W = M_L - 0.15 \pm 0.15\,. \quad (3.10)$$

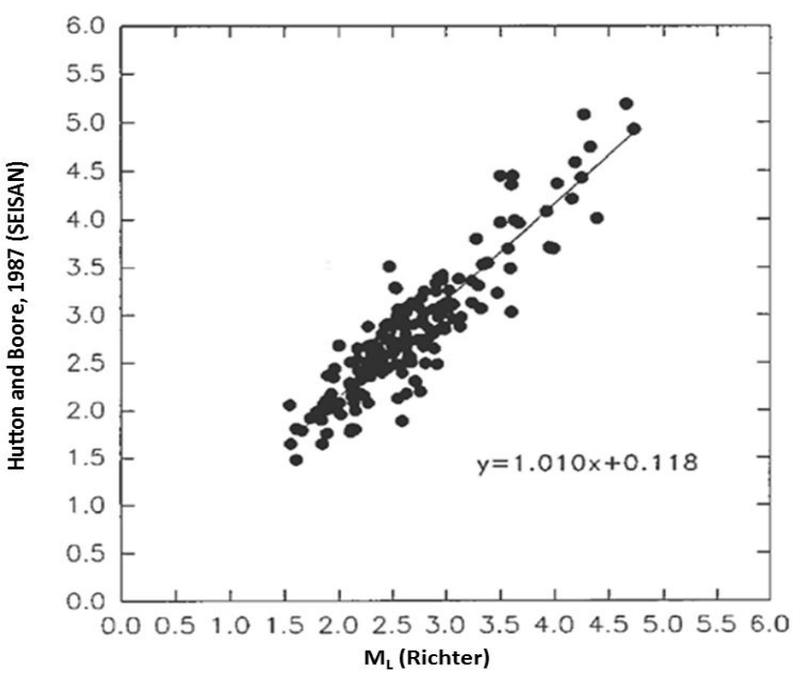

Figure 6. Comparison of magnitudes using the Hutton and Boore (1987) relation and the M_L relation of Richter (1935) used by CGS (Saunders et al., 2012).

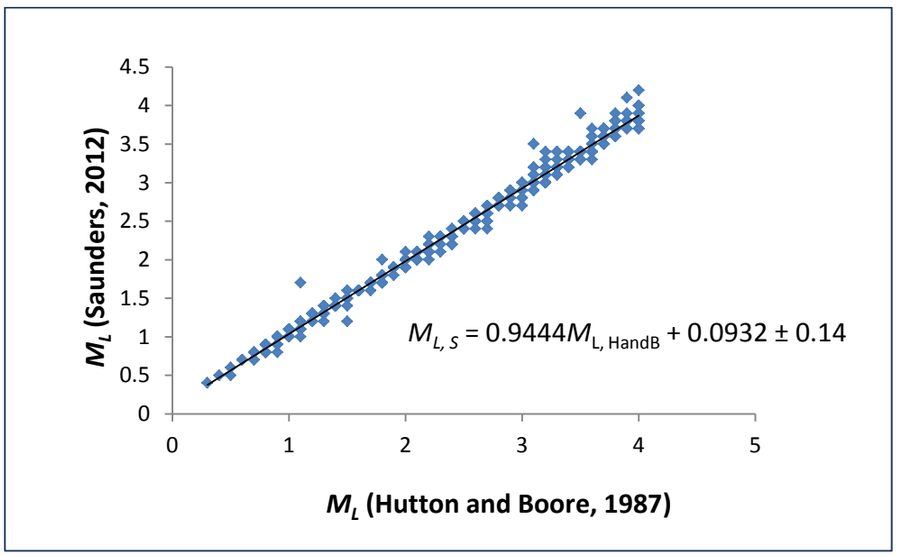

Figure 7. Comparison of the local magnitude scale using the Saunders et al. (2012) scale and the local magnitude scale of Hutton and Boore (1987).

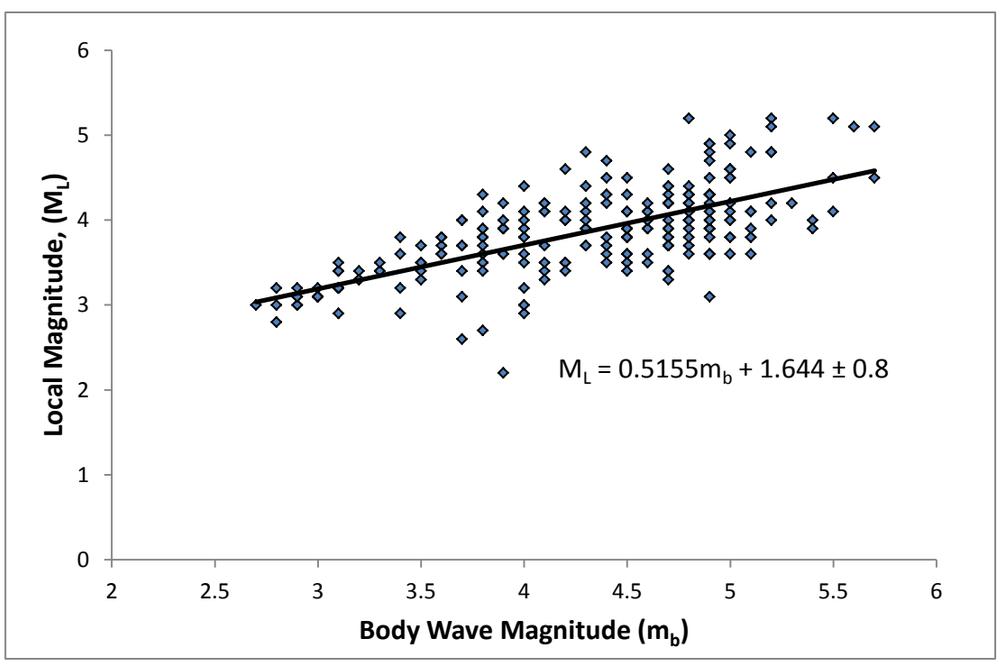

Figure 8. The relationship between local magnitude and body wave magnitude.

3.4 Catalogue Evaluation

There has been a total of 14,830 earth tremors recorded from 1908 to 1937 (Gane, 1939) and approximately 29,000 earth tremors recorded from 1938 to 1949 near to Johannesburg (Finsen, 1950). The earthquake catalogue has 33,536 seismic events recorded from 1 January 1970 up to 31 December 2015. The earthquake magnitude varies from a minimum magnitude of M_W 0.0 to a maximum magnitude M_W 4.8. The first seismic event recorded in the catalogue is the 1 January 1970 M_W 4.0 located near Edenvale, in the East Rand with a high error estimate in location because there were few seismic stations at the time in the region. The last seismic event in the catalogue is the 31 December 2015 M_W 1.0 located near Waterpan, in the West Rand with a much smaller error estimate in location compared to the first seismic event because of the improvement in the local seismic networks. There are no seismic events pre-1970 included in this catalogue because of the huge error in both location and magnitude. The error estimates are higher than 10 km, so events from one seismic zone can be mistakenly located in another seismic zone because the seismic zones being considered are small. This can result in the calculation of incorrect seismic recurrence parameters. The first time a double-digit number of seismic events were recorded from 1 January 1970 to 2 December 1970 when 12 seismic events were recorded shortly before the introduction of the SANSN.

The first significant improvement in seismic event recording was from 1971 when the SANSN became operational, even though the SANSN was analogue. A total of 93 seismic events were recorded in 1971. The seismicity recorded from 1971 gradually increased until 1974 when 306 seismic events were recorded. The first decrease in the number of seismic events recorded by the SANSN was in 1975 when only 211 seismic events were recorded due to the downtime of the SANSN. The actual seismicity had not decreased. The number of seismic events recorded then increased until 1977 when 417 seismic events were recorded. The number of seismic events recorded decreased to as low as 113 seismic events in 1979. The variation in the recorded seismicity during this period was due to the downtime of the SANSN, mainly due to maintenance. The number of seismic events recorded gradually increased from 1980, recording 365 seismic events until 1989 when 720 seismic events were recorded (Figure 9).

The number of seismic events recorded sharply decreased in 1990, when only 107 seismic events were recorded. This is the lowest ever number of seismic events recorded in a year since the introduction of the SANSN. The number of seismic events recorded steadily increased to 383 seismic events recorded in 1993 and then gradually decreased in 1994 to 273 seismic events (Figure 9). The number of seismic events recorded increased from 289 seismic events recorded in 1996 to 503 seismic events recorded in 1997. The number of seismic events recorded then increased to 556 seismic events in 1998, but then decreased down to a low 129 seismic events in 2002. The number of seismic events recorded then gradually increased to 271 seismic events recorded in 2003 and 283 seismic events recorded in 2004 (Figure 9). This was a period when some of the seismic stations SANSN were being converted from analogue to digital acquisition systems. At this stage, the SANSN consisted of a combination of analogue and digital seismograph stations, seen as a hybrid stage.

A substantial increase in the number of seismic events recorded is observed from 2005 when 767 seismic events were recorded. The number of seismic events recorded increased to 1,227 seismic events in 2006. This is the first time the number of seismic events recorded reached the 1,000 mark. The number of seismic events recorded increased to 1,828 in 2007, before decreasing again to 845 in 2012 (Figure 9). During this stage, the SANSN completed the migration to digital acquisition.

A steep increase in the number of seismic events recorded is observed from 2014 when 4,935 seismic events were recorded. The number of seismic events recorded slightly decreased in 2015 to 3,471 seismic events per year (Figure 9). This huge increase is due to the introduction of the SWMP, JICA and Mine Health and Safety Project (MHSP) cluster networks which started operating, in addition to the SANSN. The number of seismic events recorded by mining networks might not have changed significantly during these periods as they monitor at a higher sensitivity than the CGS networks.

The observed changes in the number of seismic events recorded throughout the history of the catalogue can be linked to the periods when the South African seismic networks improved or when their operation deteriorated (Saunders et al., 2016). However, the increase or decrease in the occurrence rate of events can also be linked to the production rates and level of mining in the region. However, actual records to link these last two factors to seismic rates is currently being investigated at the CGS in cooperation with students from the Tshwane University of Technology.

The number of seismic events recorded fluctuates during the day with the number of seismic events recorded increasing between 8 am and 6 pm, peaking at 4 pm and decreasing between 6 pm and 8 am (Figure 10). Cazalet (1919), Gane et al. (1949), Stokes (1936) and Wood (1914) investigated the time distribution of induced seismicity; they concluded that the peaks observed during the day are mainly due to mine blasting, which occurs at about 14H00. These mine blasts trigger forces which change the stresses in mines. The accumulated energy gets released, for example by the fracture of intact rock mass immediately ahead of the stope, or slip along a pre-existing fault. These periods correspond to the times when mining activity starts and when it stops, hence showing that this seismicity is related to mining activity.

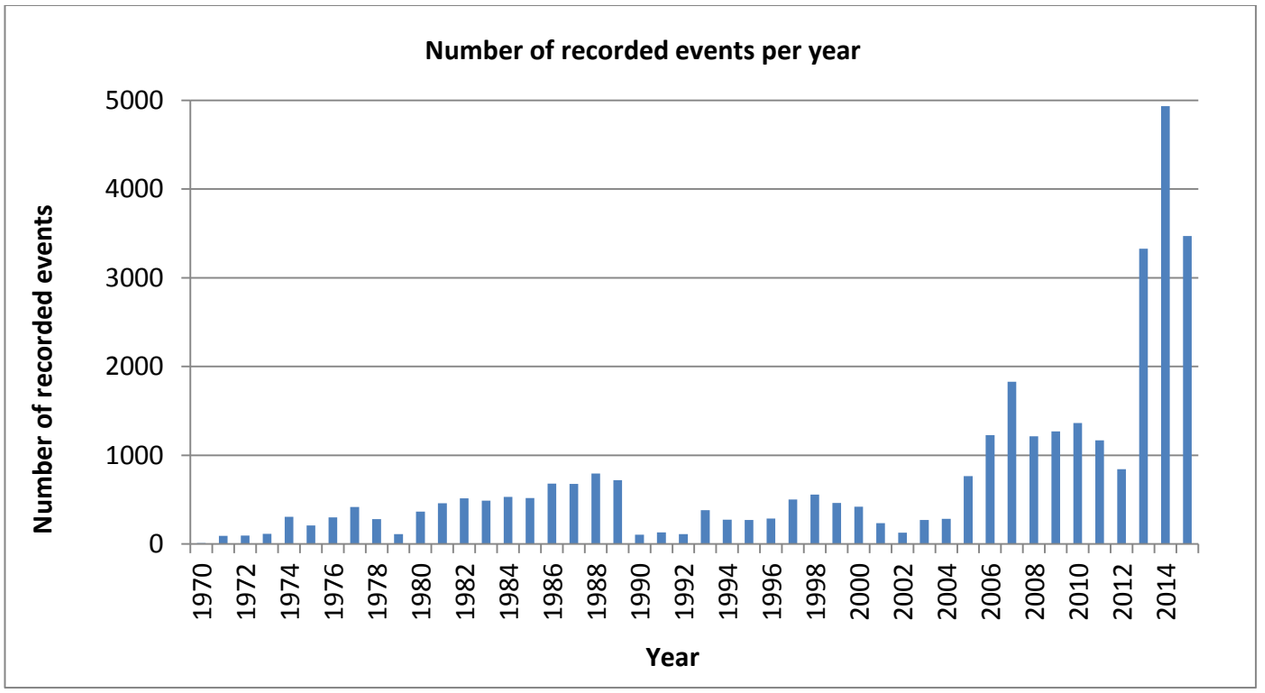

Figure 9. The number of events recorded per year by the SANSN.

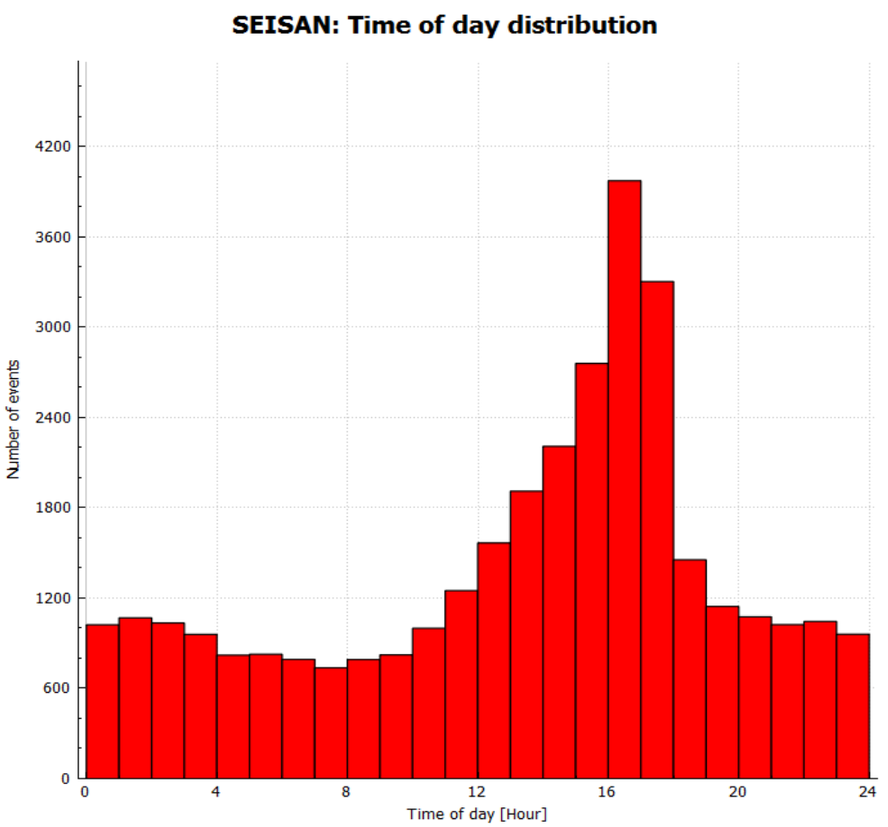

Figure 10. Variation in seismic activity in a day.

3.5 Catalogue completeness

The earthquake catalogue completeness is defined as the minimum magnitude at which all the earthquakes are recorded (Mignan and Woessner, 2012). Wiemer and Wyss (2000) define the magnitude of completeness as the magnitude at which more 90 % of the events can be modelled by a power law fit. An earthquake catalogue is said to be complete above a specific value of completeness (M_C) over a specific period of completeness (T_C) if all earthquakes with magnitudes ≥ M_c are recorded during the period T_C in the specific region of interest and listed in the catalogue. The recurrence parameters are normally calculated from M_C for each seismic source zone of the catalogue to ensure reliable estimates. The value of M_C generally improves over the years because of improvements in network capabilities (Wiemer et al., 1998; Wiemer and Wyss 2000).This phenomenon was well observed in this study, especially when the cluster networks were operational from 2010 onwards.

The completeness of the catalogue can be determined using the historical method, the maximum-curvature method and the catalogue-based method (Mignan and Woessner, 2012; Stucchi et al., 2004; Wiemer and Wyss, 2000). The historical approach, which was used in this study, is the process of obtaining a catalogue from preserved historical sources of information such as newspapers, diaries *etc*. The sources provide information which relates to the intensity of the earthquake, mostly for damaging earthquakes. The magnitude of earthquakes can be estimated with associated error estimates (Stucchi et al., 2004). The information can then be presented on a time scale similarly as the data recorded by the seismograph networks as shown in Figure 11. The historic approach has been used in San Francisco in the US, Montreal in Canada, Ica in Peru and Verona in Italy (Stucchi et al. 2004).

The maximum-curvature method (Wiemer and Katsumata, 1999; Wiemer and McNutt, 1997; Wyss et al., 2000) as implemented in SEISAN was also used in this study. The maximum-curvature method is regarded as a simpler way of computing M_C than other methods (Mignan and Woessner, 2012). The M_C is observed graphically in SEISAN software by plotting a constant moving window of 100 events with time, the maximum upward curvature of the resulting graph gives M_C (Figure 12). Wiemer and Wyss (2000) argues that the maximum-curvature method underestimates M_C and they prefer the statistical method or catalogue-based method by assessing the time and spatial distribution of seismic events as implemented in this study.

The catalogue-based method plots the frequency-magnitude distribution of events, as proposed by Gutenberg and Richter (1944) and Richter (1958). This is commonly known as the Gutenberg-Richter power law distribution of magnitudes (Wiemer and Wyss, 2000). The magnitude of completeness is the value at which the slope of the Gutenberg and Richter frequency-magnitude distribution starts to flatten out. This method of determining M_C is regarded as the simplest method (Wiemer and Wyss, 2000).

The minimum magnitude of completeness M_C and the *b*-value can vary as a function of location, time or depth (Wiemer et al., 1998). The temporally-varying of M_C is calculated by a standard moving-window technique (Wiemer and Katsumata, 1999; Wiemer et al., 1998; Wiemer and Wyss, 1997). Here M_C and the *b*-value were calculated for a time-window containing 100 seismic events,

advancing in steps of 100 events, as implemented in ZMAP. The *b*-value was determined using the maximum likelihood method, and M_C by calculating the derivative of the frequency-magnitude distribution (Wiemer et al., 1998).

The uncertainty in determining M_C is shown in Table 4 for $2 \leq M_C < 3$. The hypocentral depth was not taken into account during the assessment of M_C. Even though there was a significant improvement in the density and sensitivity of the seismic network, it was not adequate to determine depths routinely. This is because the Seismic Data Analyst at the Council for Geoscience only picks P and S arrivals. That is because there are only two Seismic Data Analysts processing thousands of seismic events per year.

Using the historical approach based on Figure 11 and the maximum-curvature method based on Figure 12, the catalogue seems to be complete at the following limits, $1.0 \leq M_W < 2.0$ from 2013 - 2015, $2.0 \leq M_W < 3.0$ from 1993 – 2015 (historic approach). It is unclear if the level of M_C was from 1993 or 2006 using the maximum-curvature method (Figure 12) for earthquakes of $2.0 \leq M_W < 3.0$. The earthquake catalogue is complete between $3.0 \leq M_W < 4.0$ from 1971 – 2015 and $4.0 \leq M_W < 5.0$ throughout the catalogue using the maximum-curvature method. The results are also shown in Table 4 which shows the range of Mc for each magnitude bin. It is worth emphasising that these two methods do not always give the same level of completeness (Table 4).Thus, it is advisable that more than one method should be used to achieve a reliable conclusion.

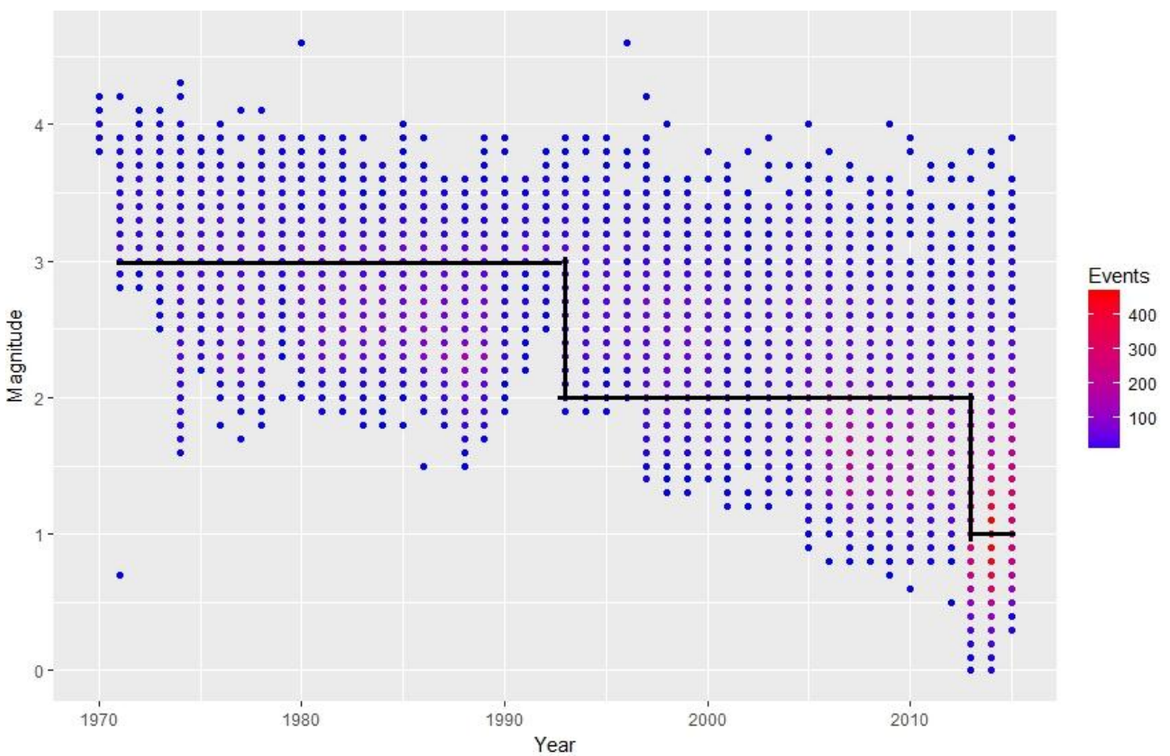

Figure 11. Catalogue completeness using historic approach.

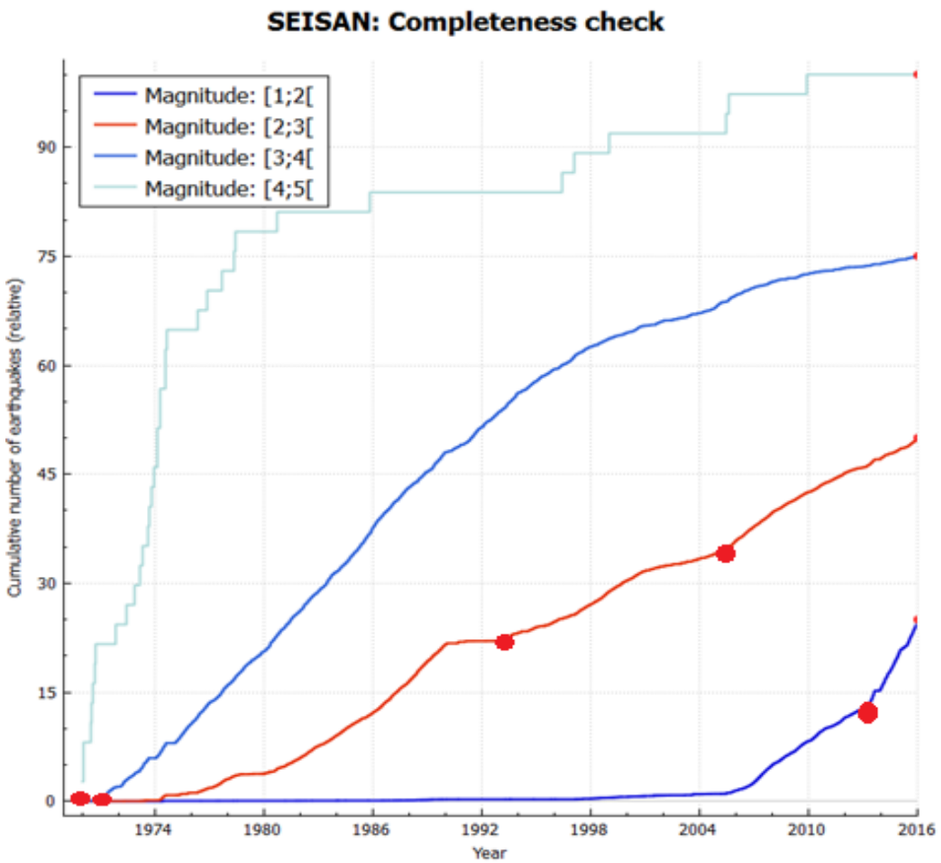

Figure 12. Catalogue completeness using maximum-curvature approach, the reverse bracket ([) is a notation from SEISAN meaning excluding number before the reverse bracket. The graph plots the standard moving-window technique of 100 earthquakes. The red dot are the inflection points at which the maximum-curvature is observed.

Table 4. Magnitude completeness using the historic approach and the maximum-curvature method.

M_C	T_C using historic approach	T_C using maximum-curvature
1-2	2013 - 2015	2013 - 2015
2-3	1993 - 2015	1993 - 2015 or 2006 - 2015
3-4	1971 - 2015	1971 - 2015
4-5	1970 - 2015	1970 - 2015

4. SEISMIC SOURCES AND RECURRENCE PARAMETERS

4.1 Assessment of seismic sources

In a typical seismic hazard assessment, seismic sources are considered to be sources that are capable of contributing to the ground-motion hazard in the region of study. The seismicity distribution in a seismic zone is assumed to be spatially uniform (Beauval et al., 2006), *i.e*. an earthquake of a given size is equally likely to occur at any point within the zone (Baker, 2008). In this study, a model of seismic sources related to mining activities was developed as follows.

The delineation of seismic source zones took into account both the spatial variation in completeness, as well as the spatial variance in the occurrence of seismicity. In order to assess these factors, the latitude of seismicity with was plotted as a function of time, revealing three prominent blocks: between latitudes -26.8° to -26.55°, latitudes -26.55° to -26.225°, and latitudes -26.225° to -25.9° (Figure 13). Similarly, the longitude of seismicity was plotted as a function of time, and six blocks were identified (Figure 14). These results were combined, yielding a source model that consists of six seismic zones. Four of the six seismic zones were assessed for temporal completeness levels (Figure 15). Two seismic zones were not considered because they are distant from the study region and the seismicity is due to opencast blasting, not earthquakes. Further assessments of completeness levels were then conducted for the four zones linked to gold mining in Gauteng. The four were identified as corresponding to the following mining regions: Far West Rand, West Rand, Central Rand and East Rand.

The study area is about 140 km x 65 km. The seismic source zones are actually quite small. The FWR zone is roughly 22 km x 35 km, which is the biggest; while the CR zone is the smallest, roughly 20 km x 20 km. The location error ellipse were large (about 33 km), but improved following the introduction of cluster seismic networks to about 5 km. It would only be possible to break these zones further if there was data from each mine network, as these have much smaller location error ellipses. The Council for Geoscience location error does not allow these seismic source zones to be made any smaller.

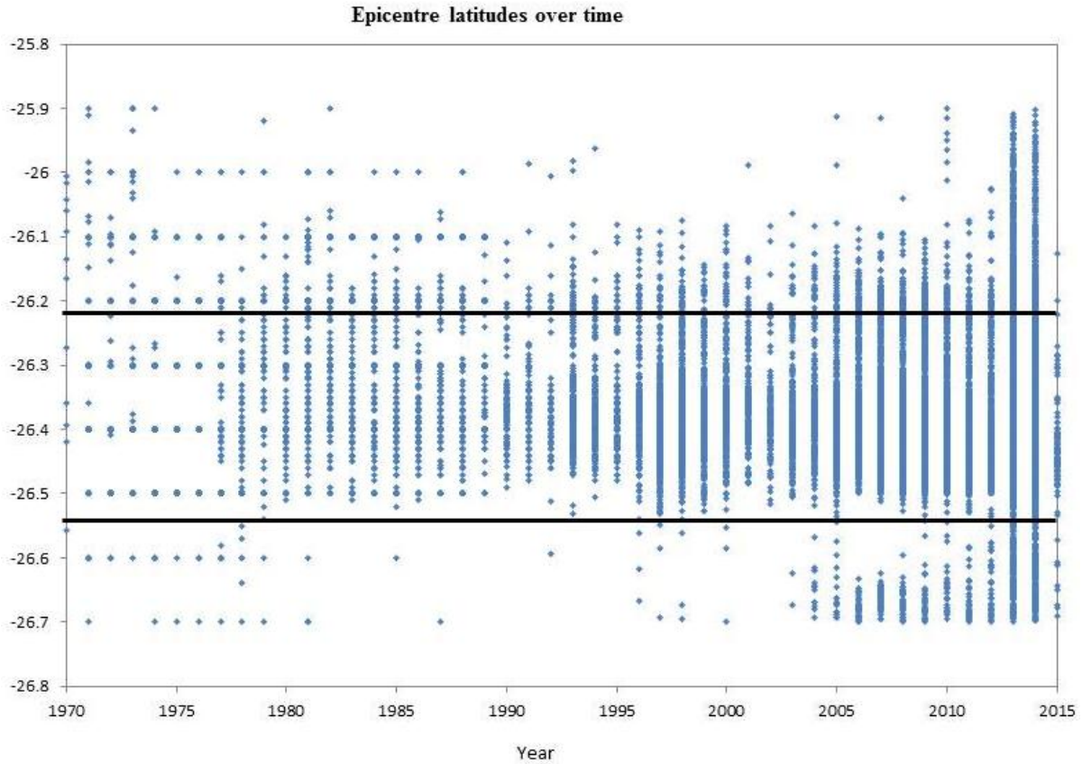

Figure 13. Epicentre latitudes over time.

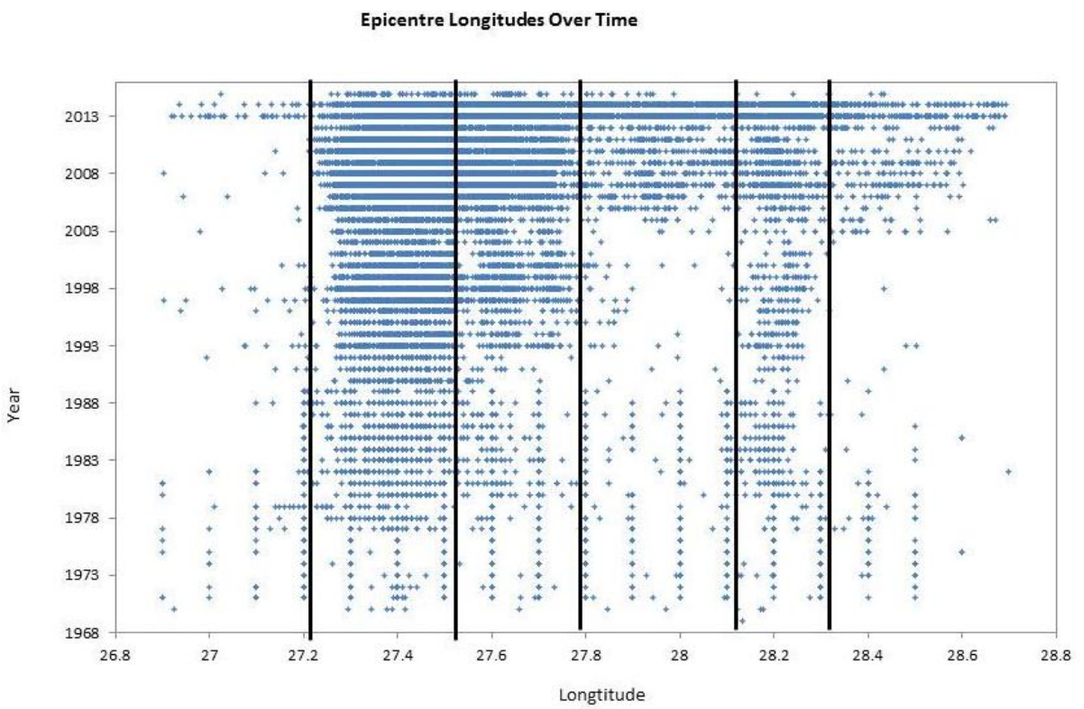

Figure 14. Epicentre longitudes over time.

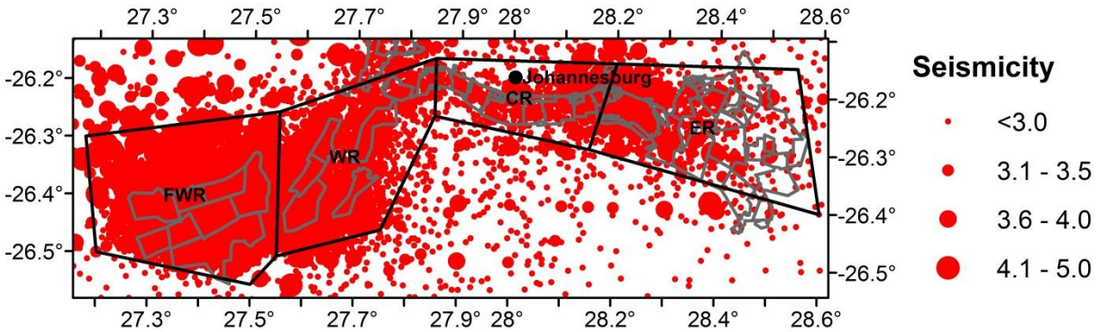

Figure 15. The four mining seismic source zones used in this study, Far West Rand (FWR), West Rand (WR), Central Rand (CR) and East Rand (ER). The black lines represent boundaries of the seismic source zones used and the blue lines represent different mine boundaries.

4.2 Seismic recurrence parameters

As it was observed in the description of seismicity in Chapter 3, it is clear that the recorded seismicity in the gold mining region of the identified seismic zones does not follow a Poisson distribution. A change in the recorded seismicity is highly influenced by changes in monitoring capabilities as well as mining activity. Thus, in characterising the four seismic zones, the time variation in seismicity was assessed and taken into consideration. Time-dependent seismic source recurrence parameters are calculated for each seismic source using various software packages and techniques suitable to each seismic source parameter namely, M_{max}, *b*-value, *a*-value and M_C. M_{max} and *b*-value were calculated using HA3 software (Kijko et al., 2016), the *a*-value was calculated using SEISAN software (Ottemöller et al., 2014) and the temporally-varying of M_C and *b*-value were calculated using the ZMAP software (Wiemer and Wyss, 2000). The catalogue for each seismic zone was used as the input to calculate the required output seismic recurrence parameters.

HA3 was used because it is developed for incomplete data files; however, HA3 doesn't show the temporally-varying of the recurrence parameters and the *a*-values produced by HA3 were too high. ZMAP was the best software to show the temporally-varying of M_C and *b*-value. SEISAN and ZMAP gave comparable results, whilst those from HA3 were different in *a*-values.

HA3 is a MATLAB-based computer program developed mainly to calculate M_{max}, but it can also be used to calculate other seismic parameters such as the *b*-value and the *a*-value (Kijko and Sellevoll, 1992; Kijko et al., 2016). Its strength is its ability to take different completeness levels of a catalogue into consideration, thus, taking into account the temporally-varying of a catalogue.

SEISAN is software developed for earthquake analysis and has a number of programs to analyse earthquakes including recurrence parameters (Ottemöller et al., 2014). SEISAN was also used because it also allows more control on the processing of the data, so it

was used to calculate the *a*-value because it provided realistic values rather than HA3 which gave unrealistic values for each seismic zone.

ZMAP is a MATLAB-based computer program developed mainly to analyse seismicity patterns and can be used to calculate a number of seismic source parameters such *b*-value, *a*-value and M_C (Wiemer and Malone, 2001). The *b*-value and *a*-value in ZMAP are derived from the Gutenberg–Richter relation and M_C is derived from the frequency-magnitude distribution (FMD), which is usually obtained by examination of the cumulative number of earthquakes (Wiemer and Malone, 2001). ZMAP was the best software to graphically show the temporally-varying of the recurrence parameters.

A common procedure in the analysis of a seismic catalogue is to analyse the relationship between the magnitude and the total number of earthquakes in a specific space, also referred as the Gutenberg-Richter relation (Gutenberg and Richter, 1944), which was firstly introduced by Ishimoto and Iida in 1939 (Wesnousky, 1994):

$$\log n = a - bM \tag{4.1}$$

where *n* is the number of earthquakes greater than magnitude *M*, and *a* and *b* are positive constants (Gutenberg and Richter, 1944; Richter 1958). The slope of this relation, commonly known as the *b*-value, relates the frequency of large earthquakes to small earthquakes; while the intercept in *log n* is commonly known as the *a*-value and provides the activity rate of earthquakes per year. A higher *b*-value ($b > 1.0$) means that the hazard is controlled by the smaller earthquakes and a lower *b*-value ($b < 1.0$) means that the hazard is controlled by the larger earthquakes (Bender, 1983).

As already mentioned above, one of the main parameters that are required for each seismic zone is the maximum expected magnitude. This value was calculated from a method described by Kijko and Sellevoll (1992) and later updated by Kijko (2004) and finally by Kijko and Singh (2011). There are eight methods of calculating maximum expected magnitude described and in implemented HA3 (Kijko et al., 2016). The recommended method of determining maximum expected magnitude in HA3 is the Kijko-Sellevoll-Bayes (KSB) method. The method assumes that the magnitudes are independent, identically distributed, random values with a cumulative distribution denoted by $F_M(m)$ (Kijko, 2004; Kijko and Singh, 2011). The method requires M_C to be noted as the minimum magnitude and the number of earthquakes recorded must be in an ascending order. The M_{max} is calculated by the iteration of the following equation:

$$M_{max} = M_{max}^{obs} + \int_{m_{min}}^{M_{max}} [F_M(m)]^n \, dm, \tag{4.2}$$

where m_{min} is M_C, the M_{max}^{obs} is the maximum observed in the region and M_{max} appears on both sides. This equation approximates the required M_{max} and providing a first approximation for M_{max}. The first M_{max} replaces the unknown M_{max} on the integral for the next

iteration. This iterative method is run until an optimal solution for M_{max} is achieved. This method is called the KSB technique, and is one of eight methods provided in HA3 to calculate M_{max}.

Another technique used to estimate M_{max} is the implementation of the equation developed by Reiter (1990) (Ayothiraman and Hazarika, 2008, p 108; Kijko and Graham, 1998):

$$M_{max}(R) = M_{max}^{obs} + 0.5, \quad (4.3)$$

where M_{max}^{obs} is the maximum observed magnitude in each seismic zone. The equation was proposed by Reiter (1990) for use in areas where the catalogues are incomplete and is commonly used in seismic hazard assessments. Equation 4.3 is a conservative method of determining M_{max} in a tectonic environment. In mines, mine engineers are responsible for controlling M_{max} to some extent by properly managing the mine seismicity. This is usually achieved by identifying hazardous seismogenic structures such as faults and dykes prior to mining, which can then be avoided (Durrheim, 2001).There are many things which are considered in mining layouts when trying to reduce M_{max}; these include the use of stiff pillars, pillar spacing, pillar width, dip-pillar, positioning of tunnels, stope dimension, backfilling, rate of mining and partially mining the reef (Durrheim, 2001; Vieira et al., 2001; Vieira and Durrheim, 2002).

4.2.1 Far West Rand (FWR) Seismic Zone

The FWR seismic zone is the most active seismic zone with a total of 20,477 earthquakes recorded between 27 June 1970 and 31 December 2015 by the SANSN and the cluster seismograph networks. The density plot of the distribution of earthquake magnitude values in the FWR seismic zone are shown in Figure 16. The seismicity in the FWR seismic zone comprises 61 % of the catalogue. Most of the seismic events have small magnitudes, even though more than 30 had magnitudes greater than M_W 4.0. The largest earthquake had a magnitude of M_W 4.6 and its epicentre was located near Welverdiend on 5 May 1996. The temporally-varying of M_C was produced using the ZMAP software and the results are shown in Figure 17. The results obtained from Figure 17 were used to filter out seismic events < constant value of M_C 2.8 and temporally-varying of M_C and results are shown in Figure 18, where the red bar represents seismic events ≥ constant value of M_C 2.8 and the blue bar represents seismic events ≥ to the temporally-varying of M_C. The number of seismic events ≥ constant value of M_C 2.8 (red bar) decreases slowly after 1999 onwards and the number of seismic events ≥ temporally-varying of M_C generally increases except between 1990 and 2004.

The narrowness of the error band in Figure 17 is due to the fact that the recorded seismic events are very close to each other in terms of magnitude size, *i.e*. mostly seismic events around M_L 2.8, although there are very few recorded seismic events in the first couple of years. The moving window approach as applied in ZMAP, a sample of 100 seismic events for each window and a step of 10 seismic events for calculation, overlapping by 90 seismic events. It is not clear in the ZMAP manual how the standard deviation of *b*-value is calculated, Kijko and Funk (1994) proposed that the standard deviation for sufficiently large number *N* of seismic event:

$$\hat{\sigma}_{\beta} = \hat{\beta}\sqrt{N} \tag{4.4}$$

where $\hat{\beta}$ is approximately normally distributed about its mean value of the classic Aki-Utsu estimate.

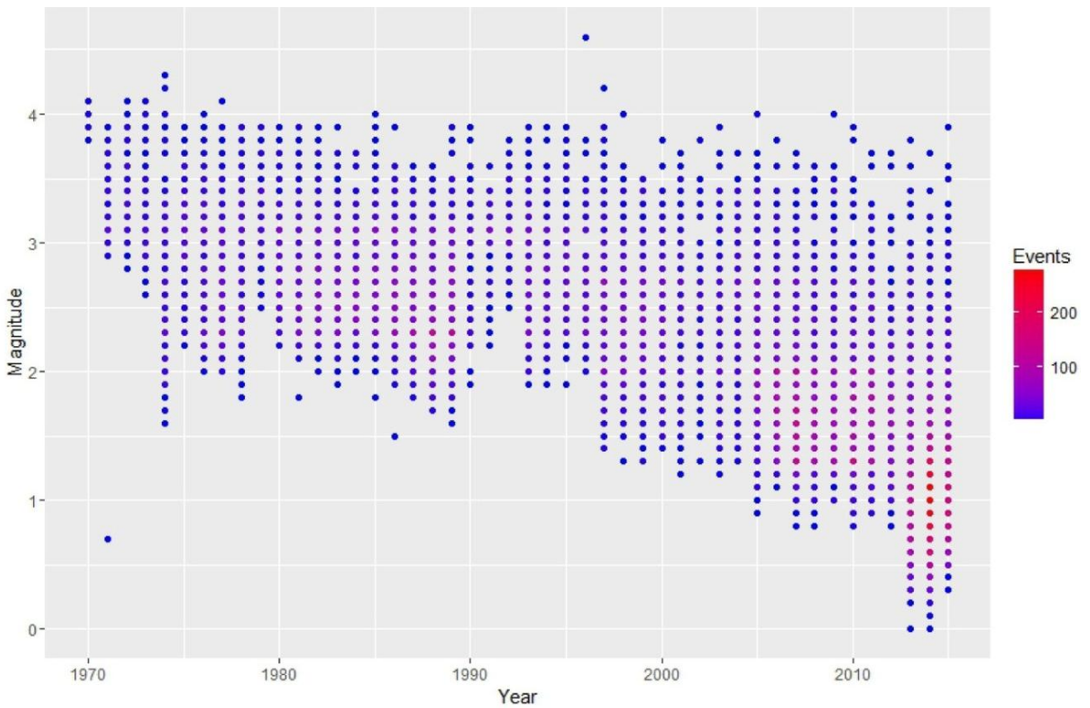

Figure 16. The temporal distribution of earthquake magnitude values in the FWR seismic zone.

This seismic zone shows a gradual increase in the number of earthquakes recorded by SANSN from January 1970 to December 1989. However, fewer seismic events were recorded between January 1990 and December 2004 but then increased between January 2005 and December 2012. An increase in the number of seismic events above the temporally-varying of M_C is observed. There is another significant increase in the recorded seismicity between January 2013 and December 2015. And increase in the number of seismic events above the temporally-varying of M_C is again observed (Figure 18) (blue bar).

This observed temporally-varying of recorded seismicity helps to identify different phases of seismic occurrence in the WR seismic zone. There are two ways considered to identify different phases. The first way is plot the cumulative number of seismic events ≥ M_C = 2.8 and the second way is to plot the cumulative number of seismic events greater or equal temporally-varying of M_C. The cumulative number of seismic events ≥ M_C = 2.8 is plotted to identify phases (Figure 19). The graph is fairly constant from year 1971 to 1999 and the slope changes from year 2000 to 2015. This implies that two phases are identify *i.e*. phase 1 (1970 - 1999) and phase 2 (2000 - 2015).

The cumulative number of seismic events greater or equal temporally-varying of M_C helps to identify different phases of seismic occurrence in the FWR seismic zone. The period from January 1970 to December 1989 corresponds to the first phase named Phase 1. The period from January 1990 to December 2004 corresponds to the second phase named Phase 2. The period from January 2005 to December 2012 corresponds to the third phase named Phase 3. The period from January 2013 to December 2015 corresponds to the fourth phase named Phase 4. These different phases can clearly be seen in Figure 20 which shows the cumulative number of earthquakes for this seismic zone. There are more earthquakes recorded per year in Phase 4.

The M_{max}^{obs} values in the FWR seismic zone for each phase are shown in Table 5. It was observed that M_C generally improves with time, as expected due to the improvement of the local networks, and the obtained values were consistent with the values obtained in Table 4. The temporally-varying of *b*-value was also calculated using the ZMAP software and the results are illustrated in Figure 21. The *b*-value fluctuates between 1.2 and 1.8 on average from January 1970 until December 2004 and reached a maximum of 2.7 in 1992 - 1993. The high value of *b*-value is a representation of lack of data when only 31 seismic events were recorded. The *b*-value then decreased to fluctuate between 0.8 and 1.4 between January 2006 and December 2015. The M_{max} calculated using the KSB technique is denoted as M_{max} (KSB) (Figure 22) and the M_{max} calculated using equation 4.3 is denoted as M_{max} (R). The *a*-values shown in Table 5 were calculated using the SEISAN software. All the recurrence parameters extracted from the FWR seismic zone using the three different software packages are shown in Table 5 for each phase.

The phases are not necessarily reflecting changes in seismic hazard with time, but were obtained from changes in the recorded seismicity after filtering out seismic events < temporally-varying of M_C. These figures aim to show the temporally-varying of *b*-value and M_C, both *b*-value and M_C do change with time and temporally-varying of *a*-value is shown in Table 5.

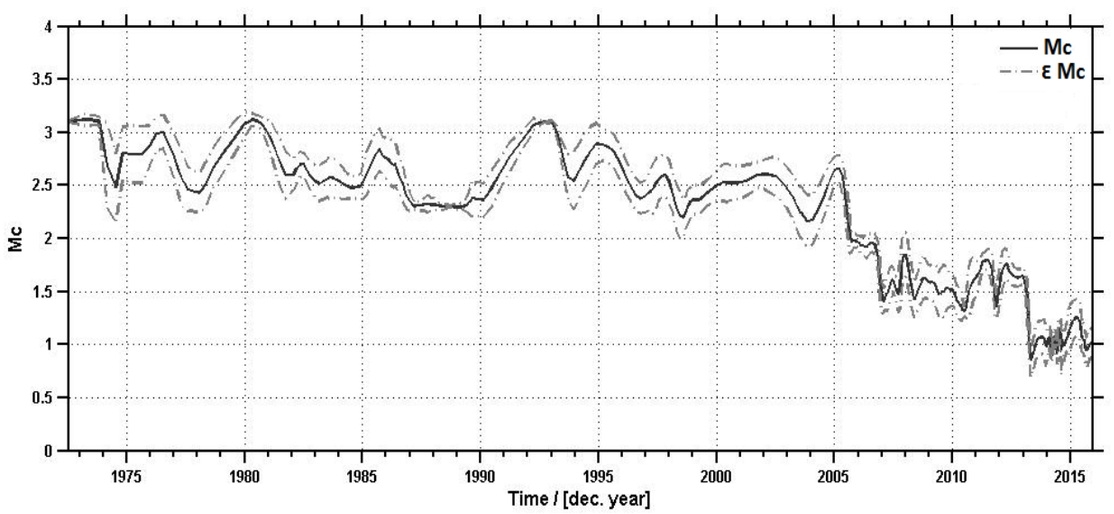

Figure 17. The temporally-varying of M_C using ZMAP for the FWR seismic zone.

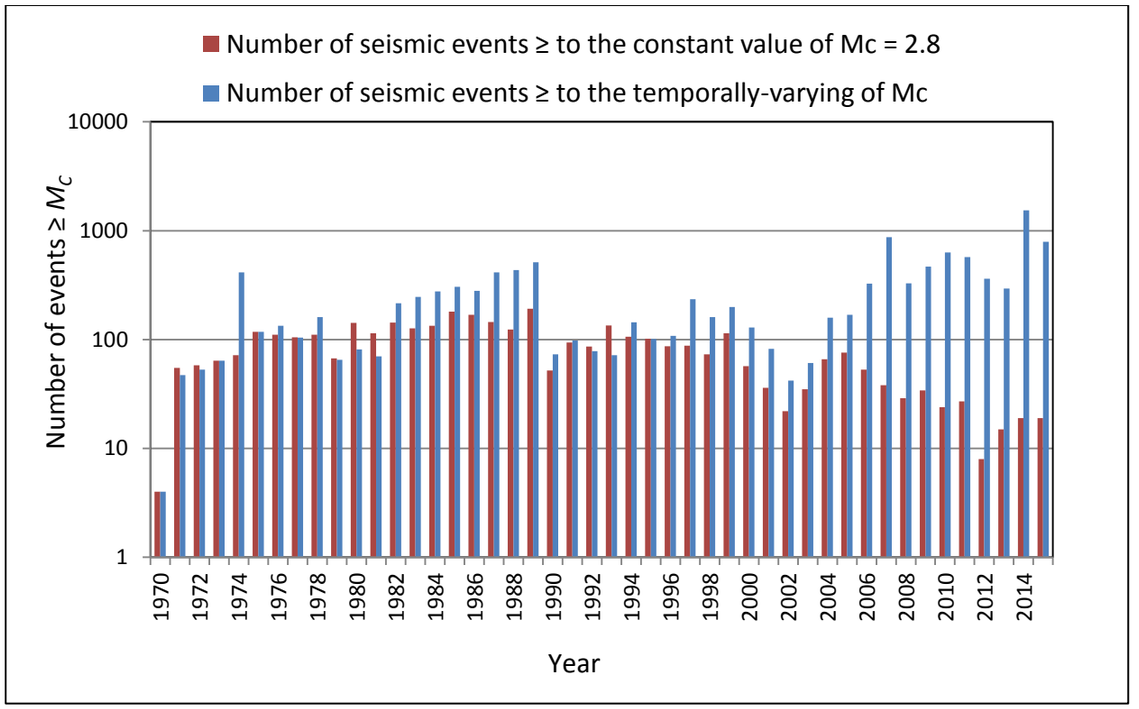

Figure 18. The number seismic events per year ≥ to the constant value of M_C = 2.8 compared to the number of seismic events per year ≥ to the temporally-varying of M_C in the FWR seismic zone.

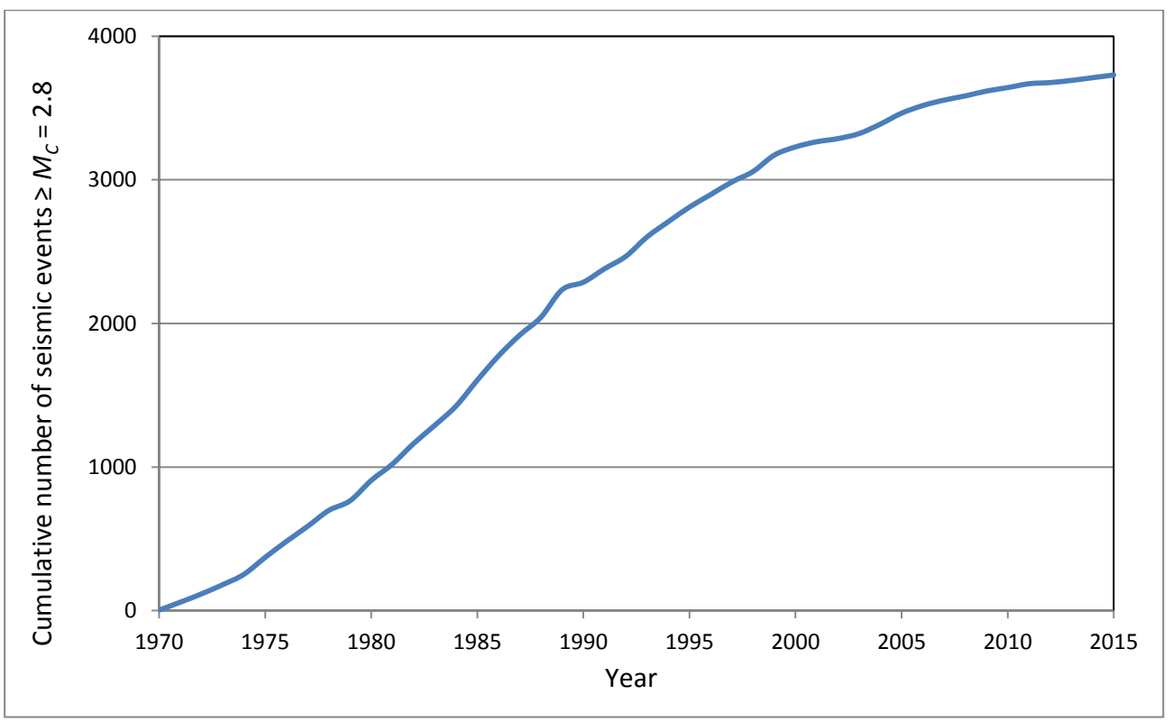

Figure 19. Cumulative number of seismic events ≥ M_C = 2.8 in the FWR seismic zone.

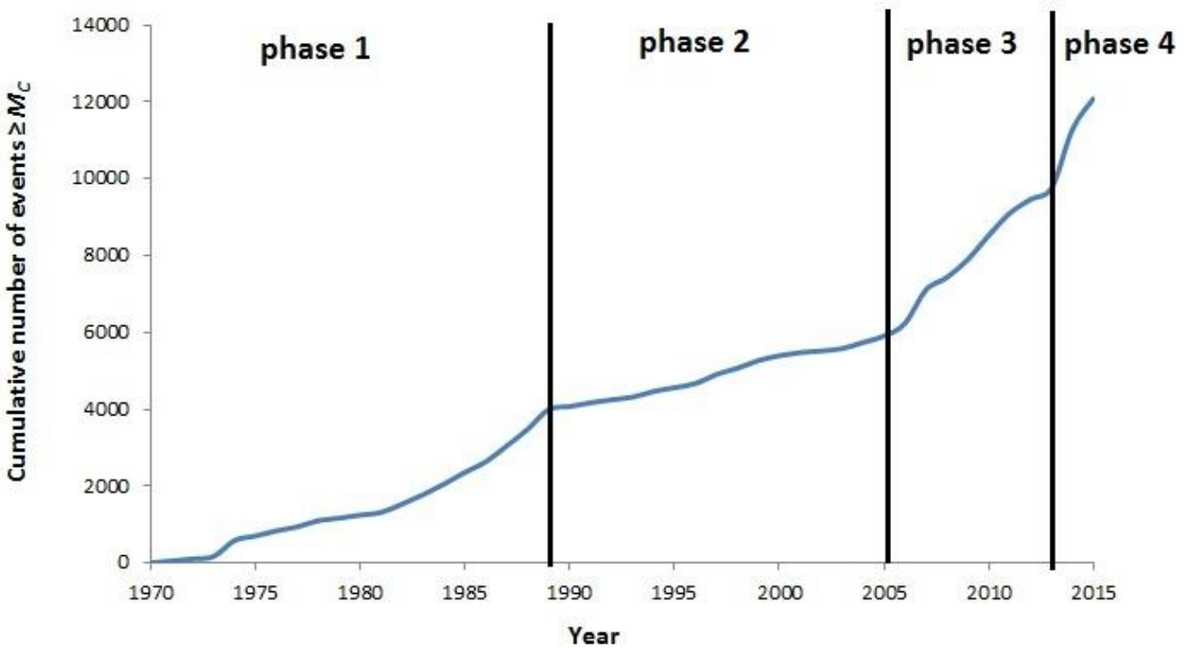

Figure 20. The cumulative number of seismic events greater or equal to temporally-varying M_C in the FWR seismic zone, phase 1 (1970-1989) inclusive, phase 2 (1990-2004) inclusive phase 3 (2005-2012) inclusive and phase 4 (2013-2015) inclusive.

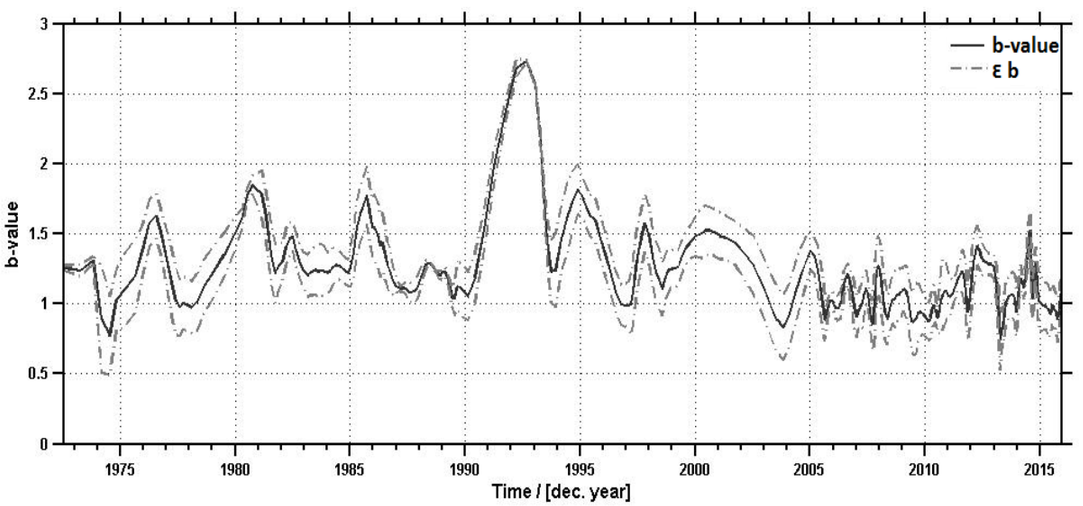

Figure 21. The temporally-varying of *b*-value using ZMAP for the FWR seismic zone.

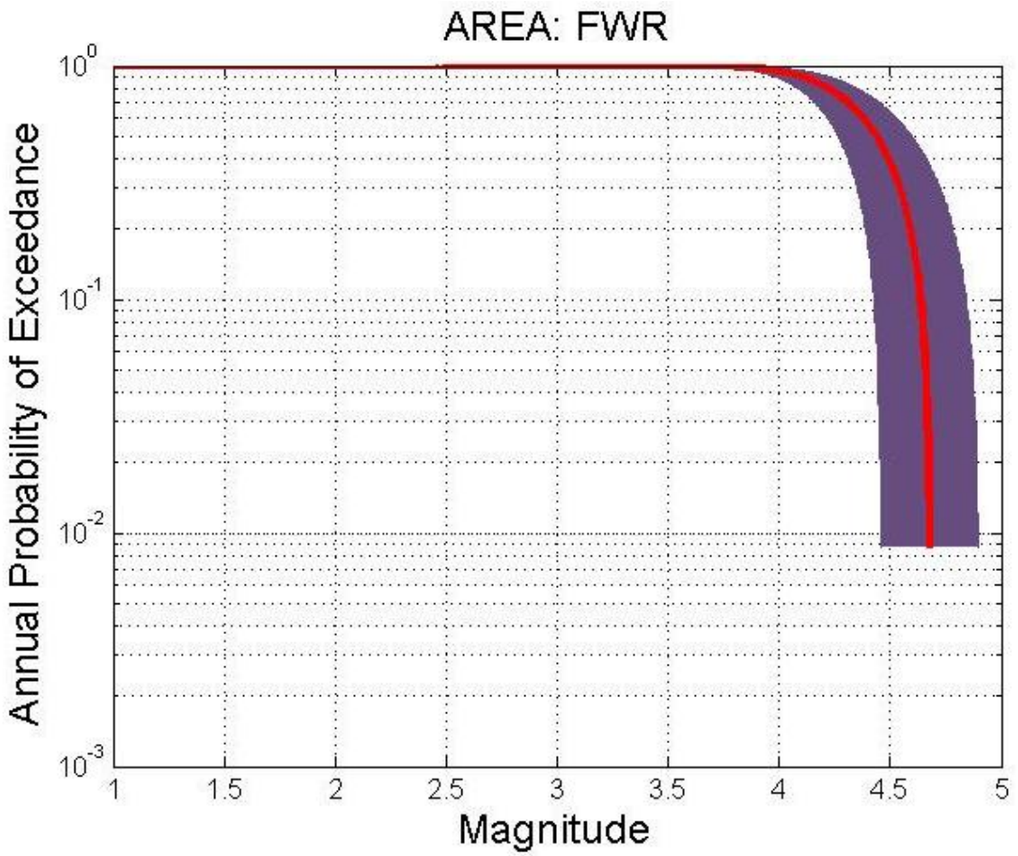

Figure 22. The M_{max} (KSB) calculated using the KSB method is 4.68 ± 0.2 for the FWR seismic zone.

Table 5. Seismic recurrence parameters of the FWR seismic zone. M_C is calculated using ZMAP software, *a*-value is calculated using SEISAN software and *b*-value is calculated using HA3 software.

Phases	M_{max}^{obs}	M_C **using ZMAP**	**Number of events >** M_C	**Average number of events per year >** M_C	***a*-value using SEISAN**	***b*-value using HA3**
Phase 1 (1970 -1989)	4.3	2.9	1165	61.3	7.95	1.58±0.2
Phase 2 (1990 - 2004)	4.6	3.1	4744	316.3	7.89	1.75±0.2
Phase 3 (2005 - 2012)	4.0	1.6	3558	444.8	5.32	1.02±0.1
Phase 4 (2013 – 2015)	3.9	1.0	2622	874	4.73	1.07±0.1

The *a*-values were calculated for $M_W > 0$ from the whole data set within each one of the phases to satisfy the conditions required by the seismic hazard software used in this study. The *b*-values are high in phase 2 due to the small number of recorded events around the period of 1992. This was important to show because it had a significant impact on the recurrence parameters. The temporal variations in M_C and b-values are shown in Figure 17 and Figure 21. The tabulated M_C and *b*-values on the tables are obtained from the whole data set within each phase, the discrepancies are due to the variation of the recorded number of events. The activity rates have decreased over the years because there has been a decrease of seismic events $M_W > 4.0$, this is clearly observed in Figure 18 (red bar) when plotting the number of seismic events ≥ to the constant value of M_C 2.8.

4.2.2 West Rand (WR) Seismic Zone

The WR seismic zone is the second most active seismic zone with a total of 8,317 earthquakes recorded from 7 January 1970 to 31 December 2015 by the SANSN and the cluster seismograph networks. The density plot of the distribution of earthquake magnitude values in the FWR seismic zone are shown in Figure 23. The seismicity in the WR seismic zone comprises 25 % of the catalogue. Most of the events have small magnitudes, with only 3 earthquakes of M_W 4.0 or more. The largest event was M_W 4.2 recorded on 14 October 1971 and its epicentre was located near Elandsvlei. The temporally-varying of M_C was produced using the ZMAP software and the results are shown in Figure 24. The results obtained from Figure 24 were used to filter out seismic events < constant value of M_C 2.8 and temporally-varying of M_C and results are shown in Figure 25, where the red bar represents seismic events ≥ constant value of M_C 2.8 and the blue bar represents seismic events ≥ to the temporally-varying of M_C. The number of seismic events ≥ constant value of M_C 2.8 (red bar) is almost constant over the study period and the number of seismic events ≥ temporally-varying of M_C generally increases especially from 2005 onwards.

There is only one seismic event recorded by the SANSN in 1970 in the WR seismic zone. The number of recorded seismic events increases in stages between the following years, January 1971 and December 2004, then between January 2005 and December 2012 and finally between January 2013 and December 2015. The increase in the number of seismic events above the temporally-varying of M_C is observed (Figure 25) (blue bar). There is another significant increase in the recorded seismicity between January 2013 and December 2015 (Figure 25).

This observed temporally-varying of recorded seismicity helps to identify different phases of seismic occurrence in the WR seismic zone. There are two ways considered to identify different phases. The first way is plot the cumulative number of seismic events ≥ M_C = 2.8 and the second way is to plot the cumulative number of seismic events greater or equal temporally-varying of M_C. The cumulative number of seismic events ≥ M_C = 2.8 is plotted to identify phases (Figure 26). The graph is fairly constant from year 1971 to 1987 and the slope changes from year 1988 to 2015. This implies that two phases are identify *i.e*. phase 1 (1971 - 1987) and phase 2 (1988 - 2015).

The cumulative number of seismic events greater or equal temporally-varying of M_C helps to identify different phases of seismic occurrence in the WR seismic zone. The period from January 1970 to December 2004 corresponds to the first phase named Phase 1. The period from January 2005 to December 2012 corresponds to the second phase named Phase 2. The period from January 2013 to December 2015 corresponds to the third phase named Phase 3. These different phases can clearly be seen in Figure 27 which shows the cumulative number of earthquakes for this seismic zone. There are more seismic events recorded per year in Phase 3.

The phases are not necessarily reflecting changes in seismic hazard with time, but were obtained from changes in the recorded seismicity after filtering out seismic events < temporally-varying of M_C. These figures aim to show the temporal variations of *b*-value and M_C, both *b*-value and M_C do change with time and temporally-varying of *a*-value is shown in Table 6.

The M_{max}^{obs} values in the WR seismic zone for each phase are shown in Table 6. The temporally-varying of M_C was produced using the ZMAP software and the results are shown in Figure 24. It was observed that M_C generally improves with time as expected due to the improvements in the local networks and the obtained values were consistent with the values obtained in Table 4. The temporally-varying of *b*-values was also calculated in the ZMAP software and the results are illustrated in Figure 28. The *b*-value fluctuates between 1.2 to 1.6 from 1970 until 2004 and then decrease to between 0.8 to 1.2 between 2005 and 2015. The M_{max} calculated using the KSB technique is denoted as M_{max} (KSB) (Figure 29) and M_{max} calculated using equation 4.3 is denoted as M_{max} (R). The *a*-values shown in Table 6 were calculated using SEISAN software. All the recurrence parameters extracted from the WR seismic zone using the three different software packages are shown in Table 6 for each phase.

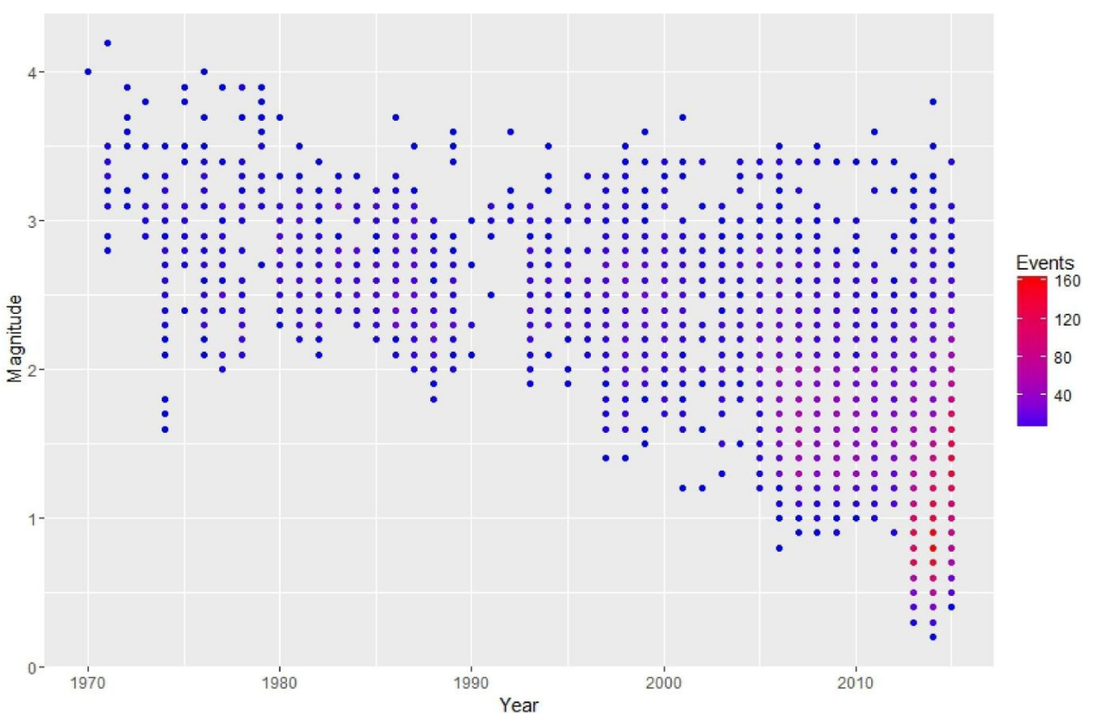

Figure 23. The temporal distribution of earthquake magnitude values in the WR seismic zone.

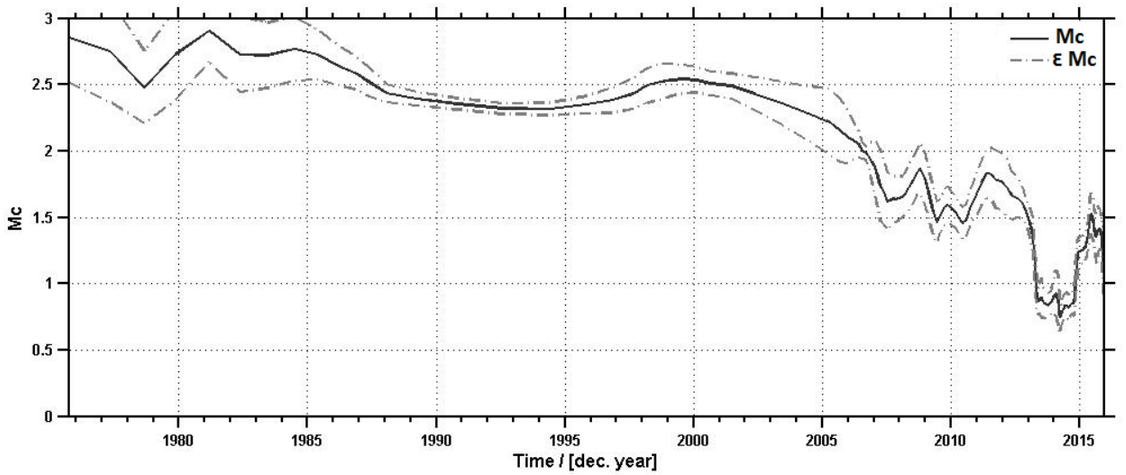

Figure 24. The temporally-varying of M_C using ZMAP for the WR seismic zone.

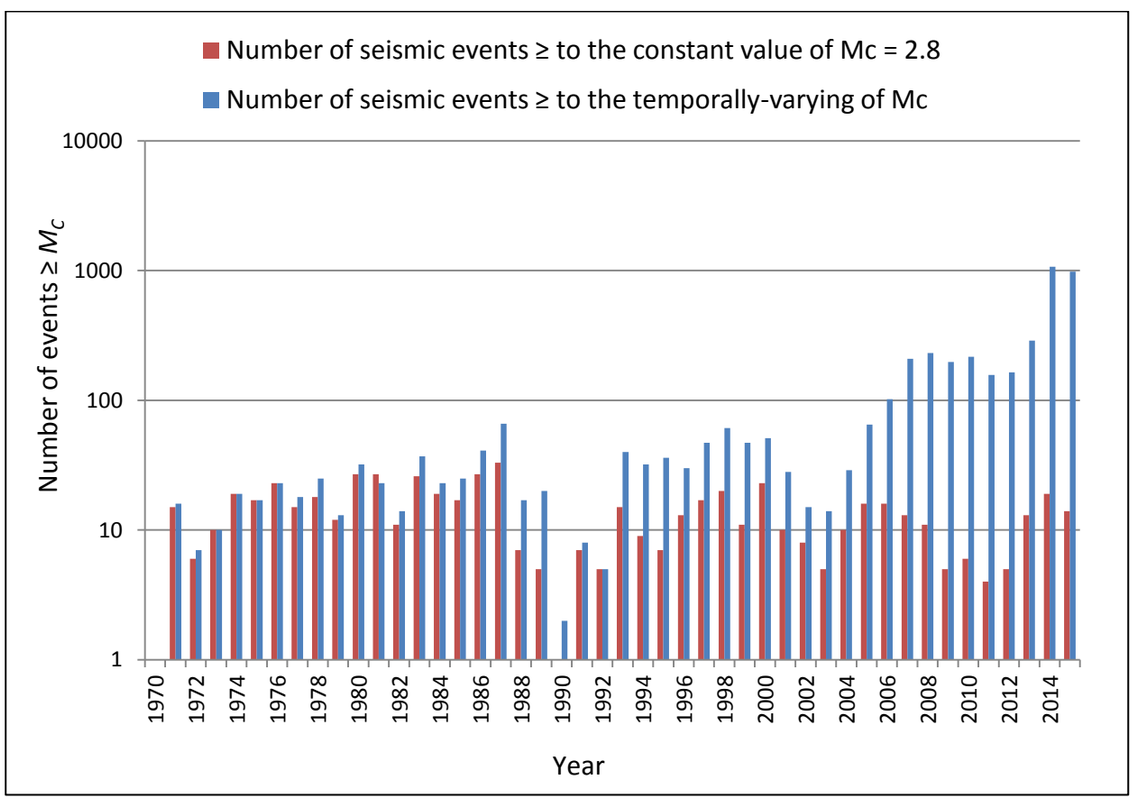

Figure 25. The number seismic events per year ≥ to the constant value of M_C = 2.8 compared to the number of seismic events per year ≥ to the temporally-varying of M_C in the WR seismic zone.

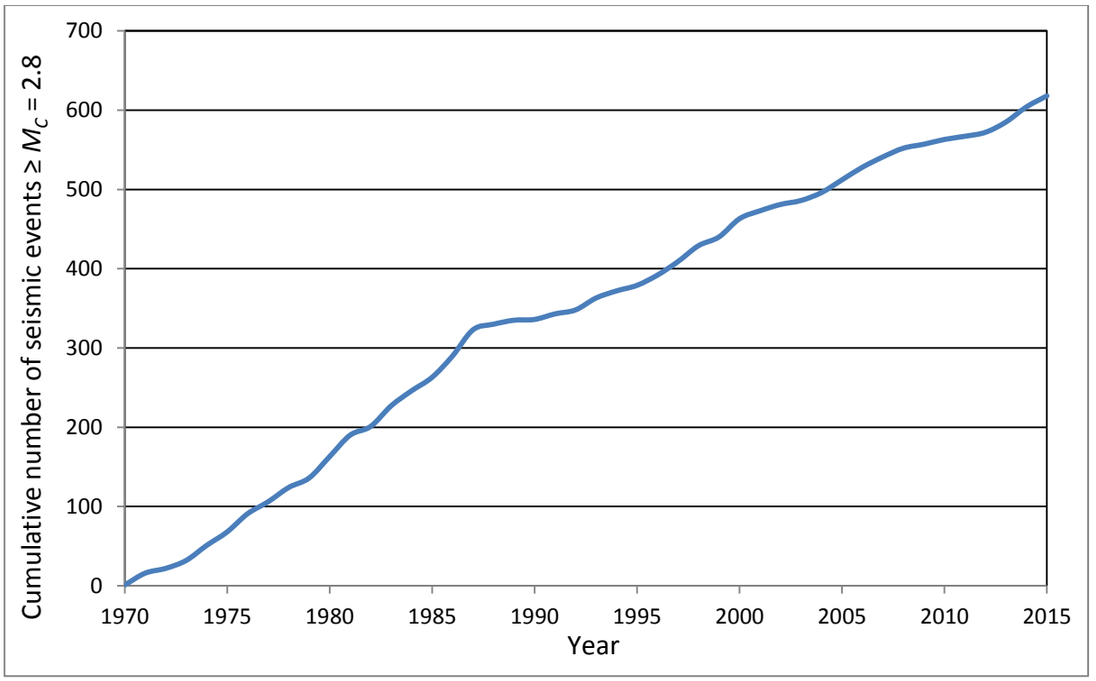

Figure 26. Cumulative number of seismic events ≥ M_C=2.8 in the WR seismic zone.

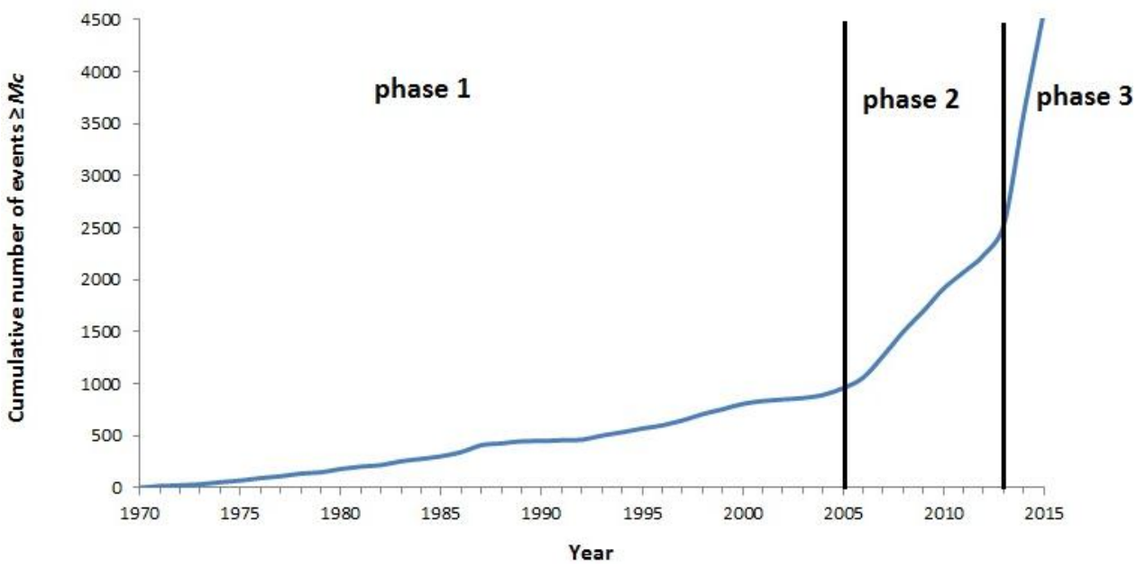

Figure 27. The cumulative number of seismic events greater or equal temporally-varying of M_C in WR seismic zone, phase 1 (1970-2004) inclusive, phase 2 (2005-2012) inclusive and phase 3 (2013-2015) inclusive.

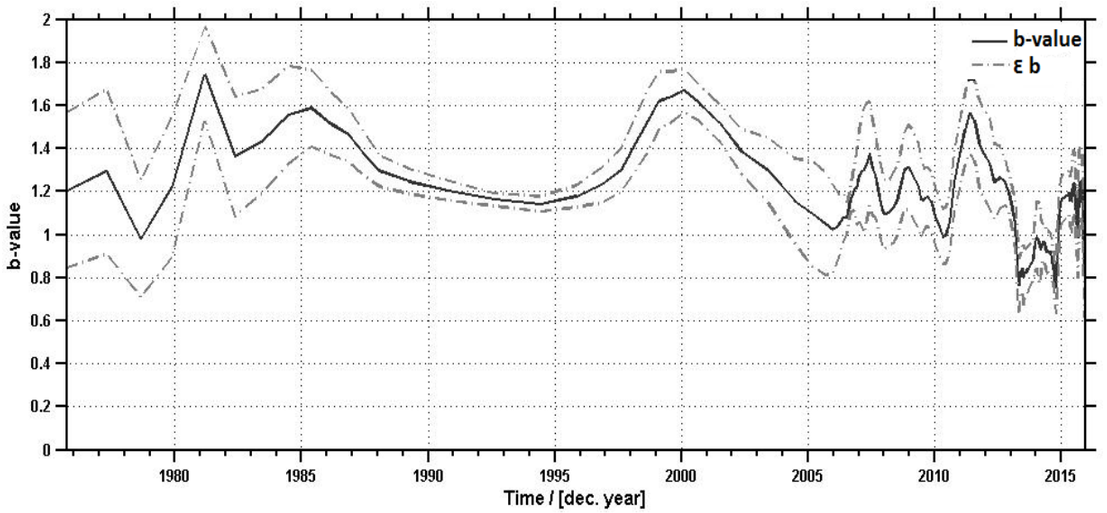

Figure 28. The temporally-varying of *b*-value using ZMAP for the WR seismic zone.

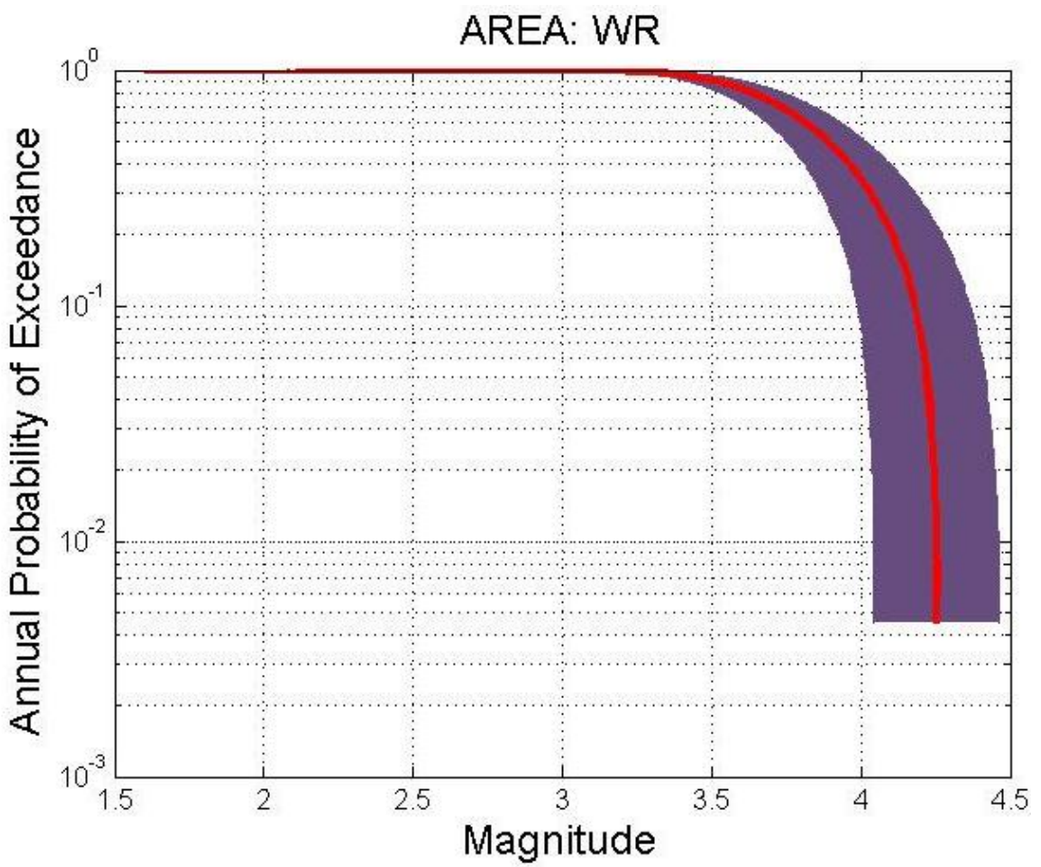

Figure 29. The M_{max} (KSB) calculated using the KSB method is 4.26 ± 0.2 for the WR seismic zone.

Table 6. Seismic recurrence parameters of the WR seismic zone, M_C is calculated using ZMAP software, *a*-value is calculated using SEISAN software and *b*-value calculated using the HA3 software.

Phases	M_{max}^{obs}	M_C using ZMAP	Number of events > M_C	Average number of events per year > M_C	*a*-value using SEISAN	*b*-value using HA3
Phase 1 (1970 - 2004)	4.2	2.6	957	35.3	6.65	1.41±0.3
Phase 2 (2005 - 2012)	3.6	1.6	1567	195.9	5.04	1.20±0.2
Phase 3 (2013 - 2015)	3.8	1.6	2055	685	5.11	1.24±0.1

4.2.3 Central Rand (CR) Seismic Zone

The CR seismic zone is the least active seismic zone with a total of 1,599 earthquakes recorded from 14 January 1971 to 29 December 2015 by the SANSN and the cluster seismograph networks. The density plot of the distribution of earthquake magnitude values in the FWR seismic zone are shown in Figure 30. The seismicity in the CR seismic zone comprises 5 % of the catalogue. This is the only seismic zone which has no earthquake larger than M_W 4.0. There are 3 large earthquakes of M_W 3.9 recorded on 26 April 1973, 10 April 1976 and 28 March 1982 and the epicentres were located near Meyersdal, Mayfair West and Denver respectively. The temporally-varying of M_C was produced using the ZMAP software and the results are shown in Figure 31. Figure 31 were used to filter out seismic events < constant value of M_C 2.8 and temporally-varying of M_C and results are shown in Figure 32, where the red bar represents seismic events ≥ constant value of M_C 2.8 and the blue bar represents seismic events ≥ to the temporally-varying of M_C. The number of seismic events ≥ constant value of M_C 2.8 (red bar) decreases sharply after 1989 onwards. This implies that seismic events generated by flooding mines from 2005 onwards do not generate high magnitudes seismic events. The number of seismic events ≥ temporally-varying of M_C generally increases between 2005 and 2015 which is the flooding period in the CR seismic zone.

There are a number of earthquakes recorded from January 1971 to December 1989. This seismic zone shows a substantial decrease in the number of earthquakes recorded from January 1990 to December 2004. This gap in recorded seismicity shows that the catalogue is incomplete owing to downtime of the SANSN. However, the increase in the recorded seismicity between January 2005 and December 2012 was substantial and the increase in the number of seismic events above the temporally-varying of M_C is observed. There is another significant increase in the recorded seismicity between January 2013 and December 2015 and the increase in the number of seismic events above the temporally-varying of M_C is observed (Figure 32) (blue bar).

This observed temporally-varying of recorded seismicity helps to identify different phases of seismic occurrence in the WR seismic zone. There are two ways considered to identify different phases. The first way is plot the cumulative number of seismic events ≥ M_C = 2.8 and the second way is to plot the cumulative number of seismic events greater or equal temporally-varying of M_C. The cumulative number of seismic events ≥ M_C = 2.8 is plotted to identify phases (Figure 33). The graph is fairly constant from year 1971 to 1987 and the slope changes from year 1988 to 2015. This implies that two phases are identify *i.e*. phase 1 (1971 - 1987) and phase 2 (1988 - 2015).

The cumulative number of seismic events greater or equal temporally-varying of M_C helps to identify different phases of seismic occurrence in the CR seismic zone. The period from January 1970 to December 1989 corresponds to the first phase named Phase 1. The period from January 1990 to December 2004 corresponds to the second phase named Phase 2. The period from January 2005 to December 2012 corresponds to the third phase named Phase 3. The period from January 2013 to December 2015 corresponds to the fourth phase named Phase 4. These different phases can clearly be seen in Figure 34 which shows the cumulative number of earthquakes for this zone. There are more earthquakes recorded in Phase 4 per year.

The M_{max}^{obs}values in the CR seismic zone for each phase are shown in Table 7. The temporally-varying of M_C was produced using the ZMAP software and the results are shown in Figure 31. It was observed that M_C generally improved with time as expected due to the improvement in the local networks and the obtained values were consistent with the values obtained in Table 4. The temporally-varying of *b*-value was also calculated using the ZMAP software and the results are illustrated in Figure 35. The *b*-value fluctuates between 0.8 and 1.2 from 1970 until 1987 and then stabilises between 1.1 and 1.2 between 1988 and 2015. The highest *b*-value of 1.86 was calculated in phase 2 using the HA3 method, this high value is due to the lack of data because only 31 seismic events were recorded. The M_{max} calculated using the KSB technique is denoted as M_{max} (KSB) (Figure 36) and M_{max} calculated using equation 4.3 is denoted as M_{max} (R). The M_{max} value obtained for the CR seismic zone was the same because the whole catalogue of the CR was used for each corresponding method for all four phases (Table 7). The corresponding *a*-values shown in Table 7 were calculated using SEISAN software. Contrary to the preceding zones, here we see an increase in the *a*-value in later phase. This must surely be the result of flooding in a region where no mining is taking place. All the recurrence parameters extracted from the CR seismic zone using the three different software packages are shown in Table 7 for each phase.

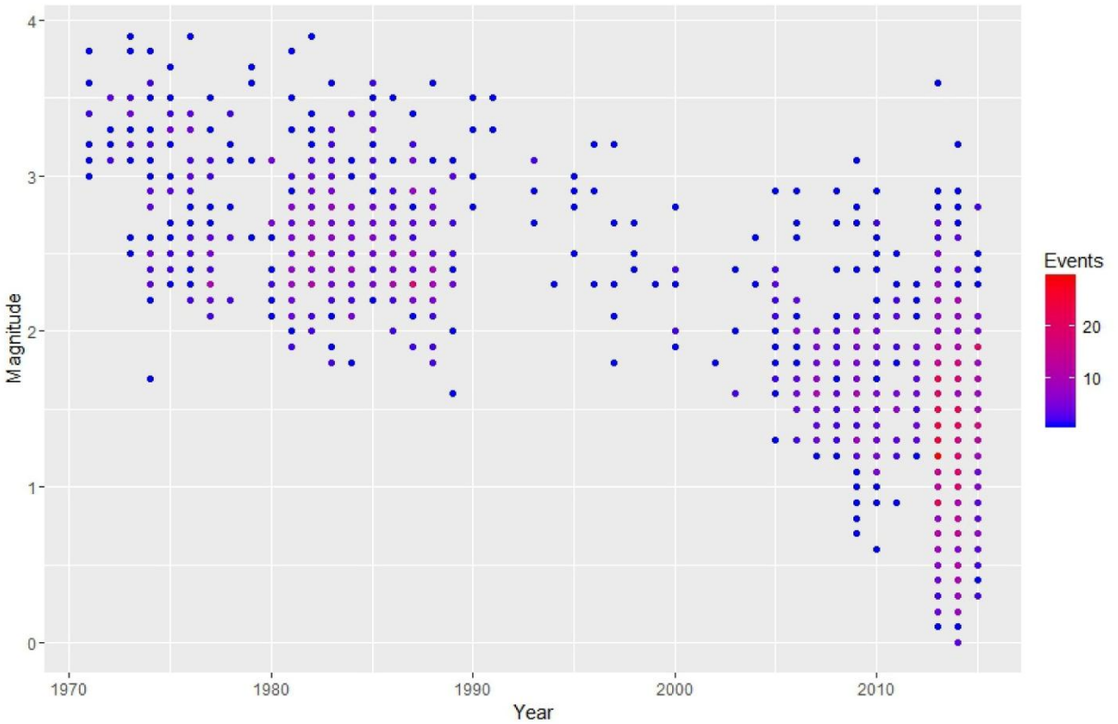

Figure 30. The temporal distribution of earthquake magnitude values in the CR seismic zone.

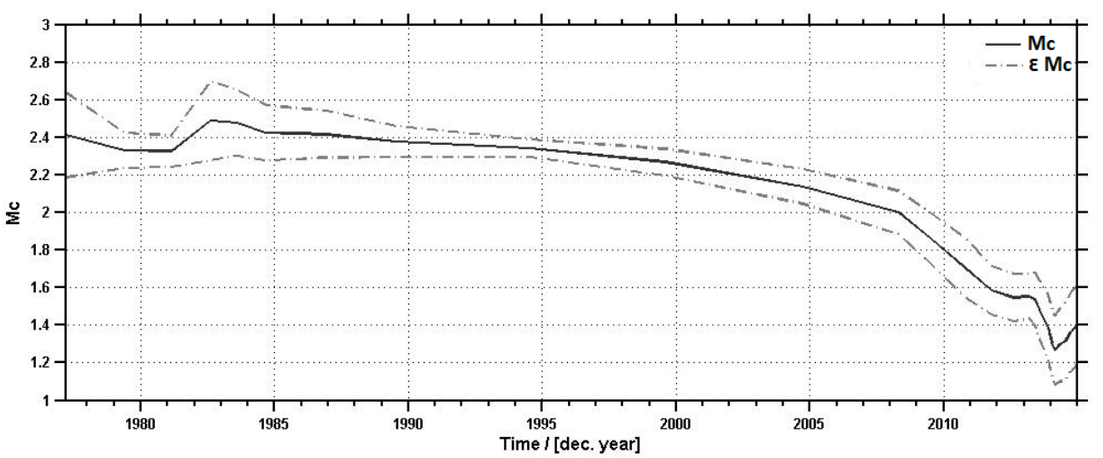

Figure 31. The temporally-varying of M_C using ZMAP for the CR seismic zone.

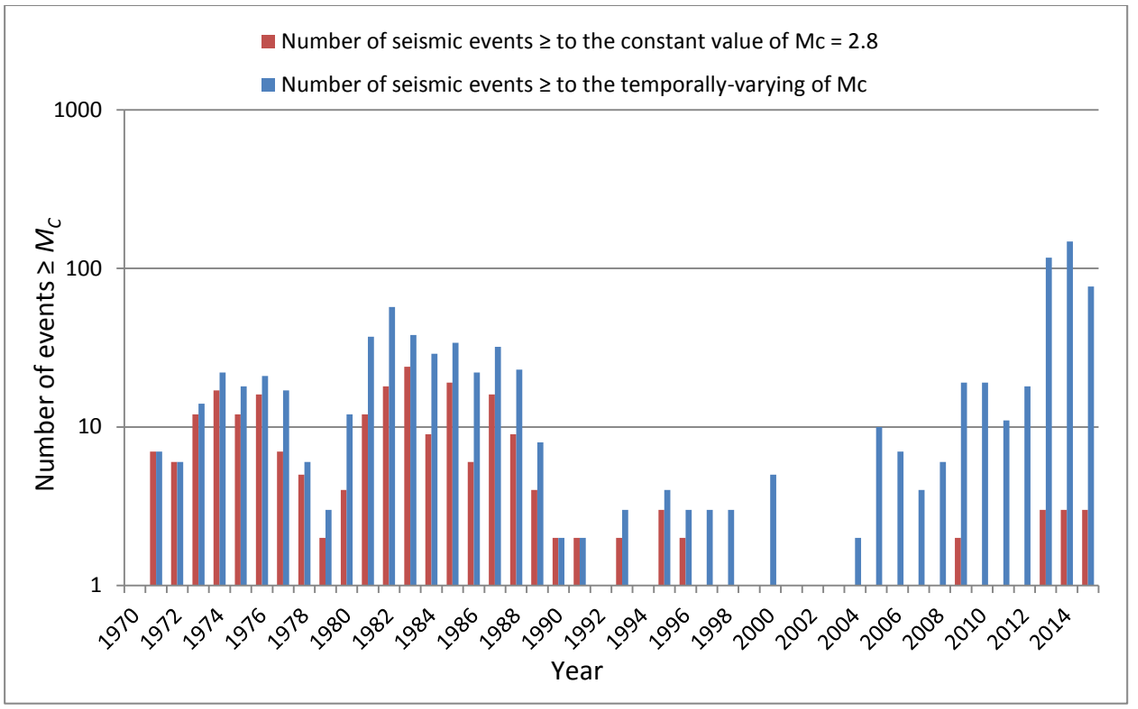

Figure 32. The number seismic events per year ≥ to the constant value of M_C = 2.8 compared to the number of seismic events per year ≥ to the temporally-varying of M_C in the CR seismic zone.

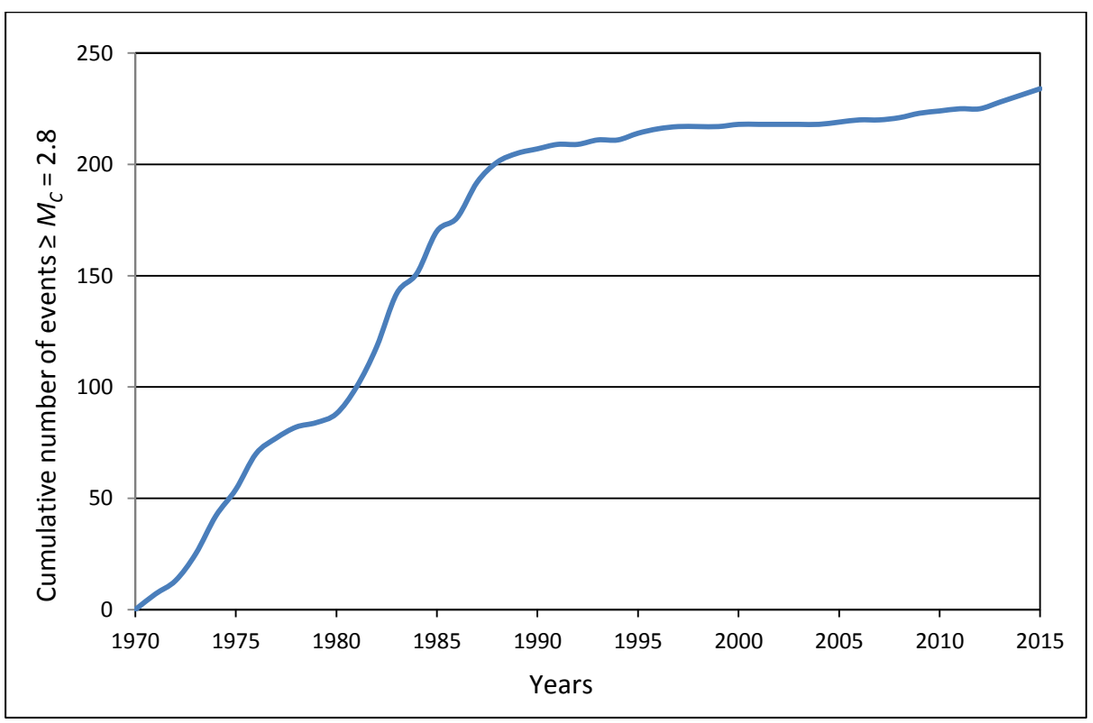

Figure 33. Cumulative number of seismic events ≥ M_C=2.8 in the CR seismic zone.

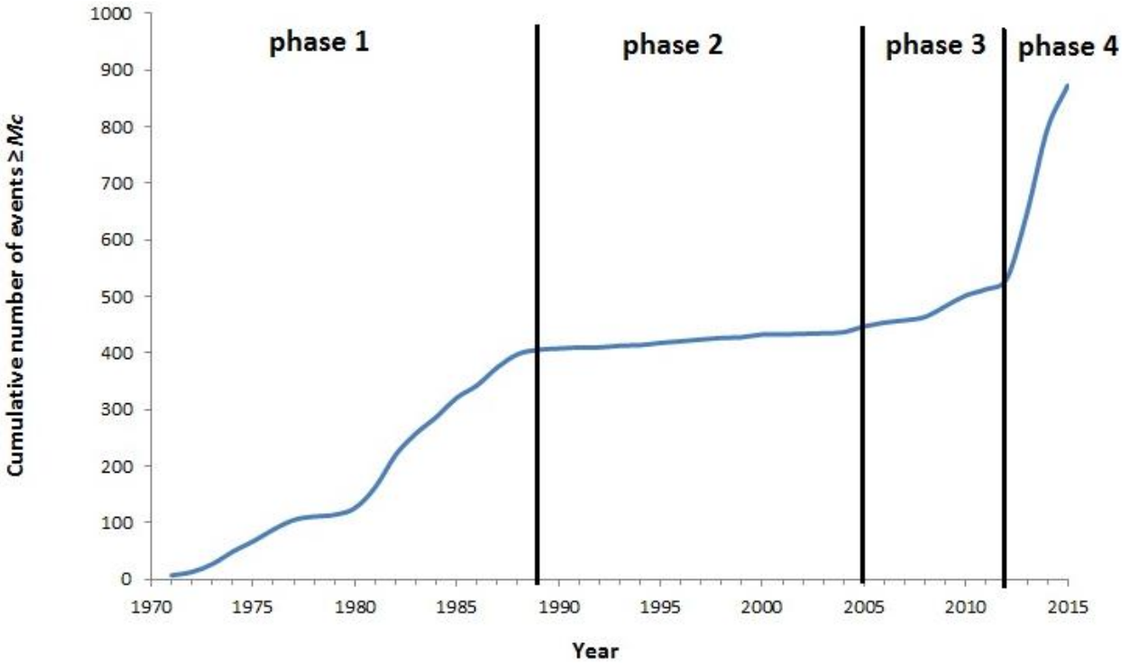

Figure 34. The cumulative number of seismic events greater or equal to temporally-varying of M_C in the CR seismic zone, phase 1 (1970-1989) inclusive, phase 2 (1990-2004) inclusive phase 3 (2005-2012) inclusive and phase 4 (2013-2015) inclusive.

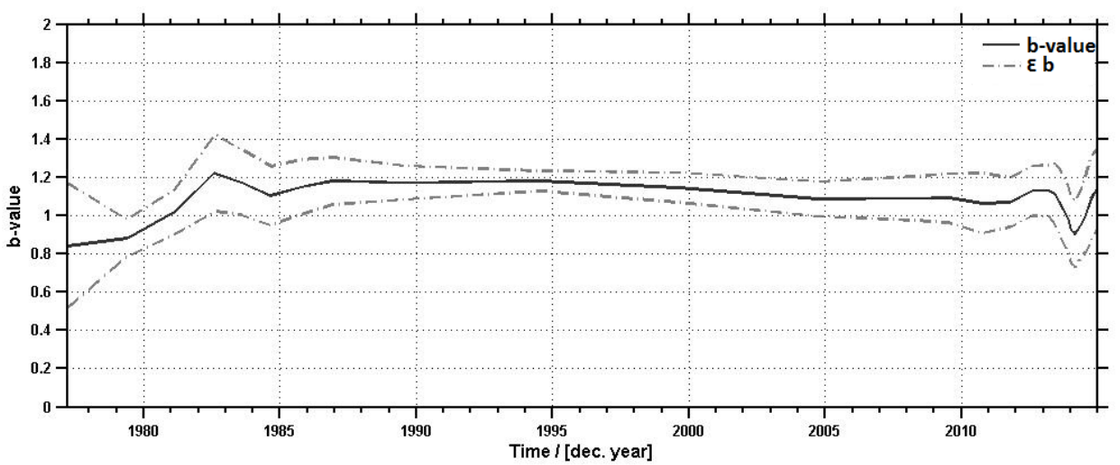

Figure 35. The temporally-varying of *b*-value using ZMAP for the CR seismic zone.

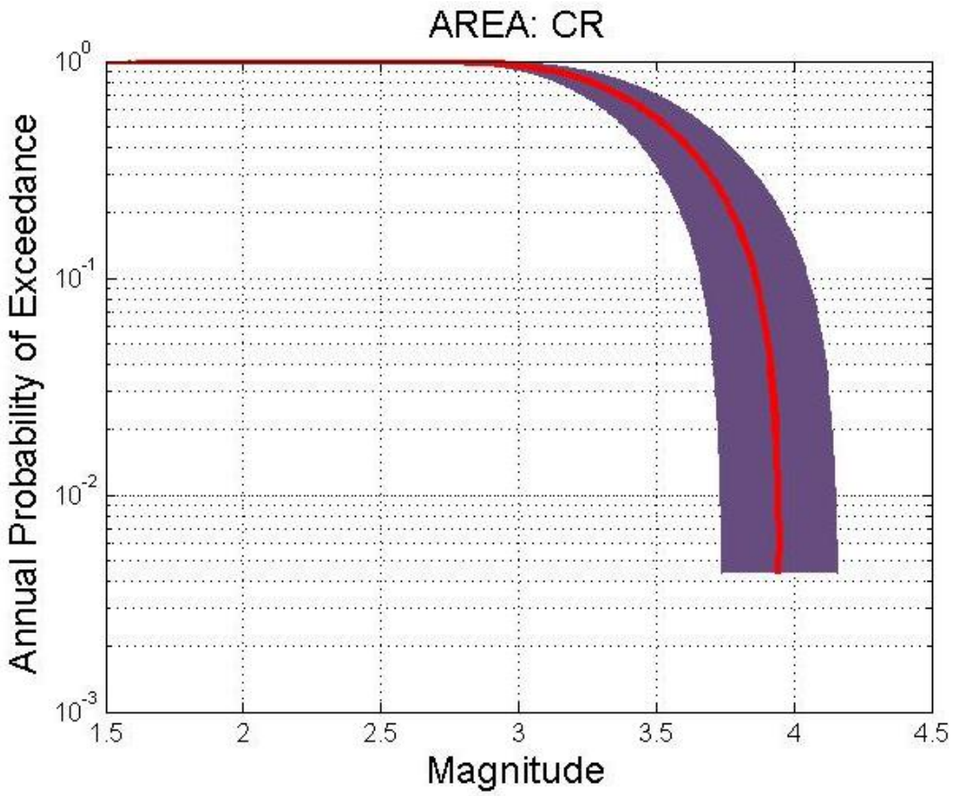

Figure 36. The M_{max} (KSB) calculated using the KSB method is 3.95 ± 0.2 for the CR seismic zone.

Table 7. Seismic recurrence parameters of the CR seismic zone, M_C is calculated using ZMAP software, *a*-value is calculated using SEISAN software and *b*-value calculated HA3 software.

Phases	M_{max}^{obs}	**M_C using ZMAP**	**Number of events > M_C**	**Average number of events per year > M_C**	***a*-value using SEISAN**	***b*-value using HA3**
Phase 1 (1970 -1989)	3.9	2.4	406	20.3	5.08	0.99±0.3
Phase 2 (1990 - 2004)	3.5	3.0	31	0.9	4.18	1.86±0.2
Phase 3 (2005 - 2012)	3.1	1.5	211	26.4	4.15	1.146±0.2
Phase 4 (2013 – 2015)	3.6	1.6	225	75	4.50	1.25±0.2

4.2.4 East Rand (ER) Seismic Zone

The ER seismic zone is the second least active seismic zone with a total of 2,713 earthquakes recorded between 1 January 1970 and 29 December 2015 by the SANSN and the cluster seismograph networks. The density plot of the distribution of earthquake magnitude values in the FWR seismic zone are shown in Figure 37. The seismicity in the ER seismic zone is 8 % of the catalogue. Most of the events were recorded since 2010 due to the establishment of the SWMP stations. The earthquakes vary from small events of M_W 0.0 to a maximum of M_W 4.6 recorded on 30 August 1980 located near Balmoral. The temporally-varying of M_C was produced using the ZMAP software and the results are shown in Figure 38. The results obtained from Figure 38 was used to filter out seismic events < constant value of M_C 2.8 and temporally-varying of M_C and results are shown in Figure 39. The number of seismic events ≥ constant value of M_C 2.8 (red bar) decreases after 1986 onwards and the number of seismic events ≥ temporally-varying of M_C generally increases between 2005 and 2015 which is the flooding period. The trend observed in this seismic zone is similar to the trend observed in the CR seismic zone which was flooding at the same period.

This seismic zone shows a gradual increase in the number of earthquakes recorded from January 1970 to December 1989. However, fewer seismic events were recorded between January 1990 and December 2004 after which the number increased between January 2005 and 2012 and the increase in the number of seismic events above the temporally-varying of M_C is observed. There was another significant increase in the recorded seismicity between January 2013 and December 2015 and the increase in the number of seismic events above the temporally-varying of M_C is observed (Figure 39) (blue bar).

This observed temporally-varying of recorded seismicity helps to identify different phases of seismic occurrence in the WR seismic zone. There are two ways considered to identify different phases. The first way is plot the cumulative number of seismic events ≥ M_C = 2.8 and the second way is to plot the cumulative number of seismic events greater or equal temporally-varying of M_C. The cumulative number of seismic events ≥ M_C = 2.8 is plotted to identify phases (Figure 40). The graph is fairly constant from year 1971 to 1989 and the slope changes from year 1990 to 2015. This implies that two phases are identify *i.e*. phase 1 (1970 - 1989) and phase 2 (2000 - 2015).

The cumulative number of seismic events greater or equal temporally-varying of M_C helps to identify different phases of seismic occurrence in the ER seismic zone. The period from January 1970 to December 1989 corresponds to the first phase named Phase 1. The period from January 1990 to December 2004 corresponds to the second phase named Phase 2. The period from January 2005 to December 2012 corresponds to the third phase named Phase 3. The period from January 2013 to December 2015 corresponds to the fourth phase named Phase 4. These different phases can clearly be seen in Figure 41 which shows the cumulative number of earthquakes for this zone. There are more earthquakes recorded in Phase 4 per year. The method of plotting cumulative number of

seismic events ≥ temporally-varying M_C was chosen over the method of plotting cumulative number of seismic events ≥ M_C 2.8 because the phases begun and ended on the same years for the FWR, CR and ER seismic zones.

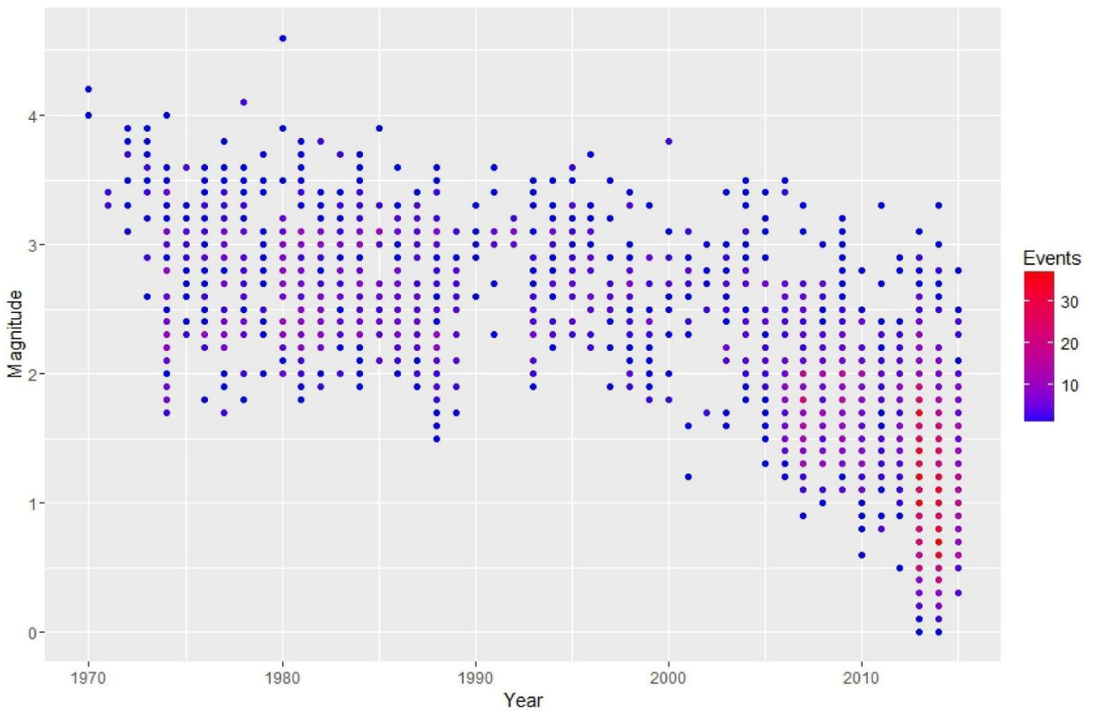

Figure 37. The temporal distribution of earthquake magnitude values in the ER seismic zone.

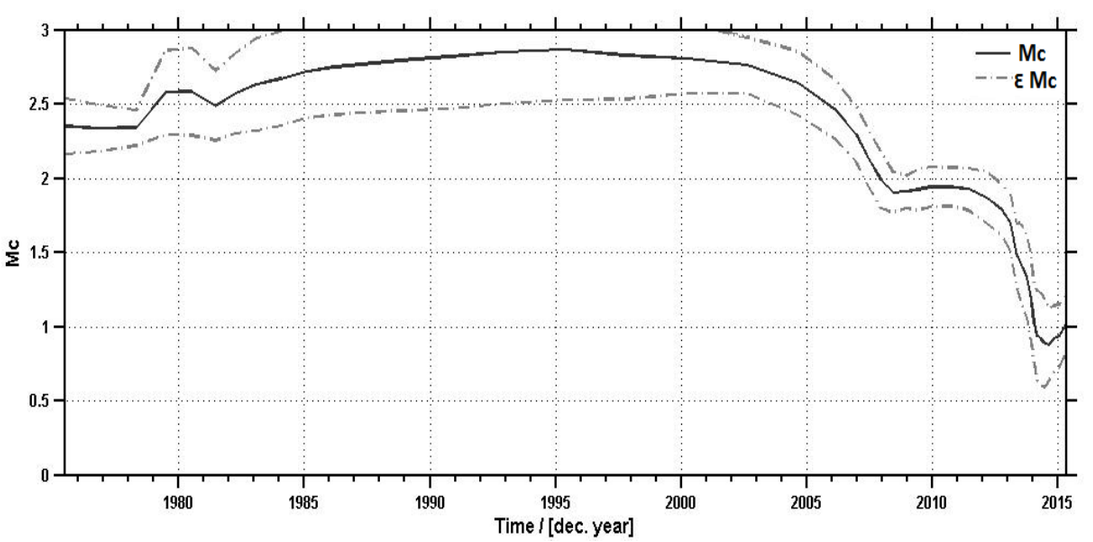

Figure 38. The temporally-varying of M_C using ZMAP for the ER seismic zone.

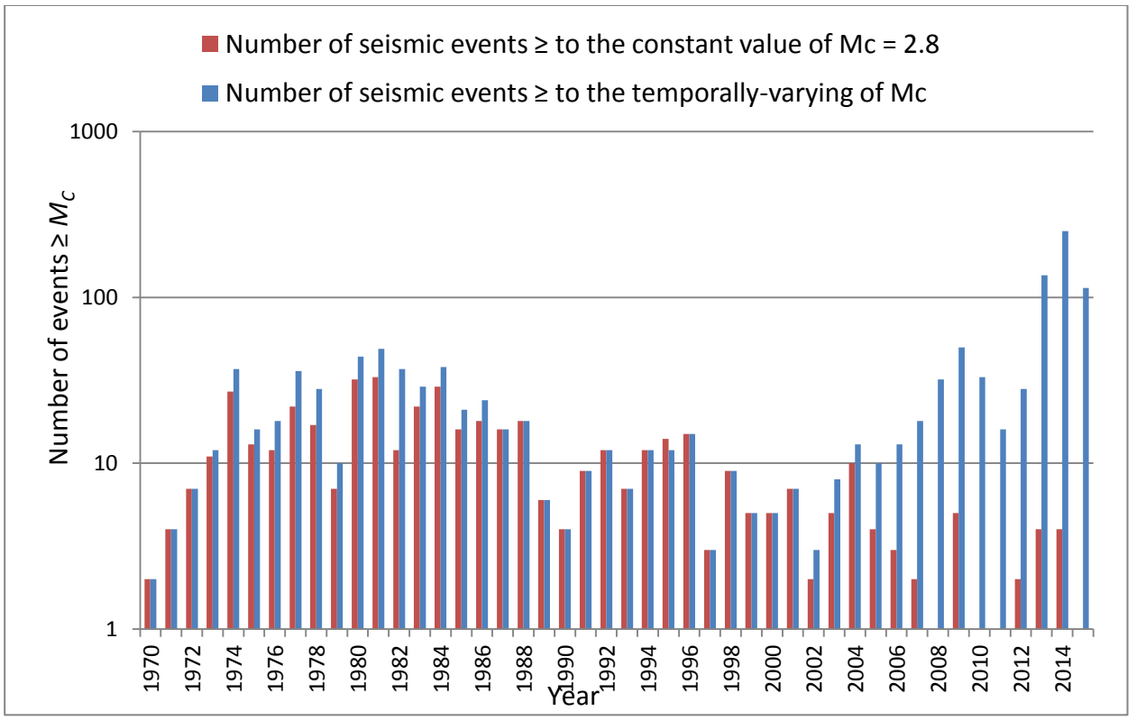

Figure 39. The number seismic events per year ≥ to the constant value of M_C = 2.8 compared to the number of seismic events per year ≥ to the temporally-varying of M_C in the ER seismic zone.

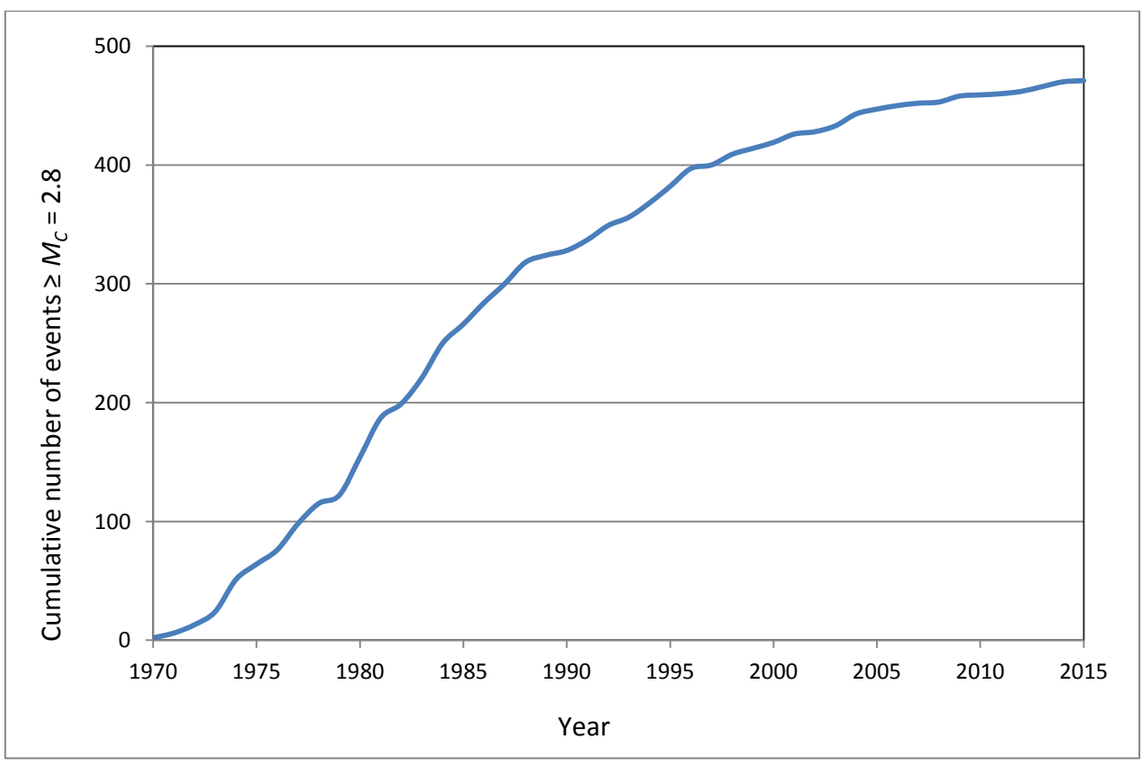

Figure 40. Cumulative number of seismic events ≥ M_C = 2.8 in the ER seismic zone.

The *b*-value for each phase is calculated using the KSB method and the temporal variations of the *b*-value is shown in Figure 42 with the corresponding *a*-values in Table 8. The M_{max} is calculated using the KSB method for the ER seismic zone and results are shown in Figure 43.

The M_{max}^{obs} values in the ER seismic zone for each phase are shown in Table 8. The temporally-varying of M_C was produced using the ZMAP software and the results are shown in Figure 38. It was observed that M_C generally improved with time as expected due to the improvement in the local networks and the obtained values were consistent with the values obtained in Table 4. The temporally-varying in the *b*-value was also calculated in the ZMAP software and the results are illustrated in Figure 42. The *b*-value increases from 0.8 in 1970 to 1.9 in 1995, decreasing down to 1.2 in 2007 and settling at around 1.0 in 2015. The M_{max} calculated using the KSB technique is denoted as M_{max} (KSB) (Figure 43) and M_{max} calculated using equation 4.3 is denoted as M_{max} (R). The *a*-values shown in Table 8 were calculated using SEISAN software. All the recurrence parameters extracted from the ER seismic zone using the three different software packages are shown in Table 8 for each phase. The number of seismic events above M_C in Phase 1 - 4 of the ER seismic source zone are 452, 134, 326 and 365 respectively.

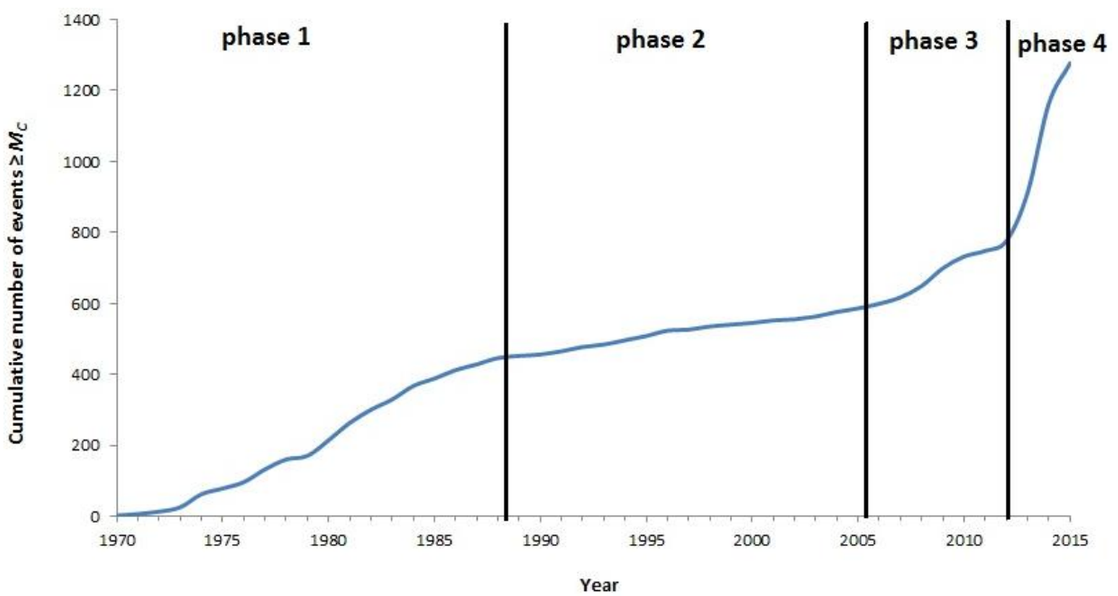

Figure 41. The cumulative number of seismic events greater or equal to temporally-varying of M_C in the ER seismic zone, phase 1 (1970-1989), phase 2 (1990-2004) inclusive phase 3 (2005-2012) inclusive and phase 4 (2013-2015) inclusive.

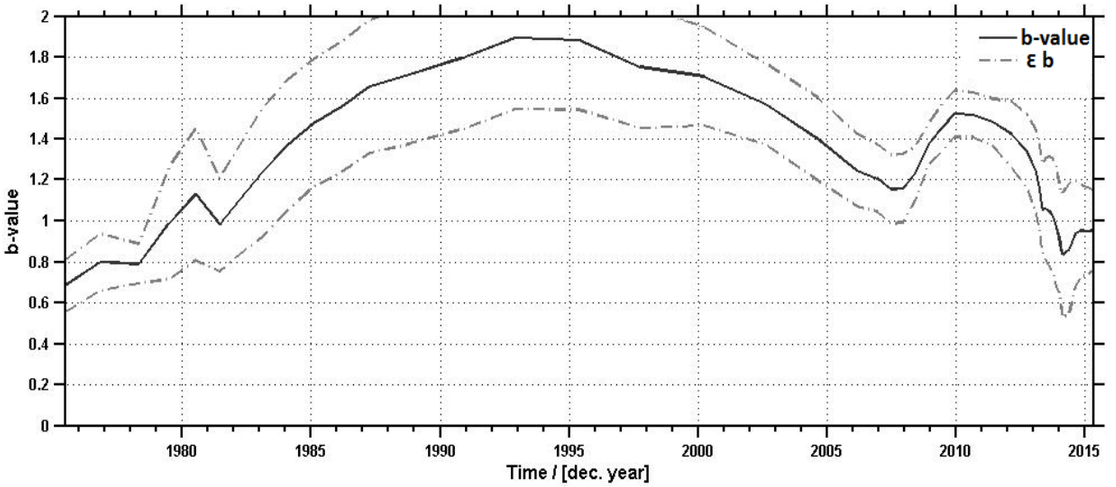

Figure 42. The temporally-varying of *b*-value using ZMAP for the ER seismic zone.

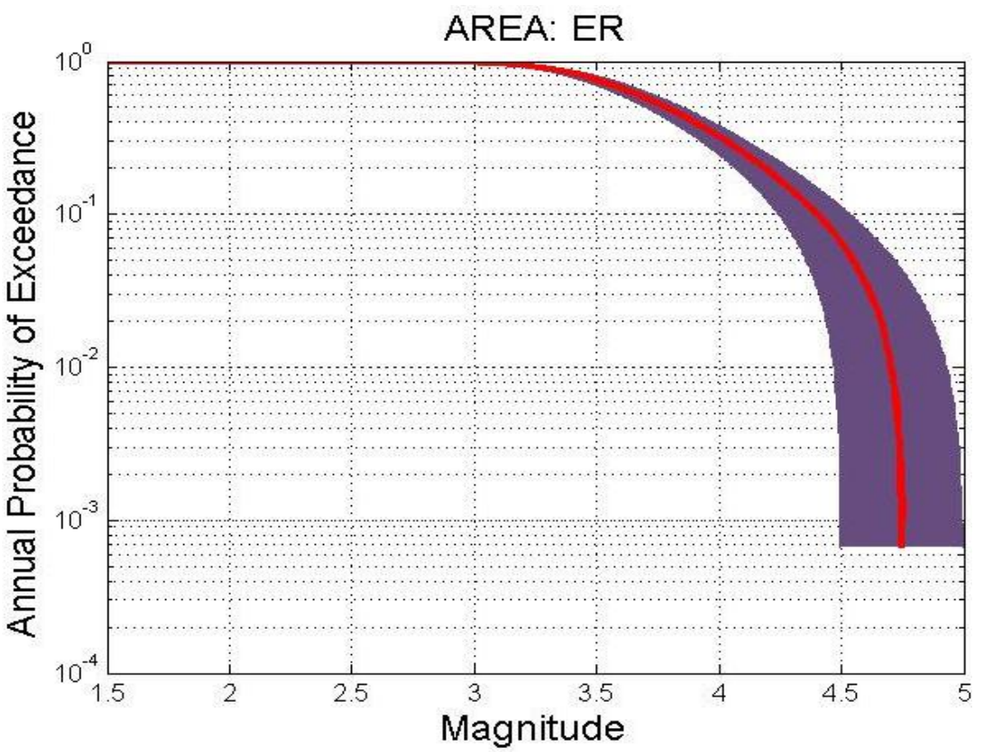

Figure 43. The M_{max} (KSB) calculated using the KSB method is 4.75 ± 0.2 for the ER seismic zone.

Table 8. Seismic recurrence parameters of the ER seismic zone, M_C is calculated using ZMAP software, *a*-value is calculated using SEISAN software and *b*-value is calculated using the HA3 software.

Phases	M_{max}^{obs}	M_C using ZMAP	Number of events > M_C	Average number of events per year > M_C	*a*-value using SEISAN	*b*-value using HA3
Phase 1 (1970 - 1989)	4.6	2.9	452	22.6	6.66	1.42±0.3
Phase 2 (1990 - 2004)	3.8	2.9	134	8.9	7.38	1.77±0.3
Phase 3 (2005 - 2012)	3.3	2.0	326	40.8	4.73	1.47±0.3
Phase 4 (2013 – 2015)	3.3	1.5	365	121.7	4.61	1.30±0.2

4.3 Seismic Source Periods and Seismic Source Recurrence Parameters

The main aim of this study is to conduct a time-dependent probabilistic seismic hazard assessment. A key step in time-dependent probabilistic seismic hazard assessments is to divide the catalogue into different periods for each seismic zone for which the hazard will be computed.

4.3.1 Seismic Periods

In Section 4.2, phases of occurrence of seismicity were defined for each source zone. Further to this, by analysing the phases of all the seismic zones together, two periods (Period A and Period B) were identified for which hazard will be calculated. Although there are 4 clearly defined phases in the FWR seismic zone, the difference between Phase 1 (period 1970 – 1989) and Phase 2 (period 1990 – 2004) in the number of earthquakes recorded is not significant and the slopes of the number of earthquakes recorded in Phase 1 and Phase 2 are not significantly different (Figure 44). This makes it possible to combine Phase 1 and 2 into Period A (period 1970 – 2004). The number of earthquakes recorded changed significantly between Phase 2 and 3, thus, they were not combined. The

number of earthquakes recorded does not change significantly between Phase 3 (period 2005 – 2013) and Phase 4 (period 2013 – 2015), making it possible to combine them to form Period B (period 2005 – 2015) (Figure 44). The CR seismic zone and ER seismic zone were flooding in Period B while active mining continued at the same period, for comparison Period B was considered at flooding period. Looking at the other three zones, the same trend was observed where there is a clear and significant change in the occurrence of events (Figure 44) as well as in the *b*-value between 2004 and 2005. This allowed the definition of two periods, Period A pre-2005 or mining period and Period B post-2005 or flooding period as the periods for which hazard will be calculated.

Period A (mining period) had a lower number of recorded earthquakes because this was when the SANSN had fewer stations close to the study area, while Period B (flooding period) has a substantially higher number of recorded earthquakes. Monitoring of earthquakes in Period B vastly improved when compared to Period A (Saunders et al., 2008; Saunders et al., 2016). Apart from improved monitoring, it was also observed that the seismicity in the CR seismic zone increased in recent times after mining activity had stopped and mines were allowed to flood (Goldbach, 2009; Ogasawara et al., 2002). Water flooding abandoned mines is said to lubricate existing faults causing them to move and create seismic events (Ogasawara et al., 2002). The SWMP cluster network was installed to monitor this effect. The seismicity recorded as a result of flooding was included in the catalogue thereby taking into account its effect on the hazard analysis of Period B for the CR seismic zone.

4.3.2 Seismic Source Recurrence Parameters

Seismic source recurrence parameters; M_{max}^{obs}, M_C, *a*-value and *b*-value for each zone for the two periods, A and B are shown in Table 9. M_{max} was determined for each seismic source zone for periods A and B combined. It was not calculated for each period because the catalogues of each phase were incomplete and the uncertainties were too great. The method adopted in this study allows to use a constant M_{max} as described in Chapter 2 and also in Convertito et al. (2012). The periods identified for each zone were used in the calculation of M_{max} and the *b*-value using the HA3 software package. The KSB technique was used in each case. HA3 allows the use of the different periods with varying completeness levels as described in Section 4.2 and incomplete catalogues (Kijko et al., 2016). The *a*-value for all seismic sources was then calculated using the SEISAN software. The information on occurrence of seismic source parameters with time after filtering out seismic events < M_C including *a*-value with time is shown in Table 9.

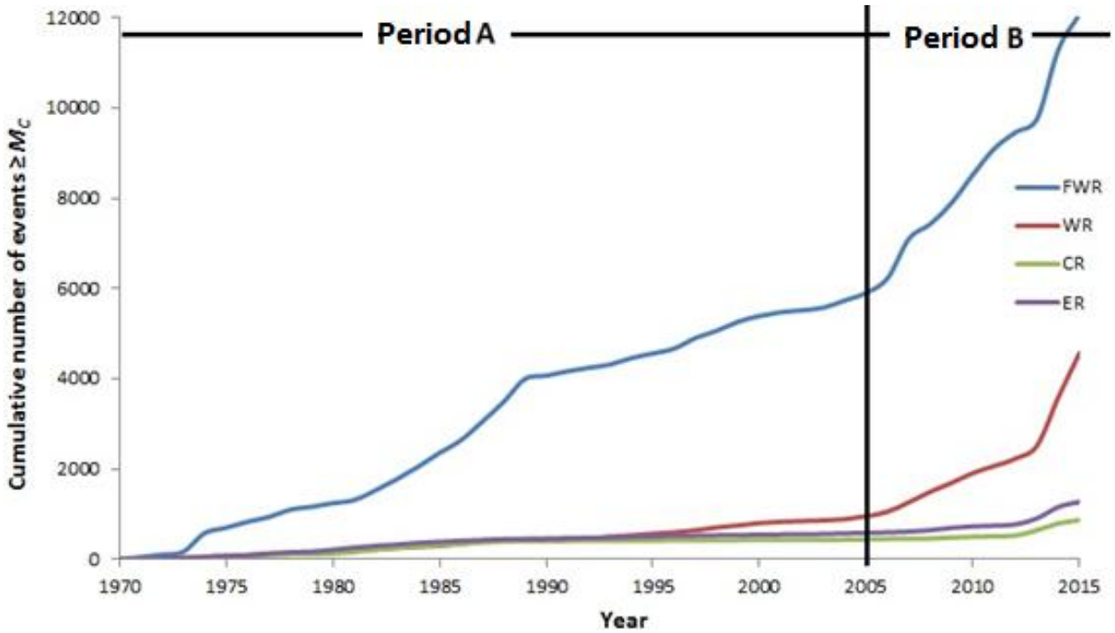

Figure 44. Cumulative numbers of events ≥ temporally-varying of M_C. Period A (1970-2004) and Period B (2005-2015). Seismic zones: ER – East Rand; CR Central Rand; WR – West Rand; FWR – Far West Rand.

It was generally observed that the *b*-value in the gold mining regions of South Africa was in the range of 1.0 to 1.5 (Table 9). These *b*-values observed are similar to those obtained by Bachmann et al. (2011) and Mena et al. (2013) for their studies in a geothermal power plant in Basel, Switzerland; Petersen et al. (2016) for the southern USA and Urban et al. (2016) for Mponeng mine in Gauteng, South Africa. Some studies show a *b*-value much closer to 1 for induced seismicity as is the case for natural seismicity (Goertz-Allmann and Wiemer, 2013), while others suggest much higher values for induced seismicity (*b* ~ 2) (Maxwell et al., 2009; Wessels et al., 2011) in hydraulic stimulation in the USA.

Table 9. Summary of the seismic recurrence parameters for each seismic source and for both Period A (1970-2004) and Period B (2005-2015). Period A is 35 years and Period B is 11 years.

Sources	M_{max}^{obs}		M_C		***a*-value**		***b*-value**	
	Period A	Period B	Period A	Period B	Period A	Period B	Period A	Period B
FWR	4.6	4.0	2.9	1.0	8.08	5.97	1.35±0.2	1.03±0.1
WR	4.2	3.8	2.6	1.6	6.56	5.32	1.41±0.2	1.34±0.1
CR	3.9	3.6	2.4	1.5	5.08	4.49	1.02±0.2	1.37±0.2
ER	4.6	3.3	2.9	1.5	7.04	4.88	1.50±0.3	1.50±0.2

5. GROUND-MOTION MODELS

Ground-motion models or ground motion prediction equations (GMPEs) predict the distribution of expected ground-motions conditional on the occurrence of a given earthquake scenario (usually characterised in terms of moment magnitude, source-to-site distance, style of faulting mechanism and site conditions) (Bora et al., 2014; Peruš and Fajfar, 2012; Thenhaus and Campbell, 2003). GMPEs predict a ground-motion parameter of interest (*e.g*. peak ground acceleration (PGA), peak ground velocity (PGV), peak ground displacement (PGD)) from the ground-shaking-intensity associated variables that describe the earthquake source, wave propagation path and local soil conditions (Douglas, 2003; Stewart et al., 2015).

There is a lack of ground-motion prediction equations derived from southern Africa using either tectonic or mining-related earthquake data. This is mainly due to a lack of sufficient records of strong ground-motion data. In such a case, GMPEs are usually selected from other regions, adjusted and used in target regions (Bommer et al., 2005; Scherbaum et al., 2004; Scherbaum et al., 2011). Such a process was followed in this study.

5.1 GMPE Selection

It has become normal to import GMPEs derived for other regions on the basis of tectonic similarity, although this may result in large epistemic uncertainties. South Africa is in a stable continental region, thus, only GMPEs from other stable continental regions were considered. The uncertainties associated with this process normally require that several GMPEs, whose variability cover the uncertainty associated with the target region be selected.

One of the most important steps in a seismic hazard analysis is the selection of models to predict the ground-motion at the target region (Scherbaum et al., 2009). There are more than 280 GMPEs for PGA and more than 180 for spectral ordinates derived all over the world, going as far back as 1964 (Douglas, 2011). Selecting appropriate models for a target region is, therefore, both important and challenging. However, several researchers have provided guidance to make the process easier. These include Cotton et al. (2006) who proposed a six-step selection procedure, which was later updated to a ten-step selection procedure by Bommer et al. (2010). GMPEs need to pass this selection procedure to be considered for use in the seismic hazard assessment in the target region. It is critical to compare observed seismic data with ground motion predicted by GMPEs as proposed by Scherbaum et al. (2009), to test if the models capture the observed ground-motions. This does not mean that the expected median ground-motions will be exactly equal to the model median ground-motions.

The selection process should result in the minimum number of independent GMPEs that capture the expected range of all possible ground-motions in the target region (Cotton et al., 2006). This minimum number of independent GMPEs must be weighted in a logic tree to address the associated uncertainty if more than one GMPE is used. The uncertainty parameters are described in the branches

of the logic tree and weighted according to the relative confidence (Bommer et al., 2005) or degree of belief by the analyst using available information.

The exclusion criteria as proposed by Cotton et al. (2006) and used in other major projects such as the Global Earthquake Model (GEM) (Stewart et al., 2015), was applied in this study to select suitable GMPEs. The exclusion criteria from Cotton et al. (2006) are listed as follows:

1. *The model is from a clearly irrelevant tectonic regime (e.g. models from subduction zones cannot be used),*
2. *The model is not published in an international peer-reviewed journal,*
3. *The model has been superseded by more recent publications,*
4. *The frequency range of the model is not appropriate for engineering application,*
5. *The model has an inappropriate functional form (e.g. models which don't represent the proper physical mean of attenuation),*
6. *The regression method or regression coefficients are judged to be inappropriate, mainly due to insufficient data.*

The GMPEs can be divided into three groups according to the methodology used to derive them, (1) Empirical models, (2) Stochastic models, (3) Hybrid empirical models. Empirical models are derived by regression of observed data in regions with large amounts of strong ground-motion data, like the western North America and Japan (Campbell, 2003a; Pezeshk et al., 2011). Stochastic simulation processes involve repeatedly exercising the model for a range of magnitudes and distances, as well as other parameters, adopting a proper functional form for a regression equation. The final step is to performing regression analyses to determine coefficients for mean predictions, median predictions and percentile predictions as well as variability about the mean, median and percentile for the target region (Silva et al., 2002). The hybrid empirical method is usually used to develop GMPEs in areas with sparse ground-motions like northern Europe, eastern North America and Australia. This method employs the stochastic simulation to adjust empirical GMPEs developed for a region with infinite strong-motion recordings, like the western North America and Japan in order to estimate strong-motion parameters in a region with small amounts of native dataset (Campbell, 2014). The adjustments account for regional differences between the host and the target region in the earthquake source, wave propagation, and site-response characteristics between the two regions (Pezeshk et al., 2011).

During the GEM project (Stewart et al., 2015), ten GMPEs were selected for stable continental regions. The pre-selected models are Silva et al. (2002, SEA02); Toro et al. (2002, TEA02); Campbell (2003a, CAMP03), Pankow and Pechmann (2004, PP04); Atkinson and Boore (2006, AB06); Kanth and Iyengar (2007, KI07); Akkar and Bommer (2010, AKB10); Pezeshk et al. (2011, PZT11) (Table 10). Two models included in the GEM project, Douglas et al. (2006) and Sommerville et al. (2009) were excluded in this study. The Douglas et al. (2006) model was excluded because it is essentially the same as the CAMP03 model, producing very similar results. The functional form and the regression coefficients are exactly the same. The Sommerville et al. (2009) was excluded because of the selection criterion number 2 above, which states *"The model is not published in an international peer-reviewed journal"*. This model was presented at the Annual Conference of the Australian Earthquake Engineering Society, Newcastle, 11-13 December 2009 and is not

published in a scientific journal. In addition to the GEM recommended GMPEs, a new model developed for a stable continental region (United Kingdom) was included. This model was developed by Rietbrock et al. (2013) (RSE13) using stochastic simulation using weak earthquake data recorded in the United Kingdom. The characteristics of the pre-selected GMPEs, such as the tectonic region for which each model was created, method used to create each model, the magnitude range of data used to create each model, the magnitude type used in each model, the distance metric type used in each model, the distance capability of each model, site conditions used in each model, frequency range, ground motion amplitude type used in each model and coefficients regression techniques used in each model are listed in Table 10.

However, most existing GMPEs are derived from records of natural earthquakes of magnitude ranges of interest in terms of structural damage, which is generally M_W 5 and above (Akkar and Bommer, 2010; Boore et al., 1997; Campbell, 2003a; Pankow and Pechmann, 2004; Pezeshk et al., 2011; Toro et al., 2002). The Orkney earthquake of M_W 5.5 which occurred on 5 August 2015 is the only earthquake with M_W > 5.0 that has been recorded by the strong ground-motion network and can be used to test the pre-selected GMPEs, although this earthquake was slightly outside the study region.

5.2 Comparison of pre-selected GMPE predictions to the observed Orkney earthquake data

Prior to the Orkney earthquake, McGarr et al. (1989) recorded PGA value of 0.45 g for an event (M_W 4.0) and the corresponding PGV value of 6.7 cm/s at an epicentral distance of 2.4 km in Klerksdorp. The strike-slip M_W 5.5 Orkney earthquake of 5 August 2014, which occurred in the North West Province, South Africa at about 10:22 GMT was recorded by the SANSN as well as the strong ground-motion networks; MHSC, JICA and SWMP. Of the 47 accelerographs, 35 seismic stations recorded the event, 18 seismic stations from the MHSC network, 8 seismic stations from the JICA network and 9 seismic stations from the SWMP network (Figure 45). The MHSC stations are located within a distance of 4.3 to 35 km from the epicentre, whilst those from the JICA network were located at an epicentral distance ranging between 80 to 120 km, and 150 to 190 km for the SWMP stations (Figure 45). Each ray in Figure 45 represents a distance from each seismic station to the epicentre. There are no stations between 35 and 80 km, and limited azimuthal coverage in the areas between the three networks, with no stations to the east and south.

The closest station to the epicentre is the Vaal River Visiting Wives Village (VRVW) station located approximately 4.3 km west of the epicentre. This station recorded a PGA value of 0.21 g of the north-south component and a PGA value of 0.24 g of the east-west component (Figure 46). The station which recorded the highest PGA was the Slimmer and Jack station at shaft number 10 (SAJ10) located about 6 km NNE of the epicentre. This station recorded a maximum PGA value of 0.265 g of the north-south component and 0.088 g of the east-west component (Figure 47).The huge difference at SJ10 was because the station was north of the event which was why the EW component was weak because the event was a strike-slip event with NS orientation.

Table 10. The main characteristic of the pre-selected GMPEs (Douglas, 2010).

Reference	Area	Model Type	M range	M scale	R range (km)	R scale (km)	S	Ts	T range (s)	C	R
Akkar and Bommer (2010)	Europe and Middle East	532 accelerograms, Empirical model	5-7.6	M_W	1-100	Rjb	Soft soil/ Hard rock	PGA, PSA	0.05-3.0	G	1WM
Atkinson and Boore (2006)	Eastern North America	34800 simulated records	3.5-8	M_W	1-1000	Rrup	I,C	24, PGA, PGV	0.025-5.0	G	1
Campbell, 2003a	Eastern North America	Hybrid empirical + simulations	5-8.2	M_W	1-1000	Rrup	Vs30 = 2.8 km/s	16, PGA (0.01s)	0.02-4.0	G	1
Kanth and Iyengar (2007)	India	900, Simulated records	4-8	M_W	1-300	Rhyp	Hard rock, NEHRP	27, PGA	0.010-4.0	G	2M
Pankow and Pechmann (2004)	Worldwide data	Empirical Model	5-7.7	M_W	1-100	Rjb	Hard rock or Soft soil	46, PGA, PGV	0.1-2.0	G	1M
Pezeshk et al., (2011)	NGA models	Hybrid empirical	5-8	M_W	1-1000	Rrup	NEHRP class A	22, PGA	0.01-10	G	1
Silva et al.,(2002)	Central and Eastern North America	Stochastic simulations	4.5-8.5	M_W	1-400	Rjb	Vs30 = 2.8 km/s	26, PGA, PGV, PGD	0.01-10	G	1
Toro et al., (2002)	Central and Eastern North America	Stochastic simulations	5-8	M_W	1-100	Rjb	Vs30 = 2.8 km/s	7, PGA	0.028-2.0	G	1
Rietbrock et al., 2013	United Kingdom	Stochastic simulations from weak data	3-7	M_W	1-300	Rjb	Vs30 = 2.3 km/s	23, PGA, PGV	0.03-5.00	G	1

where:

M range Magnitude rage,

M scale Magnitude scale,

M_W Moment magnitude,

R range Source-to-site distance,

R scale Distance scale used

- Rjb Distance to projection of rupture place on surface,

- Rrup Distance to rupture plane,
- Rhyp Hypocentral distance,

S Number of different site conditions modelled,

C Continuous classification,

- I Individual classification for each site,
- Ts Number of periods for which attenuation equations are derived,

T range Range of periods for which attenuation equations are derived,

C Use of the two horizontal components of each accelerogram,

G Geometric mean,

R Regression method used,

- 1WM Weighted maximum likelihood one-stage,
- 1 Ordinary one-stage,
- 1M Maximum likelihood one-stage (Joyner and Boore, 1993),
- 2M Maximum likelihood two-stage (Joyner and Boore, 1993).

5.3 GMPE Adjustments

Before using GMPEs imported from one region to another, adjustments usually need to be made, especially where the host and target regions are of different tectonic regimes (Bommer et al., 2005; Scherbaum et al., 2004; Scherbaum et al., 2011). The parameters which were considered for adjustment in this study are those discussed below and listed in Table 11. These adjustments were made on all the GMPEs that were compared to the ground motion observed during the Orkney earthquake.

5.3.1 Horizontal component definition

Ground-motions calculated in seismic hazard analysis are usually for the geometric mean of the two horizontal components of motion, which is the most commonly used horizontal component definition. No adjustment is necessary for all the pre-selected GMPEs because they all use a geometric mean of the two horizontal components of motion (Table 10).

5.3.2 Magnitude

The seismic catalogue of this study is homogenised to moment magnitude as described in section 3.3. All of the GMPEs adopted for the hazard calculations use moment magnitude (M_w). Thus, no adjustment is necessary (Table 10).

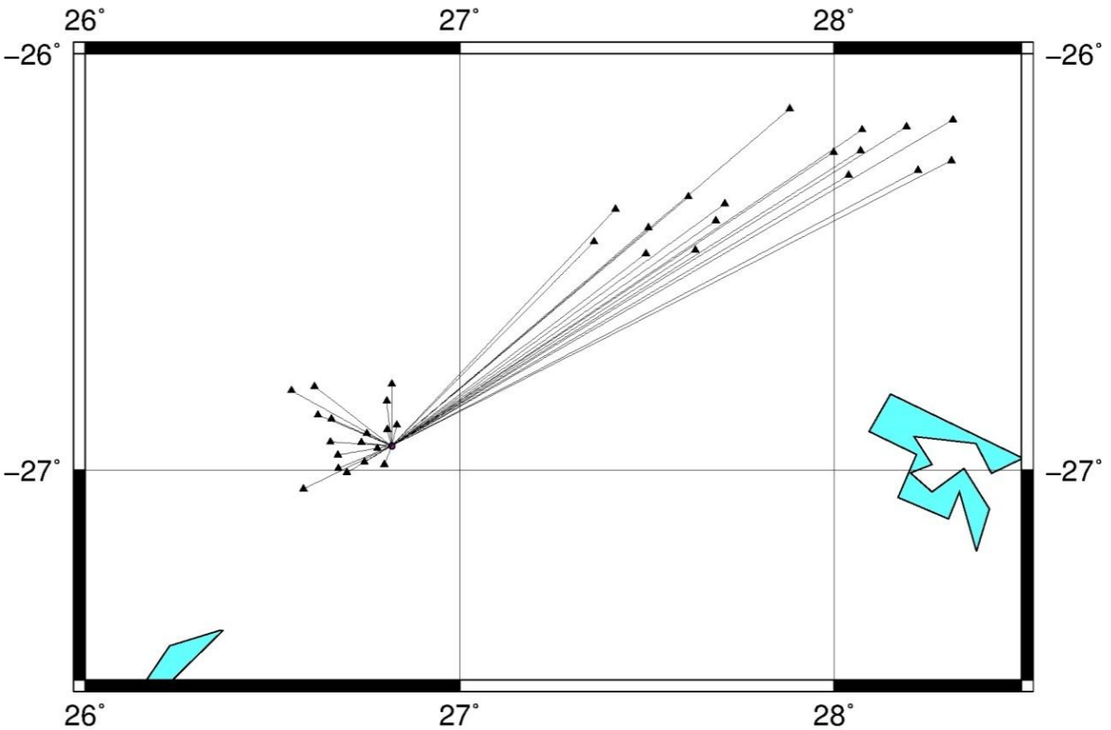

Figure 45. Epicentre to station ray paths (epicentre indicated by a black dot).

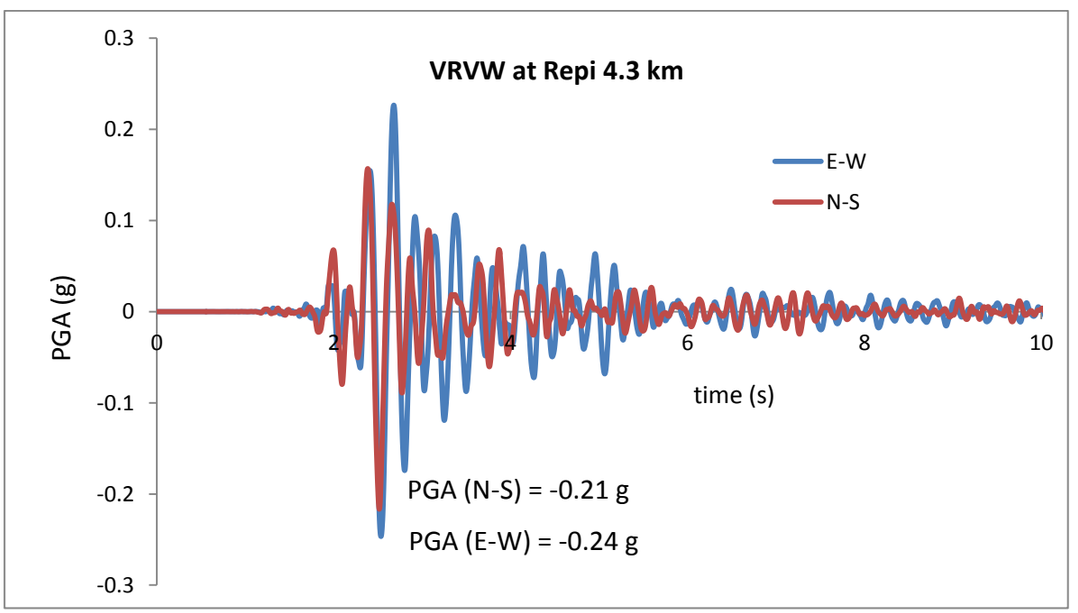

Figure 46. Orkney earthquake waveforms at the Vaal River Visiting Wives Village (VRVW) station with the PGA value of 0.21 g of the north-south component and PGA value of 0.24 g of the east-west component.

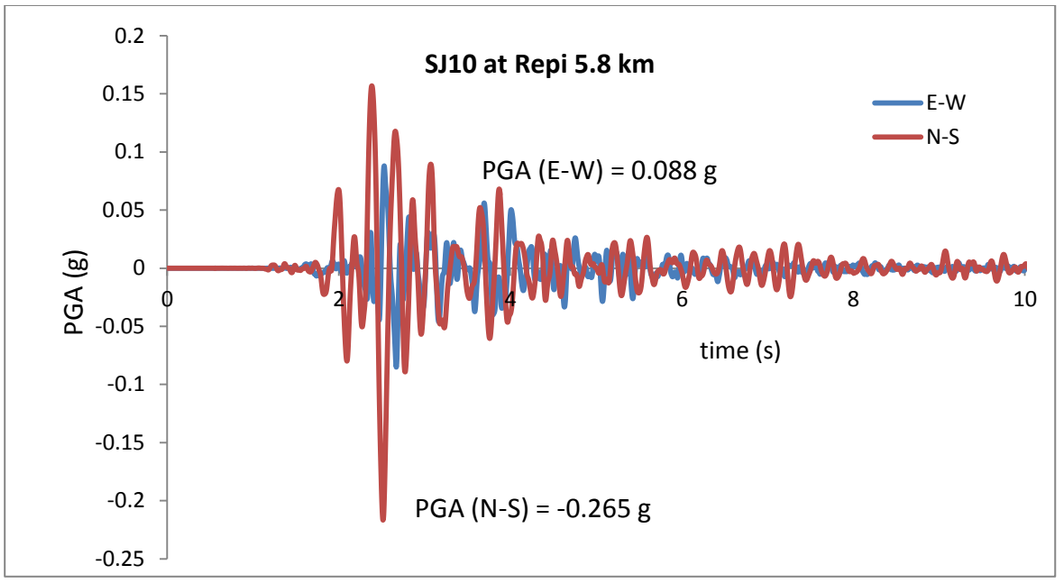

Figure 47. Orkney earthquake waveforms at the Simmer and Jack Shaft 10 (SJ10) station with the PGA value of 0.265 g of the north-south component and PGA value of 0.088 g of the east-west component.

5.3.3 Distance

The different equations used different distance metrics (Table 11), no adjustment for this parameter is necessary since the software to be used in the hazard calculation (OPENQUAKE) computes the appropriate distance for each model.

5.3.4 Style-of-faulting

An analysis of the style-of-faulting has been conducted for a few recent seismic events $M_L \geq 3.5$ at CGS. Most of these seismic events are normal or strike-slip faulting suggesting that the region of study is under extension. This requires adjustments of the GMPEs derived with reverse faulting data.

Although the GMPE used in the hazard calculations has been pre-selected in order to be compatible with the tectonic setting of South Africa, the composition of the underlying dataset in terms of style-of-faulting (SOF) is not always consistent with the predominantly normal faulting mechanisms of South African tectonic earthquakes. South Africa is in a stable continental region generally under extensional forces (Johnston et al., 1994), hence, in the absence of a well-defined seismotectonic model in the mining region, it is assumed that the mining region under consideration in this study is under extension. Most of the GMPE models do not require adjustment, either because they are stochastic (simulated) models or they allow for the selection of the style of faulting during the hazard calculation. The Pankow and Pechmann (2004) model was derived using a dataset made up of 55% strike–

slip and 45% normal faulting. Thus, this model was adjusted (Table 11) following the technique presented by Bommer et al., (2003). This is necessary because it was found that earthquakes generated by strike-slip faulting generate higher ground-motions compared to earthquakes generated by normal faulting (Schorlemmer et al., 2005) by a factor of approximately 1.042 (Bommer et al., 2003). Style-of-faulting in Akkar and Bommer (2010) is explicitly used in the GMPE model; hence there is no need for adjustment.

5.3.5 Local site conditions

The ground-motion predictions for the region of interest (northern part of the Witwatersrand Basin in Gauteng) need to take into consideration the local site conditions. The study area is mainly underlain by quartzite and conglomerate of the Turffontein Formation and Johannesburg Formation of the Witwatersrand Supergroup (Johnson et al., 2006, p 7). Though the weighted average shear-wave velocity over the uppermost 30m, V_{S30}, was not measured, typical values fall around 760 m/s (Zulu and Manzunzu, 2015). Thus, we considered a value of 760 m/s in the calculations. All the GMPEs are derived for hard rock conditions and some include soil conditions (Akkar and Bommer, 2010; Atkinson and Boore, 2006; Pankow and Pechmann, 2004), these conditions can be used explicitly in the GMPE models (Table 10).

Table 11. Distance metrics used in the pre-selected GMPE.

Equation	Distance Metric	Distance adjustment	Stochastic model	SOF adjustment
Kanth and Iyengar (2007)	Closest vertical distance to the occurrence of the earthquake Rhyp	Not be required	Explicitly used in the model	Not be required
Akkar and Bommer (2010)	Closest distance to surface projection of fault rupture (Rjb)	Not be required	Not included explicitly. Dataset is assumed to be 55% Strike-slip, 45% Normal	FN:EQ = 1.042 at all periods
Pankow and Pechmann (2004)	Closest distance to surface projection of fault rupture (Rjb)	Not be required	Stochastic model	Not be required
Silva et al. (2002)	Closest distance to surface projection of fault rupture (Rjb)	Not be required	Stochastic model	Not be required
Toro et al. (2002)	Closest distance to surface projection of fault rupture (Rjb)	Not be required	Stochastic model	Not be required
Atkinson and Boore (2006)	Closest distance from a site to a rupture surface (Rrup)	Not be required	Stochastic model	Not be required
Campbell (2003a)	Closest distance from a site to a rupture surface (Rrup)	Not be required	Hybrid empirical	Not be required
Pezeshk et al. (2011)	Closest distance from a site to a rupture surface (Rrup)	Not be required	Stochastic model	Not be required
Rietbrock et al. (2013)	Closest distance from a site to a rupture surface (Rrup)	Not be required	Stochastic model	Not be required

5.4 Comparison of the Orkney earthquake strong-motion data with pre-selected GMPEs

5.4.1 GMPEs from induced earthquakes.

There are several GMPEs derived from induced seismic events and they were compared against the Orkney strong ground-motion data. There is very little precedent in predicting ground-motions from mining-related events beyond the perimeter of the mine itself. To the knowledge of the author, one GMPE that was derived specifically for mining-related events is the equation by McGarr and Fletcher (2005), which was calculated as part of the seismic hazard assessment of a dam located in the immediate vicinity of coal mines in Utah. This equation has been found to be in good agreement with extrapolations of equations derived from strong-motion data up to magnitudes of about M_L 4.0, but predicts very low amplitudes of ground-motion when extrapolated to magnitudes of M_L 5.0 and above at distance higher than 10 km (Figure 48), which could be because this model is not data constrained above M_L 4.1. Considering that the current study considers a M_{max} value of at least M_W 5.5, the McGarr and Fletcher (2005) model is deemed inappropriate as it would grossly under-predict any ground-motion of interest.

The GMPE developed by Convertito et al. (2012) derived from shallow earthquakes in the Geyser geothermal field northern California was also considered because it was derived from induced seismicity and earthquakes with depths similar to the mines in the gold mining regions of South Africa. This equation predicts PGA values that match the observed data up to a distance of 30 km and then predicts very large PGA values when extrapolated to distances beyond 30 km (Figure 48). Considering that the current study considers seismic sources beyond 30 km from the epicentre, this model is deemed inappropriate as it would grossly over-predict any ground-motion of interest.

Douglas et al. (2013) developed an empirical GMPE using various ground-motion datasets of natural and induced seismicity from 6 datasets. These datasets are from Basel (Switzerland), Campi Flegrei (Italy), Geysers (United States), Hengill (Iceland), Roswinkel and Voerendaal (the Netherlands), and Soultz-sous-Forêts (France). This model is derived for moment magnitude range of M_W 1 – 5 for short hypocentral distance range of 1 – 50 km (Figure 48). On comparing to the Orkney earthquake data, this model is observed to over-predict PGA values at higher magnitudes. This model is also deemed inappropriate as it would result in grossly over-predicted any ground-motions. Therefore all GMPEs from induced earthquakes are not appropriate in this region of study, then tectonic GMPEs were investigated.

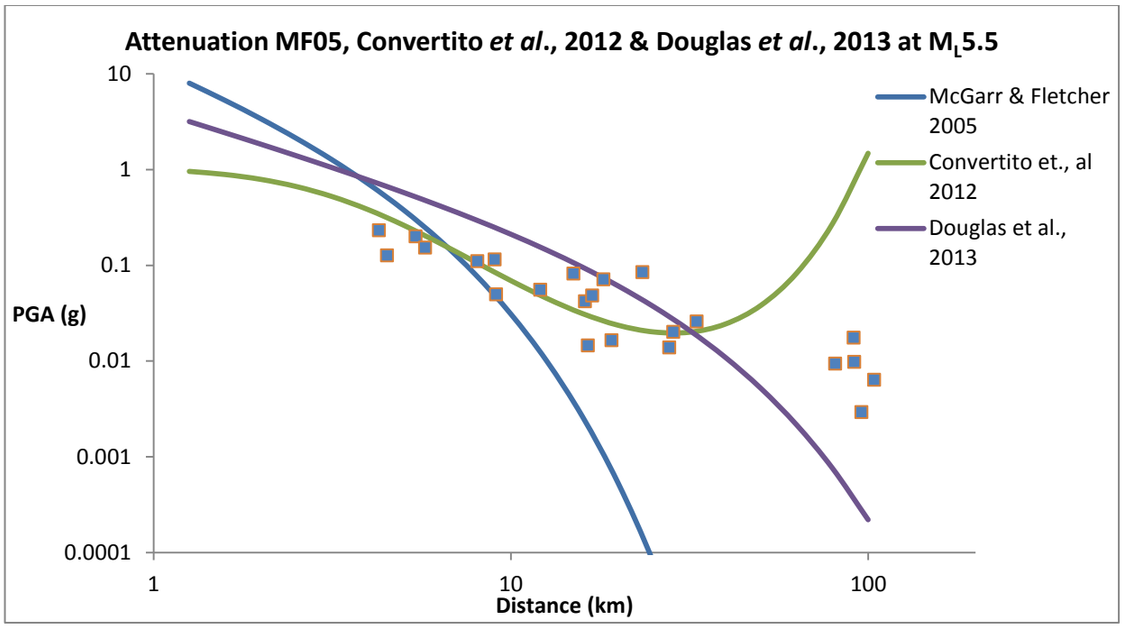

Figure 48. The comparison of induced GMPEs with Orkney strong-motion data up to 100 km.

5.4.2 GMPEs from tectonic earthquakes

The two horizontal components of PGA values recorded by the MHSC, JICA and SWMP networks are listed in Table 12. The geometric mean of PGA for the two horizontal components was calculated for the epicentral distance of each seismic station (Table 12). The predicted ground-motion obtained from the pre-selected GMPEs was compared with the observed Orkney strong-motion data (Figure 49). It should be noted here that GMPEs are not being compared amongst themselves nor are they being judged. The ultimate goal of this study is to select a minimum number of GMPEs which can be assumed to represent strong ground motion in the Gauteng gold mining region. The selected models should cover the centre, body and range of all possible ground-motions. Hence the selected models should cover the mean PGAs, the upper and the lower PGAs. The limitation of this study is that there is only one earthquake with M_W > 5.0 which has been recorded by the South African strong ground motion networks.

The observed data from the Orkney earthquake is represented by the blue rectangles and the tectonic GMPEs are represented by the eight different colour lines except for the black line which is the regression line derived from the Orkney earthquake. The best model should be the one closest to the black line. The models are compared against the data at distances 4 - 200 km (Figure 49).

The models; AB06, CAMP03, SEA02 and TEA02 overestimate PGA at distances less than 30 km from the epicentre (Figure 49). AB06, CAMP03 and TEA02 predict PGA values of up 1 g at about 1 km from the epicentre. AKB10, PP04 and KI07 are the closest to the observed data (black line) at distances of up to 30 km. The KI07 model also reaches PGA value of 1 g at about 1 km from the

epicentre and PP04 predicts a PGA value of about 0.16 g, underestimating PGA at very short distances. The PZT11 model predicts the lowest PGA values at distances of about 30 km although it is higher than PP04 at about 1 km from the epicentre.

The models; AB06, CAMP03, PP04, SEA02 and TEA02 models estimate high PGA values at distances 80 – 200 km from the epicentre, whilst AKB10 is the closest to the black at the same distance (Figure 49). On the other hand, the models PZT11 and KI07 models underestimate PGA values again at the same distance range.

According to the results in Figure 49, it observed that AKB10 represents the mean of the observed data, while TEA02 and PZT11 cover the upper and lower range respectively. Therefore, these three models were selected to be used in the study region and the RSE13 model.

These four GMPEs [ASB14 (update of AKB10), PZT11, TEA02 and RSE13] were then used in hazard calculations in the study region using calculated recurrence parameters for Period A. The results are shown in Figure 50. The PSHA calculation method is discussed in chapter 6. The obtained PGA values are clearly overestimated by ASB14, PZT11 and TEA02. These GMPEs estimate maximum PGA values of 0.655 g, 1.634 g and 1.500 g respectively, which are unrealistically high. The RSE13 estimate maximum PGA value of 0.25 g which is more reasonable compared to the other GMPEs. Thus, RSE13 was chosen as the most reliable model and used in the hazard calculations going forward.

Table 12. Stations with horizontal PGA component, geometric mean PGA and Epicentral distance.

Station	Network	PGA (E-W) (g)	PGA (N-S) (g)	Geometric mean PGA (km)	Epicentral Distance (km)
VRVW	KOSH	0.247	0.217	0.231	4.3
BSP	KOSH	0.201	0.080	0.127	4.5
MOAB	KOSH	0.218	0.185	0.201	5.4
SJ10	KOSH	0.088	0.265	0.153	5.8
AG5	KOSH	0.090	0.136	0.110	8.1
AGHS	KOSH	0.120	0.110	0.115	9.0
KPNG	KOSH	0.051	0.048	0.050	9.1
MWC	KOSH	0.069	0.045	0.056	12.1
VRCP	KOSH	0.027	0.245	0.082	15.0
TLEK	KOSH	0.028	0.064	0.042	16.1
FBF	KOSH	0.015	0.014	0.015	16.4
OGC	KOSH	0.032	0.073	0.048	16.9
VMBD	KOSH	0.048	0.105	0.071	18.1
KDGC	KOSH	0.015	0.017	0.016	19.1

Station	Network	PGA (E-W) (g)	PGA (N-S) (g)	Geometric mean PGA (km)	Epicentral Distance (km)
RCAS	KOSH	0.078	0.091	0.084	23.3
PNMR	KOSH	0.013	0.015	0.014	27.7
WDF	KOSH	0.018	0.023	0.020	28.5
KMDR	KOSH	0.027	0.025	0.026	33.1
ELND	JICA	0.011	0.008	0.009	80.9
FOCH	JICA	0.014	0.022	0.018	91.1
KEVO	JICA	0.010	0.010	0.010	91.5
DRF5	JICA	0.003	0.003	0.003	95.7
WBHF	JICA	0.007	0.006	0.006	104.0
LEBN	JICA	0.010	0.018	0.014	110.2
SDEP	JICA	0.006	0.005	0.005	113.3
EZUL	JICA	0.003	0.004	0.004	118.0
KFND	SWMP	0.016	0.012	0.014	148.3
ORMO	SWMP	0.003	0.004	0.003	152.6
RDWR	SWMP	0.002	0.003	0.002	153.5
CTDP	SWMP	0.003	0.003	0.003	159.7
OBSV	SWMP	0.002	0.003	0.002	162.9
SPCM	SWMP	0.004	0.006	0.005	172.5
GOUD	SWMP	0.002	0.005	0.003	174.8
CNVL	SWMP	0.001	0.002	0.001	182.5
BNON	SWMP	0.002	0.002	0.002	187.7

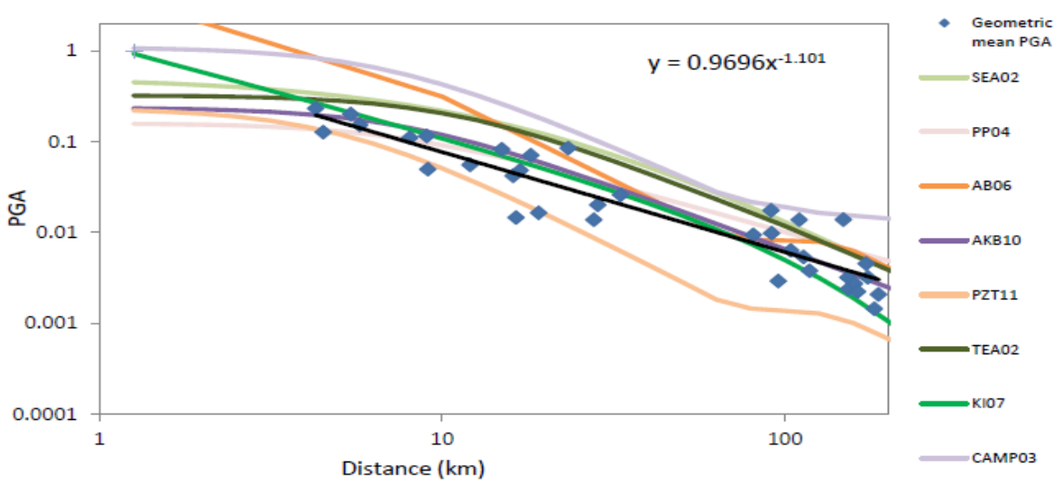

Figure 49. The comparison of ground motion predicted by the eight pre-selected GMPEs with Orkney strong-motion data. The black curve is a best-fit model of the Orkney data.

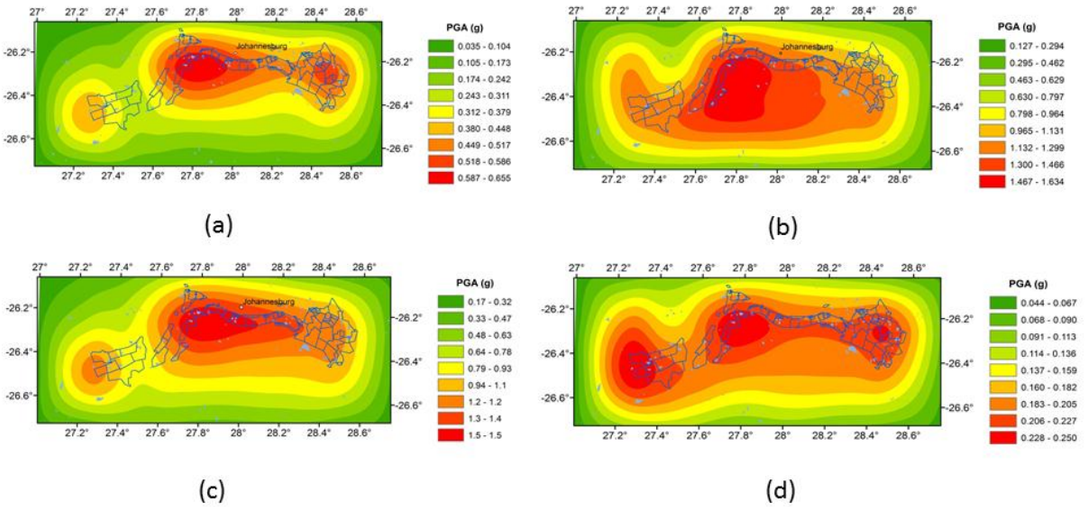

Figure 50. Peak ground acceleration at a return period of 475 years map for Period A (mining period) using ASB14 (a), PZT11 (b), TEA02, (c) and RSE14 (d) (full figure images in Appendix).

6. PSHA CALCULATIONS

Seismic hazard estimates were calculated in terms of PGA and 5 % damped response spectra at periods of 0.1 s, 0.5 s, 1.0 s and 2.0 s for 10 % probability of exceedance in 50 years which corresponds to a 475 year return period, using the OPENQUAKE software (Pagani et al., 2014). The RSE13 GMPE was the only GMPE used as it provided reasonable results, as well as different seismic recurrence parameters were implemented using the logic tree approach in order to account for epistemic uncertainties. The weighted parameters are shown in the logic tree in Figure 51. The other corresponding recurrence parameters are shown in Table 9 for each period.

This logic tree is not necessarily the probability of occurrence but it is a degree-of-belief on the occurrence of the seismic recurrence parameters. Most seismic events in the mining region occur at a depth of about 2 km and few occur at distances up to 5 km, hence the depth of 2 km was weighted higher than depth of 5 km. The KSB method is weighted higher because it is the recommended method to calculate M_{max} on HA3 and it provided more stable results than the other methods. Overpopulating a logic tree does not necessarily reduce epistemic uncertainty associated with an input parameter, overpopulating a logic tree is a misuse of a logic tree (Bommer and Scherbaum, 2008).The test results shown in Figure 50 allowed only one GMPE to be used this study.

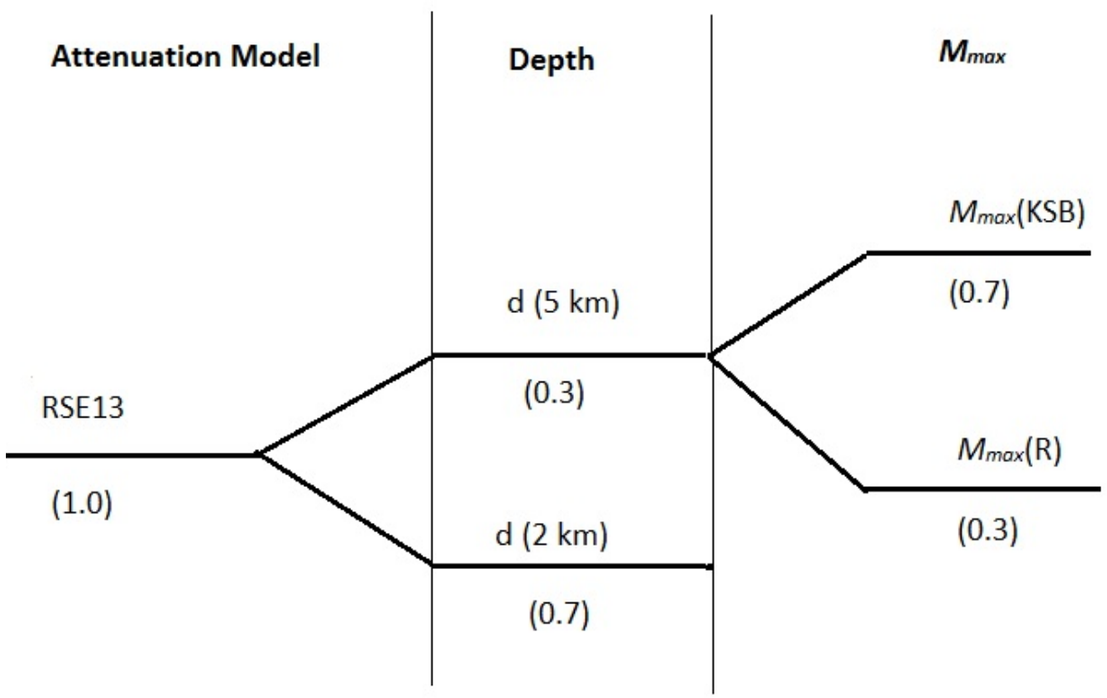

Figure 51. Logic tree with weights.

OPENQUAKE is an open-source software developed at the University of Pavia, Italy by the GEM Foundation working group (Pagani et al., 2014) to compute seismic hazard assessment and seismic risk assessment at site, local, regional and global level. OPENQUAKE is designed to compute modern state-of-the-art probabilistic seismic hazard assessment. Although this software is still under development, it has been extensively tested and compared to commercial software like FRISK88, in numerous projects like the ESKOM project in South Africa (Bommer et al., 2013).

To meet the objective of computing time-dependent seismic hazard for Johannesburg, the calculations were carried out at bedrock of seismic velocity of 760 m/s for the two time periods *i.e.* Period A (Figure 52) and Period B (Figure 53). Sensitivity analysis studies were also performed to test the influence of each source zone to the hazard results.

6.1 PSHA Results and Discussions

The aim of this study is to conduct a time-dependent probabilistic assessment of the seismic hazard in the northern rim of the Witwatersrand Basin of the Gauteng Province, South Africa, mainly due to seismicity in the gold mining regions.

The highest estimated PGA value was approximately 0.250 g in the western part of the region in Period A (mining period) and the corresponding estimated PGA value was 0.206 g in the same region in Period B (flooding period) (Figure 52a and Figure 53a). The spectral acceleration values also decreased from Period A to Period B (Figure 52b - d and Figure 53b - d).

The second highest hazard levels were observed in the eastern part of Johannesburg, although the western part of Johannesburg was seismically more active than the eastern part. This was because the eastern part of Johannesburg had a higher maximum expected magnitude than the western part. It was once again observed that the hazard levels were higher in Period A than in Period B in the eastern parts, with PGA value range 0.183 - 0.205 g in Period A to a range of PGA value range 0.048 g - 0.067 g in Period B. This shows a significant reduction in the hazard level between the two periods in the eastern parts of Johannesburg. The spectral acceleration values also decreased from Period A to Period B in the western part of Johannesburg (Figure 52b - d and Figure 53b - d). This shows that seismic hazard decreases in flooding period compared to mining period.

The central part of Johannesburg has the lowest hazard estimated with PGA value in a range of 0.160 - 0.182 g in Period A and the corresponding estimated PGA value in a range of 0.068 - 0.087 g in Period B (Figure 52a and Figure 53a). The spectral values also decreased from Period A to Period B in the central part of Johannesburg (Figure 52b - d and Figure 53b - d). Therefore, it was observed that the hazard generally decreased from Period A to Period B in all seismic zones although the number of the recorded events increases due to the improved of the capabilities of the network. It is important to understand which seismic zones contribute more the hazard of the entire region of study.

It was generally observed that the hazard estimates were higher close to the proximity of the mining boundaries, this is in good agreement with what was observed in the studies of Petersen et al. (2014) and Petersen et al. (2016). The inclusion of mining-induced seismic events does increase the hazard level in the areas of low to moderate seismic region. The hazard estimates from this study are higher than those from the GSHAP project. The GSHAP project predicted seismic hazard values less than 0.20 g while this study predicts values up to 0.25 g. The hazard level estimated in this study was comparable to the hazard level observed in the areas of low to moderate seismicity such as the southern part of the USA from the GSHAP project.

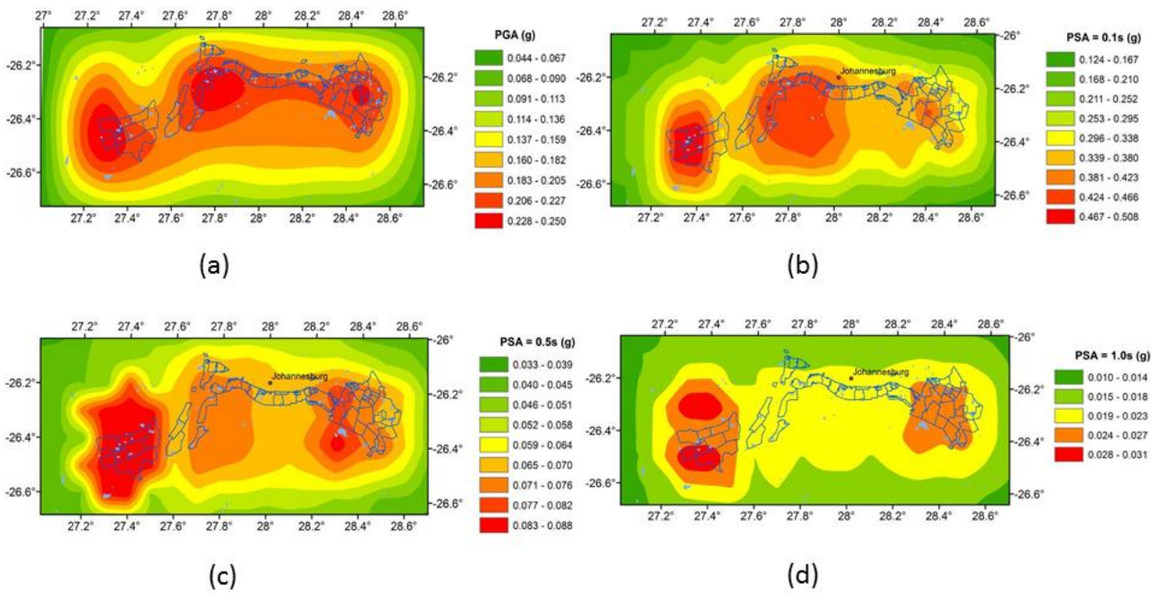

Figure 52. Seismic hazard maps for Period A for the Gauteng gold mining regions of South Africa, (a) PGA map, (b) Spectral acceleration at period 0.1s, (c) Spectral acceleration at period 0.5s, (d) Spectral acceleration at period 1.0s (full figure images in Appendix).

In sensitivity assessments to investigate the influence of the seismic zones to the hazard, calculations were conducted only for PGA values. It was observed that the FWR seismic zone contributes in the range of 70 – 80 % of the hazard in Period A for FWR seismic zone, while the other zones contributing between 20 – 30 % range. In Period B, the FWR seismic zone contributes in the range of 80 – 90 % in the FWR seismic zone while other zones contributing between the range of 10 – 20 % of the hazard of the FWR seismic zone (Figure 54a and Figure 55a). This was mainly due to a lower *b*-value, the lower the *b*-value the higher is the hazard and higher the *b*-value the lower is the hazard (Table 9). The contribution of the WR seismic zone doesn't change much in the range of 50 – 60 % in both Period A and Period B for the WR seismic zone, while other zones contributing in the range of 40 – 50 % towards the hazard of the WR seismic zone (Figure 54b and Figure 55b) as expected because the recurrence parameters didn't change much (Table 9). The contribution of CR seismic zone decreased from the region of 40 – 50 % in Period A to the range of 30 - 40% in Period B for the CR seismic zone (Figure 54c and Figure 55c), this was mainly due to a higher *b*-value (Table 9). The contribution of ER seismic zone decreased significantly from the range of 70 – 80 % in Period A to the range of 40 – 50 % in Period B (Figure 54d and Figure 55d) this

was mainly due to a lower activity rate (Table 9). The FWR seismic zone contributes more hazard to the study region due to lower *b*-value and higher activity rates, followed the WR seismic zone and then the ER seismic zone. The CR seismic zone contributes the least to the hazard due to the lowest activity rates.

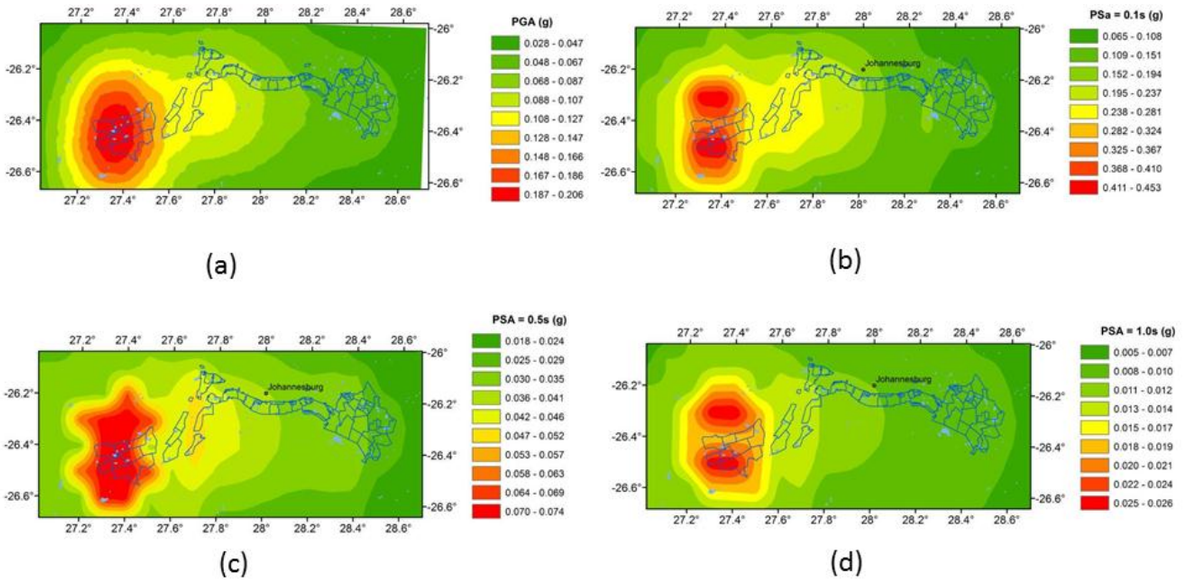

Figure 53. Seismic hazard maps for Period B for the Gauteng gold mining regions of South Africa, (a) PGA map, (b) Spectral acceleration at period 0.1s, (c) Spectral acceleration at period 0.5s, (d) Spectral acceleration at period 1.0s (full figure images in Appendix).

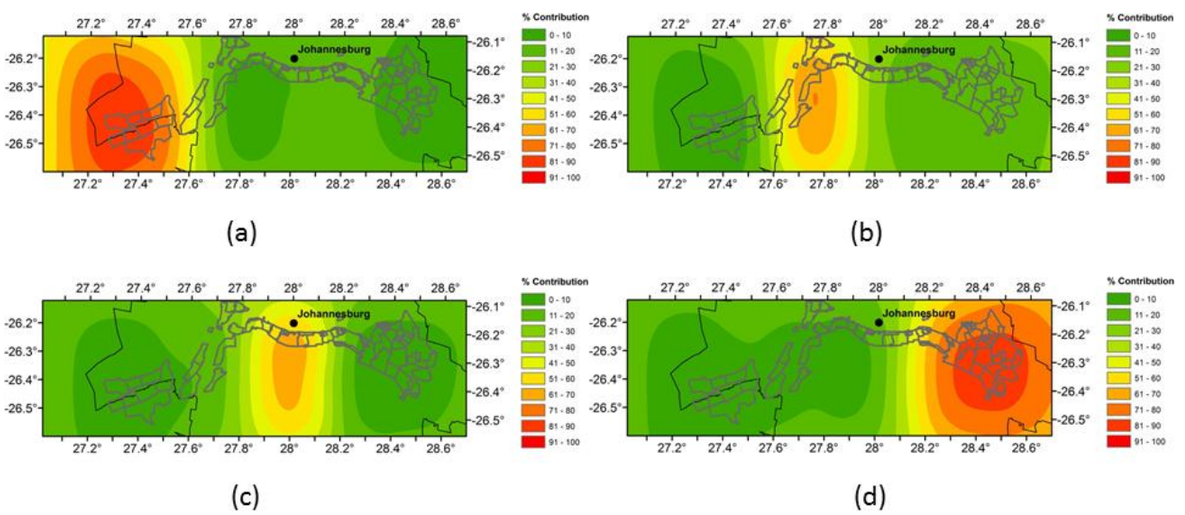

Figure 54. Percentage hazard contribution of seismic zones in Period A (a) FWR seismic zone, (b) WR seismic zone (c) CR seismic zone, (d) ER seismic zone (full figure images in Appendix).

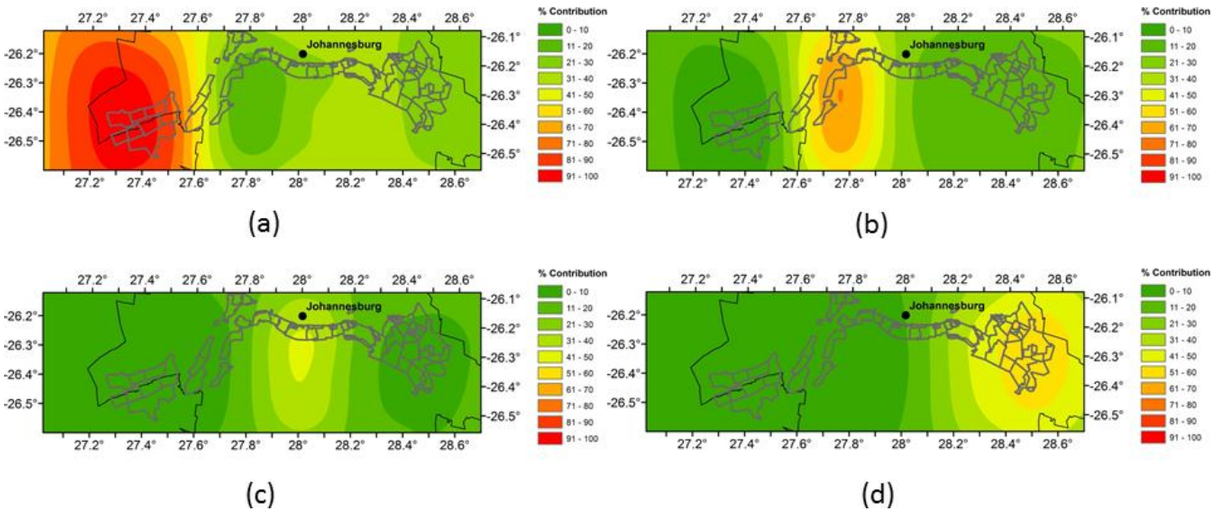

Figure 55. Percentage hazard contribution of seismic zones in Period B (a) FWR seismic zone, (b) WR seismic zone (c) CR seismic zone, (d) ER seismic zone (full figure images in Appendix).

7. CONCLUSIONS

A seismic hazard assessment in the gold mining regions of South Africa has not been incorporated in global projects such as the Global Earthquake Model project, although the seismicity related to the gold mining activities accounts for about 90 % of the seismicity in South Africa. This type of seismicity is solely considered for this study. Furthermore, the time-dependency of the seismicity was taken into account with respect to monitoring, the occurrence of events, recurrence parameters such as M_C, M_{max}, *b*-value, and *a*-value. All of these factors were addressed in the assessment.

The earthquake catalogue of South Africa has evolved over the last 100 years. Different earthquake magnitude scales have been used in different studies. In this study, different local magnitude scales are homogenised into a single local magnitude scale and then converted to moment magnitude. A set of GMPEs has been pre-selected using a procedure consistent with other global projects such as Global Earthquake Model. The Orkney earthquake strong-ground motion data was then used to identify the ground-motion prediction equations which are suitable for our study region. The ground-motion prediction equations derived from induced seismicity were not used because they were found to be inappropriate for the magnitude-distances required for this study. There is a need to derive a ground-motion prediction equation specifically for our region in order to improve our seismic hazard estimates.

The time-dependent seismic hazard estimates are given in terms of PGA and 5 % damped response spectra at periods of 0.1 s, 0.5 s, 1.0 s and 2.0 s for a 10 % probability of exceedance in 50 years, which corresponds to a 475 year return period, for two different time periods, namely Period A (mining period) (1970-2004) and Period B (flooding period) (2005-2015). Seismic hazard was observed to be higher in Period A than in Period B due to the change in the recurrence parameters. The seismic hazard estimates are mainly influenced by the temporal-variation in the number of the events recorded by the South African National Seismograph Network. The number of seismic events above temporally-varying of M_C increases over time but the number of seismic events below a constant value of M_C = 2.8 decrease over time and hence the hazards decreases. A decrease in *b*-value implies that there is an increase in the relative number of large events, meaning the hazard should increase; while a decrease in the activity rates implies that the frequency of events has decreased, meaning the hazard should decrease. The general observation for this study area is that M_{max}, *a*-value and *b*-value decrease over time for most sources during Period B, while the hazard also decreases. Flooding in the mines which occurs in Period B does not appear to have any significant influence on the hazard. While flooding of abandoned mines certainly led to an increase in seismic activity and some alarm, the activity and maximum magnitude of events was less than that experienced during the period of active mining. Seismic activity is likely to diminish once the level of the water table stabilises. Higher hazard values are found in the western parts of Johannesburg and Gauteng. This is due to the proximity of the FWR zone, which has the highest occurrence of seismicity as well as the largest events. The FWR source zones contribute about 80 % of the total hazard in the western part of the region.

REFERENCES

Akkar, S. and Bommer, J. J. (2010). Empirical equations for the prediction of PGA, PGV and spectral accelerations in Europe, the Mediterranean region and the Middle East, *Seismological Research Letters*, **81**, 195-206.

Albini, P., Strasser, F.O. and Flint, N. S. (2014). Earthquakes from 1820 to 1936 in Grahamstown and surroundings (Eastern Cape Province, South Africa), *Bulletin of Earthquake Engineering,* **12**, 45-78.

Atkinson, G. M. and Boore, D. M. (2006). Earthquake ground-motion prediction equations for eastern North America, *Bulletin of the Seismological Society of America*, **96**, 2181-2205.

Atkinson, G. M., Ghofrani, H. and Assatourians, K. (2015). Impact of induced seismicity on the evaluation of seismic hazard: Some preliminary considerations, *Seismological Research Letters*, **86**, 1009-1021.

Ayothiraman, R and Hazarika, H. (2008). Earthquake hazard and mitigation, *I.K International Publishing House Pvt. Ltd*, New Delhi, 564 pp.

Bachmann, C. E., Wiemer, S., Woessner, J. and Hainzl, S. (2011). Statistical analysis of the induced Basel 2006 earthquake sequence: introducing a probabilistic-based monitoring approach for enhanced geothermal systems, *Geophysical Journal International*, **186**, 793-807.

Baker, J. W. (2008). An introduction to probabilistic seismic hazard analysis (PSHA). Report for the US Nuclear Regulatory Commission, version 1.3, 72 pp.

Beauval, C., Hainzl, S. and Scherbaum, F. (2006). The impact of the spatial uniform distribution of seismicity on probabilistic seismic-hazard estimation, *Bulletin of the Seismological Society of America,* **96**, 2465-2471.

Bender, B. (1983). Maximum likelihood estimation of *b* values for magnitude grouped data, *Bulletin of the Seismological Society of America,* **73**, 831-851.

Bommer, J. J., Crowley, H. and Pinho, R. (2015). A risk-mitigation approach to the management of induced seismicity. Journal of *Seismology*, **19,** 623-646.

Bommer, J. J., Douglas, J., Scherbaum, F., Cotton, F., Bungum, H. and Fäh, D. (2010). On the selection of ground-motion prediction equations for seismic hazard analysis. *Seismological Research Letters*, **81** 783-793.

Bommer, J. J., Douglas, J. and Strasser, F. O. (2003). Style-of-faulting in ground-motion prediction equations, *Bulletin of Earthquake Engineering,* **1**, 171-203.

Bommer, J. J. and Scherbaum, F. (2008). The use and misuse of logic trees in probabilistic seismic hazard analysis, *Earthquake Spectra,* **24**, 997-1009.

Bommer, J. J., Scherbaum, F., Bungum, H., Cotton, F., Sabetta, F. and Abrahamson, N. (2005). On the use of logic-trees for ground-motion prediction equations in seismic-hazard analysis, *Bulletin of the Seismological Society of America,* **95**, 377-389.

Bommer, J. J., Strasser, F. O., Ranthje, E. M., Rodriguez-Marek, A., Stafford, P. J. and Hattingh, E. (2013). Verification and validation report for calculations performed for the Thyspunt PSHA and compliance with RD-0016. Council for Geoscience, Report No. 2013-0032.

Boore, D. M., Joyner, W B. and Fumal, T E. (1997). Equations for estimating horizontal response spectra and peak acceleration from western North American earthquakes: a summary of recent work, *Seismological Research Letters*, **68**, 128-153.

Bora, S. S, Scherbaum, F., Keuhn, N. and Stafford, P. (2014). Fourier spectral- and duration models for the generation of response spectra adjustable to different source-, propagation-, and site conditions, *Bulletin of Earthquake Engineering*, **12**, 467-493.

Brandt, M. B. C. (1997). Implementation of the SEISAN earthquake software for the SUN to analyze the data obtained through the South African National Seismograph Network. Council for Geoscience, Report No. 1997-0263, 48 pp.

Brandt, M. B. C., Bejaichund, M., Kgaswane, E. M., Hattingh, E. and Roblin, D. L. (2005). Seismic history of southern Africa. *Seismological Series,* **37**. Pretoria: Council for Geoscience, 32 pp.

Brandt, M. B. C. and Saunders, I. (2015). First look at an M_W-M_L earthquake magnitude relation for South Africa, *24th Institute of Mine Seismology Seminar*, Stellenbosch, South Africa.

Budnitz, R. J., Apostolakis, G., Boore, D. M., Cluff, D., Coppersmith, J. and Morris, A. (1997). Recommendations for probabilistic seismic hazard analysis: guidance on uncertainty and use of experts, **1,** *US Nuclear Regulatory Commission*, 278 pp.

Campbell, K. W. (2003a). Prediction of strong ground-motion using the hybrid empirical method and its use in the development of ground-motion (attenuation) relations in eastern North America, *Bulletin of the Seismological Society of America,* **93**, 1012-1033.

Campbell, K.W. (2003b). Strong-motion attenuation relations. In Lee, W.H., Kanamori, H., Jennings, P.C. and Kisslinger, C (Eds), Earthquake and engineering seismology, Part B. *Academic Press*, New York, 937-1945.

Campbell, K. W. (2014). An evaluation of eastern North America ground-motion models developed using the hybrid empirical methods, *Bulletin of the Seismological Society of America,* **104**, 347-359.

Cazalet, P. (1919). Notes on the study of records of earth tremors on the Central Rand, *Journal of South African Institute of Engineers*, **18**, 211-228.

Convertito, V., Maercklin, N., Sharma, N. and Zollo, A. (2012). From induced seismicity to time-dependent seismic hazard, *Bulletin of the Seismological Society of America,* **102**, 2563-2573.

Cornell, C. A. (1968). Engineering seismic risk analysis, *Bulletin of the Seismological Society of America,* **58**, 1583-1606.

Cotton, F., Scherbaum, F., Bommer, J. J. and Bungum, H. (2006). Criteria for selecting and adjusting ground-motion models for specific target regions: Application to central Europe and rock sites. *Journal of Seismology*, **10**, 137-156.

Douglas, J. (2003). Earthquake ground motion estimation using strong-motion records: A review of equations for the estimation of peak ground acceleration and response spectral ordinates. *Earth-Science Reviews*, **61**, 43-104.

Douglas, J. (2011). Ground-motion prediction equations 1964-2010. Final report RP-59356-FR, *BRGM*, Orleans, France, 444p, http:///www.brgm.fr/publication/rechRapportSP.jsp.

Douglas, J., Bungum, H. and Scherbaum, F. (2006). Ground-motion prediction equations for southern Spain and southern Norway obtained using the composite model perspective, *Journal of Earthquake Engineering*, **10**, 33-72.

Douglas, J., Edwards, B., Convertito, V., Sharma, N., Tramelli, A., Kraaijpoe, D., Cabrera, B. M., Maercklin, N. and Troise, C. (2013). Predicting ground motion from induced earthquakes in geothermal areas. *Bulletin of the Seismological Society of America,* **103 (3)**, 1875-1897.

Durrheim, R.J. (1999). Rockbursting. In Jager, A. J. and Ryder, J. A (Eds). A handbook on rock engineering practice for tabular hard rock mines, *The Safety in Mines Research Advisory Committee (SIMRAC)*, Braamfontein, Johannesburg, South Africa, 249-286.

Durrheim, R. J. (2001). Management of mining-induced seismicity in ultra-deep South African gold mines, Rockbursts and seismicity in mines. In: Proceedings of the 5th International Symposium on Rockbursts and Seismicity in Mines (RaSiM5). Johannesburg: *South African Institute of Mining and Metallurgy*, 213-219.

Durrheim, R. J. (2007). The risks to miners, mines and the public posed by large seismic events in the gold mining districts of South Africa, changes in deep and high stress Mining, *Australian Centre for Geomechanics*, Perth, Australia, 35-42.

Durrheim, R. J. (2010). Mitigating the risk of rockbursts in the deep hard rock mines of South Africa: 100 years of research, In Brune, J. (Ed), Extracting the Science: a century of mining research*, Society for Mining, Metallurgy, and Exploration*, Inc., ISBN 978-0-87335-322-9, 156-171.

Fernández, L. M. (1973). Program to evaluate epicentral distance, origin time and local magnitude of regional tremors. Report no. Gh 1968, *Geological Survey of South Africa*, 11 pp.

Fernández, L. M. (1977). Evaluation of epicentral distances, origin times and local magnitudes of local seismic events. A computer program for the HP-9830. Report no. Gh 2256, *Geological Survey of South Africa,* 12 pp.

Fernández, L. M. and Guzman, J. A. (1979). Seismic history of southern Africa, *Seismologic Series*, Council for Geoscience, Report No. 1980-0175, 38 pp.

Fernández, L. M. and Guzman, J. A. (1980). Adaptation of the Richter seismic local magnitude scale to South Africa, *Seismologic Series*, Council for Geoscience, Pretoria, Report 9, 22 pp.

Finsen, A. (1950). The statistics of Witwatersrand earth tremors 1938.5 to 1949. *Union Observatory. Circular*, **110**, 444-456.

Gane, P. G. (1939). A statistical study of Witwatersrand earth tremors, *Journal of the Chemical Metallurgical and Mining Society of South Africa*, **40**, 155.

Gane, P. G., Hales, A. L. and Oliver, H. A. (1946). A seismic investigation of the Witwatersrand earth tremors, *Bulletin of the Seismological Society of America*, **36**, 115-173.

Gane, P. G., Logie, H. J. and Stephen, J. H. (1949). Triggered telerecording seismic equipment, *Bulletin of the Seismological Society of America*, **39**, 117-143.

Giardini, D., Grünthal, G., Shedlock, K. M. and Zhang, P. (1999). The GSHAP global seismic hazard map, *Annali Di Geofisica*, **42**, 1225-1230.

Goertz-Allmannm, B. P. and Wiemer, S. (2013). Geomechanical modelling of induced seismicity source parameters and implications, *Geophysics*, **78**, 25-39.

Goldbach, O. D. (2009). Seismic risk posed by mine flooding. *The South African Institute of Mining and Metallurgy*, Hard Rock Safety Conference, South Africa, 149-174.

Gutenberg, B. and Richter, C. F. (1944). Frequency of earthquakes in California, *Bulletin of the Seismological Society of America*, **34**, 185-188.

Hanks, T. C. and Kanamori, H. (1979). A moment magnitude scale, *Journal of Geophysical Research*, **84**, 2348-2350.

Hussein, H. M., Abou Elenean, K. M., Marzouk, I. A., Peresan, A., Korrat, I. M., Abu El-Nader, E., Panza, G. F. and El-Gabry, M. N. (2008). Integration and magnitude homogenization of the Egyptian earthquake catalogue, *Natural Hazards*, **47**, 525-546.

Hutton, L. K. and Boore, D. M. (1987). The M_L scale in Southern California, *Bulletin of the Seismological Society of America*, **77**, 2074-2094.

International Atomic Energy Agency (2010). Seismic hazards in site evaluation for nuclear installations, IAEA safety standards series No. SSG-9, available on: www-pub.iaea.org/MTCD/publications/PDF/Pub1448_web.pdf, downloaded on: 11 February 2015.

Ishimoto, M. and Iida, K. (1939). Observations of earthquakes registered with the microseismograph constructed recently, *Bulletin of the Earthquake Research Institute*, **17**, 443-478.

Johnson, M. R., Anhaeusser, C. R. and Thomas, T. R. (2006). The geology of South Africa. *Geological Society of South Africa*, Johannesburg, Council for Geoscience, Pretoria, 691 pp.

Johnston, A. C., Coppersmith, K. J., Kanter, L. R. and Cornell, C. A. (1994). The earthquakes of stable continental regions, Final report submitted to Electric Power Research Institute (EPRI), TR- 102261, Vols. 1 and 3.

Joyner, W. B. and Boore, D. M. (1993). Methods for regression analysis of strong-motion data, *Bulletin of the Seismological Society of America*, **83**, 469-487.

Kanth, S. T. G. and Iyenger, R. N. (2007). Estimation of seismic spectral acceleration in Peninsular India, *Journal of Earth System Science*, **116**, 199-214.

Kijko, A. (2004). Estimation of the maximum earthquake magnitude, Mmax, *Pure and Applied Geophysics*, **161**, 1-27.

Kijko, A. (2011). Introduction to probabilistic seismic hazard analysis. In Gupta, H. K (Ed). Encyclopedia of Solid Earth Geophysics, *Springer*, vol **1**, 1107-1120.

Kijko, A. and Graham, G. (1998). Parametric-historic procedure for probabilistic seismic hazard analysis Part I: estimation of maximum regional magnitude m_{max}, *Pure and Applied Geophysics*, **152**, 413-442.

Kijko, A. and Funk, C. (1994). The assessment of seismic hazards in mines, *The Journal of the South African Institute of Mining and Metallurgy*, 179-285.

Kijko, A. and Sellevoll, M. A. (1992). Estimation of earthquake hazard parameter from incomplete data files. Part II. Incorporation of magnitude heterogeneity, *Bulletin of the Seismological Society of America*, **82**, 120-134.

Kijko, A., and Singh, M. A. (2011). Statistical tools for maximum possible earthquake magnitude estimation, *Acta Geophysicie*, **59**, 674-700.

Kijko, A., Smit, A., and Sellevoll, M. A. (2016). Estimation of earthquake hazard parameters from incomplete data Files. Part III. Incorporation of uncertainty of earthquake-occurrence model. *Bulletin of the Seismological Society of America*, **106**, 12010-1222.

Lehotla, P. J. (2015). Mining: production and sales, *Statistics South Africa*, Report no: P2041, 14 pp.

Lasocki, S. (2005). Probabilistic analysis of seismic hazard posed by mining induced events, In Potvin, Y., and Hudyma, M (Eds). Proceedings of Sixth International Symposium on Rockbursts and Seismicity in Mines. *Australian Centre for Geomechanics*, 9-11 March 2005, 151-156.

Lasocki, S. (2008). Some unique statistical properties of the seismic process in mines. In: *Proceedings of the 1st Southern Hemisphere International Rock Mechanics Symposium.* Vol. **1**, 667-678.

Maxwell, S., Jones, M., Parker, R., Miong, S., Leaney, S., Dorval, D., D'Amico, D., Logel, J., Anderson, E. and Hammermaster, K. (2009). Fault activation during hydraulic fracturing, *79th Annual International Meeting*, SEG, Houston.

McGarr, A. (1976). Seismic moments and volume changes, *Journal of Geophysical Research*, **81**, 1487-1494.

McGarr, A., Bicknell, J., Sembera, E. and Green, R. W. E. (1989). Analysis of exceptional large tremors in two gold mining districts of South Africa, *Pure and Applied Geophysics*, **129**, 295-307.

McGarr, A. and Fletcher, J. B. (2005). Development of ground–motion prediction equations relevant to shallow mining–induced seismicity in the Trail Mountain area, Emery County, Utah, *Bulletin of the Seismological Society of America*, **95**, 31-47.

McGarr, A., Simpson, D. and Seeber, L. (2002). Case histories of induced and triggered seismicity. In Lee. W. H. K., Kanamori, H., Jennings, P. C. and Kisslinger, C (Eds). *International Handbook of Earthquake and Engineering Seismology*, **81A**(Academic Press, 2002).

McGuire, R. K. (1976). FORTRAN computer program for seismic risk analysis, *U.S. Geological Survey*, Open-File Report. 76-67, 1-94.

Mena, B., Wiemer, S. and Bachmann, C. (2013). Building robust models to forecast the induced seismicity related to geothermal reservoir enhancement, *Bulletin of the Seismological Society of America*, **103**, 383-393.

Midzi, V., Zulu, B., Manzunzu, B., Mulabisana, T., Pule, T., Myendeki, S. and Gubela, W. (2015). Macroseismic survey of the ML5.5, 2014 Orkney earthquake, *Journal of Seismology*, **19**, 741-751.

Mignan, A. and Woessner, J. (2012). Estimating the magnitude of completeness for earthquake catalogs, community online resource for statistical seismicity analysis, doi:10.5078/corssa-00180805. Available at http://www.corssa.org.

Nakatani, M., Yabe, Y., Philipp, J., Morema, G., Stanchits, S. and Dresen, G. and JAGUARS Group. (2008). Acoustic emission measurements in a Deep Gold Mine in South Africa-project overview and some typical waveforms, *Seismological Research Letters*, **79**, 311.

Ogasawara, H., Kuwabara, Y., Miwa, T., Fujimori, K., Hirano, N. and Koizumi, M. (2002). Post-seismic effects of an M 7.2 earthquake and microseismicity in an abandoned, flooded, deep mine, *Pure and Applied Geophysics*, **159**, 63-90.

Ottemöller, L., Voss, P. and Havskov, J. (2014). SEISAN earthquake analysis software for windows, Solaris, Linux and MacOSX. *University of Bergen*. http://seisan.info/ (downloaded on November 2014).

Padhy, S. and Subhadra, N. (2010). Attenuation of high-frequency seismic waves in northeast India, *Geophysical Journal International*, **181**, 453-467.

Pagani, M., Monelli, M., Weatherill, G. A. and Garcia, J. (2014). The OpenQuake-engine Book: Hazard. *Global Earthquake Model (GEM) Technical Report 2014-08, doi: 10.13117/GEM.OPENQUAKE.TR2014.08*, 67 pp.

Pankow, K. L. and Pechmann, J. C. (2004). The SEA99 ground-motion predictive relations and new peak ground velocity relation, *Bulletin of the Seismological Society of America,* **94**, 341-348.

Peruš, I. and Fajfar, P. (2012). Ground-motion prediction by a non-parametric approach*, Earthquake Engineering and Structural Dynamics*, **39**, 1395-1416.

Petersen, M. D., Moschetti, M. P., Powers, P. M., Mueller, C. S., Haller, K. M., Frankel, A. D., Zeng, Y., Rezaeian, S., Harmsen, S. C. and Boyd, O. S. (2014). Documentation for the 2014 update of the United States national seismic hazard maps, *U.S. Geological Survey*, Open‐File Report. 2014-1091, 243 pp., doi: 10.3133/ofr20141091.

Petersen, M. D., Mueller, C. S., Moschetti, M. P., Hoover, S. M., Llenos, A. L., Ellsworth, W. L., Michael, A. J. Rubinstein, J. L., McGarr, A. F. and Rukstales, K. S. (2016). One-year seismic hazard forecast for the central and eastern United States from induced and natural earthquakes*: U.S. Geological Survey,* Open-File Report 2016–1035*, 52 pp.,* doi:10.3133/ofr20161035.

Pezeshk, S., Zandieh, A. and Tavakoli, B. (2011). Hybrid empirical ground-motion prediction equations for eastern North America using NGA models and updated seismological parameters, *Bulletin of the Seismological Society of America,* **101**, 1859-1870.

Plenkers, K., Kwaitek, G., Nakatani, M., Dresen, G., and JAGUARS Group. (2010). Observation of seismic events with frequency f > 25 kHz at Mponeng Deep Gold Mine, South Africa. *Seismological Research Letters*, **83**, 467-479.

Reiter, L. (1990). Earthquake hazard analysis: issues and insights. Columbia University Press, 254 pp.

Richter, C. F. (1935). An instrumental earthquake magnitude scale, *Bulletin of the Seismological Society of America*, **25**, 1-32.

Richter, C. F. (1958). Elementary seismology, *W.H. Freeman,* New York, 1-32.

Riemer, K. L. and Durrheim, R. J. (2012). Mining seismicity in the Witwatersrand Basin: monitoring, mechanisms and mitigation strategies in perspective, *Journal of Rock Mechanics and Geotechnical Engineering*, **4**, 228-249.

Rietbrock, A., Strasser, F. and Edwards, B. (2013). A stochastic earthquake ground-motion prediction model for the United Kingdom, *Bulletin of the Seismological Society of America,* **103**, 57-77.

Ross, M. R. (2014). Introduction to probability models, *Academic Press*, Elsevier, UK, ISBN978-0-12-407948-9.

Saunders, I., Brandt, M. B. C, Molea, T., Akromah, L. and Sutherland, B. (2010). Seismicity of southern Africa during 2006 with special reference to the M_W 7 Machaze earthquake, *South African Journal of Geology*, **113**, 396-380.

Saunders, I., Brandt, M. B. C., Steyn, J., Roblin, D. and Kijko, A. (2008). The South African National Seismograph Network. *Seismological Research Letters,* **97**, 203-210.

Saunders, I., Kijko, A. and Fourie, C. J. S. (2016). Statistical evaluation of seismic events location accuracy by the South African national seismograph network over four decades, *South African Journal of Geology*, **119**, 291-304.

Saunders, I., Ottemöller, L., Brandt, M. B. C. and Fourie, C. J. S. (2012). Calibration of an M_L scale for South Africa using tectonic earthquake data recorded by the South African national seismograph network: 2006 to 2009, *Journal of Seismology*, **17**, 437-451.

Scherbaum, F., Delavaud, E. and Riggelsen, C. (2009). Model selection in seismic hazard analysis: an information-theory perspective, *Bulletin of the Seismological Society of America*, **99**, 3234-3247.

Scherbaum, F., Schmedes, J. and Cotton, F. (2004). On the conversion of source-to-site distance measures for extended earthquake source models, *Bulletin of the Seismological Society of America*, **94**, 1053-1069.

Scherbaum, F., Seif, S. and Kuehn, N.M. (2011). On the relationship between Fourier and response spectra: consequences for the adjustment of empirical ground-motion prediction equations for regional differences, *American Geophysical Union*, Fall Meeting, 5-9 December 2011, San Francisco, California, Abstract No. S53B-2298.

Schorlemmer, D., Wiemer, S. and Wyss, M. (2005). Variation in earthquake-size distribution across different stress regimes, *Nature*, **437**, 539-542.

Silva, W. J., Gregor, N. and Darragh, R. (2002). Development of regional hard rock attenuation relations for central and eastern North America, Tech. rept., Pacific Engineering and Analysis.

Singh, M. and Hattingh, E. (2009). Short communication: Collection of isoseismal maps for South Africa, *Natural Hazards*, **50**, 403-408.

Sommerville, P. G., Graves, R. W., Collins, N. F., Song, S. G., Ni, S. and Cummins, P. (2009). Source and ground motion models of Australian earthquakes. In: *Proceedings of the 2009 Annual Conference of the Australian Earthquake Engineering Society*, Newcastle, December 11 - 13.

Stewart, J. P., Douglas, J., Javanbarg, M., Bozorgnia, Y., Abrahamson, N. A., Boore, D. M., Campbell, K. W., Delavaud, E., Erdik, M. and Stafford, P. J. (2015). Selection of ground-motion prediction equations for the Global Earthquake Model. *Earthquake Spectra,* **31**, 19-45.

Stokes, R. S. G. (1936). Recent developments in mining practice in the Witwatersrand, *Institute of Mining and Metallurgy*, **45**, 191.

Strasser, F. O. and Mangongolo, A. (2012). TNSP earthquake catalogue, Council for Geoscience, Report No. 2012-0166, 183 pp.

Stucchi, M., Albini, P., Mirto, C. and Rebez, A. (2004). Assessing the completeness of Italian historical earthquake data. *Annals of Geophysics*, **47**, 659-673.

Thenhaus, P.C. and Campbell, K. W. (2003). Seismic hazard analysis, in Chen, W. F. and Scawthorn, C (Eds). Earthquake engineering handbook, *CRC Press*, Boca Raton, FL, USA, 8, 1-43.

Toro, G. R. (2002). Modification of the Toro et al. (1997) attenuation equations for large magnitudes and short distances, *Technical Report*, Risk Engineering.

Toro, G. R., Abrahamson, N. A. and Schneider, J. F. (1997). Model of strong ground motions from earthquakes in central and eastern North America: Best estimates and uncertainties, *Seismological Research Letters*, **68**, 41-57.

Urban, P., Lasocki, S., Blascheck, P., Farias do Nascimento, A, Van Giang. N. and Kwiatek, G. (2016). Violations of Gutenberg-Richter relations in anthropogenic seismicity, *Pure and Applied Geophysics*, **173**, 1517-1537.

Vaccari, F., Romanelli, F. and Panza, G. (2005). Detailed modelling of strong ground-motion in Trieste. United Nations Educational Scientific and Cultural Organization and International Atomic Energy Agency, 39 pp.

Vieira, F. M. C. C., Diering, D. H. and Durrheim, R. J. (2001). Methods to mine the ultra-deep tabular gold-bearing reefs on the Witwatersrand Basin, South Africa. In Hustrulid, W. A. and Bullock, R. L., Underground mining methods. 691-704. *Society for Mining, Metallurgy, and Exploration, Inc.* Colorado.

Vieira, F. M. C. C. and Durrheim, R. J. (2002). Probabilistic mine design methods to reduce rockburst risk, *The Journal of The South African Institute of Mining and Metallurgy*, **102**, 231-242.

Wesnousky, S. G. (1994). The Gutenberg-Richter or characteristic earthquake distribution, which Is It?, *Bulletin of the Seismological Society of America*, **84**, 1940-1959.

Wessels, S., Kratz, S. M. and Pena, A. D. L. (2011). Identifying fault activation during hydraulic stimulation in the Barnett shale: Source mechanism, *b* values, and energy release analyses of microseismicity, *81st Annual International Meeting*, SEG, San Antonio, Texas.

Wiemer, S. and Katsumata, K. (1999). Spatial variability of seismicity parameters in aftershock zones, *Journal of Geophysical Research*, **104**, 135-151.

Wiemer, S. and Malone, S. (2001). A software package to analyze seismicity: ZMAP, *Seismological Research Letters*, **72**, 374-383.

Wiemer, S. and McNutt, S. R. (1997). Variations in frequency-magnitude distribution with depth in two volcanic areas, *Geophysical Research Letters*, **24**, 189-192.

Wiemer, S. McNutt, S.R and Wyss, M. (1998). Temporal and three-dimensional spatial analysis of the frequency-magnitude distribution near Long Valley caldera, California, *Geophysical Journal*, **134**, 409-421.

Wiemer, S. and Wyss, M. (1997). Mapping the frequency-magnitude distribution in asperities: An improved technique to calculate recurrence times?, *Journal of Geophysical Research*, **102**, 15115-15128.

Wiemer, S. and Wyss, M. (2000). Minimum magnitude of completeness in earthquakes catalogs: Examples from Alaska, the western United States and Japan, *Bulletin of the Seismological Society of America*, **90**, 859-869.

Woessner, J., Hardebeck, J. L. and Haukkson, E. (2010). What is an instrumental seismicity catalog? Theme IV – Understanding Seismicity Catalogues and their Problems [Online], IV. Available: http://www.corssa.org/articles/themeiv/woessner_et_al/woessner_et_al.pdf, downloaded on 21/06/2014.

Wood, H. E. (1913). On the occurrence of earthquakes in South Africa, *Bulletin of the Seismological Society of America*, **3**, 113-869.

Wood, H. E. (1914). The Witwatersrand earth tremors, *Journal of the Chemical, Mineralogical and Meteorological Society of South Africa,* **14**: 423-427.

Wyss, M., Schorlemmer, D. and Wiemer, S. (2000). Mapping asperities by minima of local recurrence time: The San Jacinto-Elsinore fault zones, *Geophysical Research Letters*, **105**, 7829-7844.

Zulu, B. S. and Manzunzu, B. (2015). Surface seismic hazard due to mining-induced earthquakes in Gauteng, South Africa, Council for Geoscience, Report No. 2015-0108, 64 pp.

APPENDIX

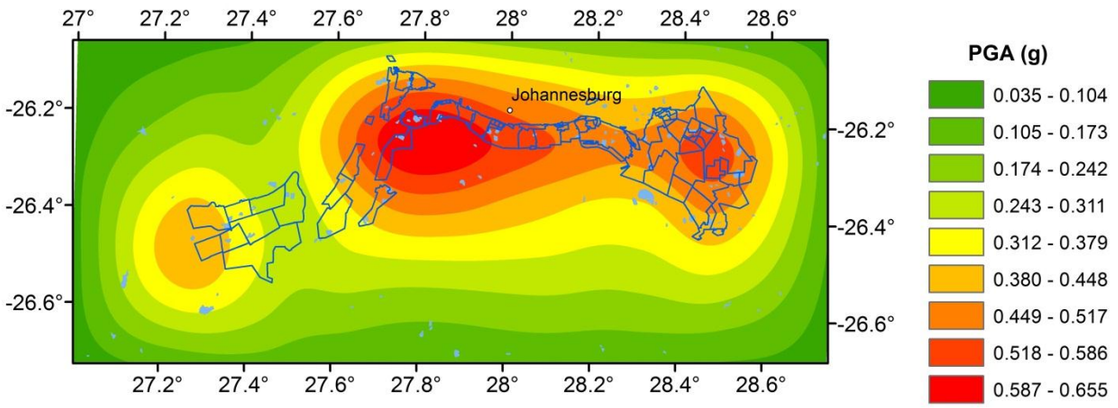

Figure 50 (a). Peak ground acceleration map using ASB14 (a)

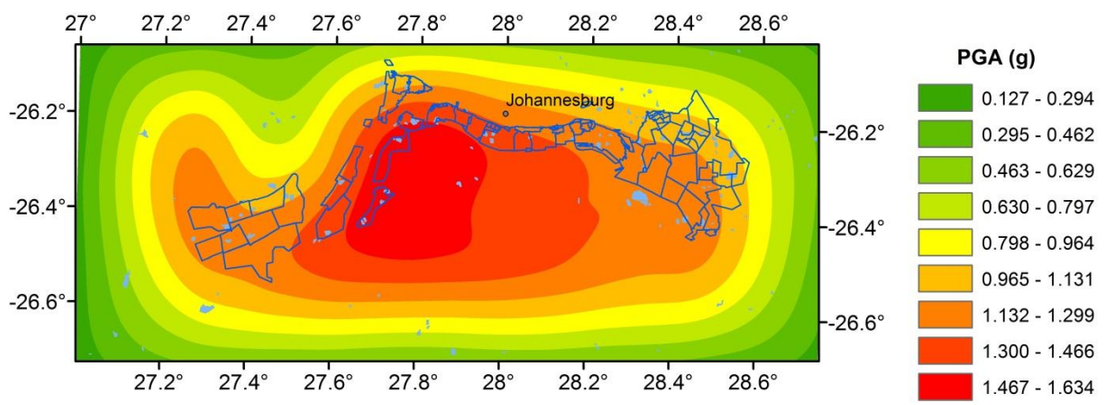

Figure 50 (b). Peak ground acceleration map using PZT11.

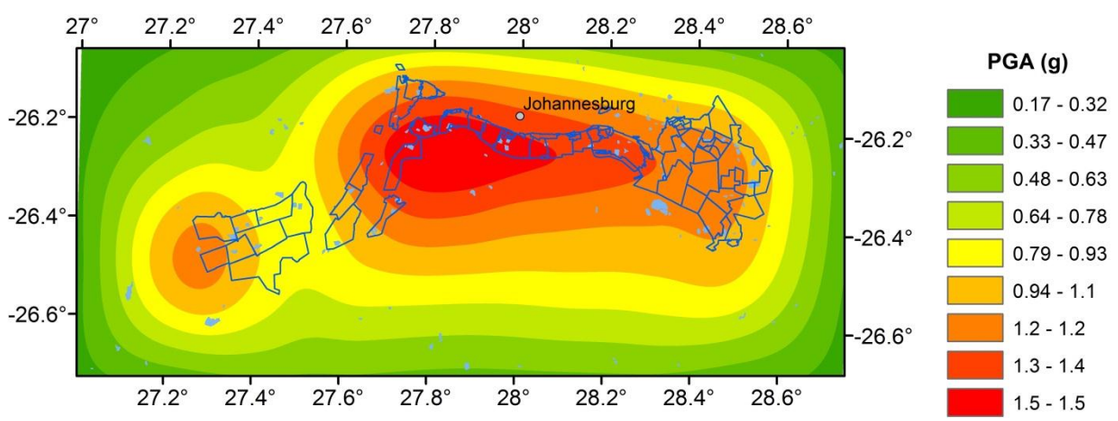

Figure 50 (c). Peak ground acceleration map using TEA02.

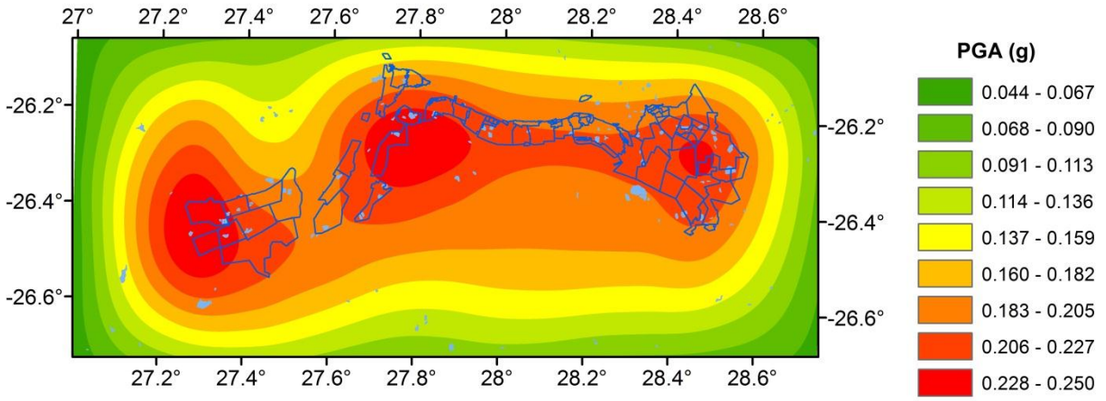

Figure 50 (d). Peak ground acceleration map using RSE14.

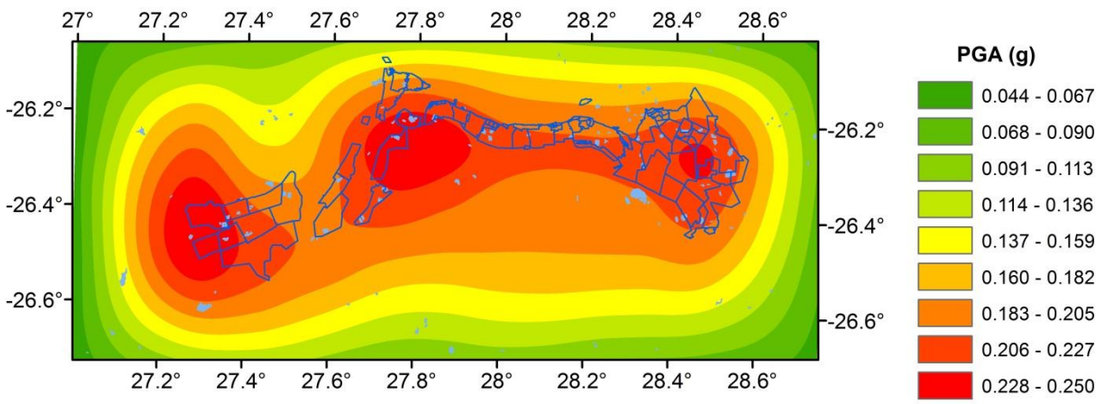

Figure 52 (a). Seismic hazard maps for Period A for the Gauteng gold mining regions of South Africa for PGA map.

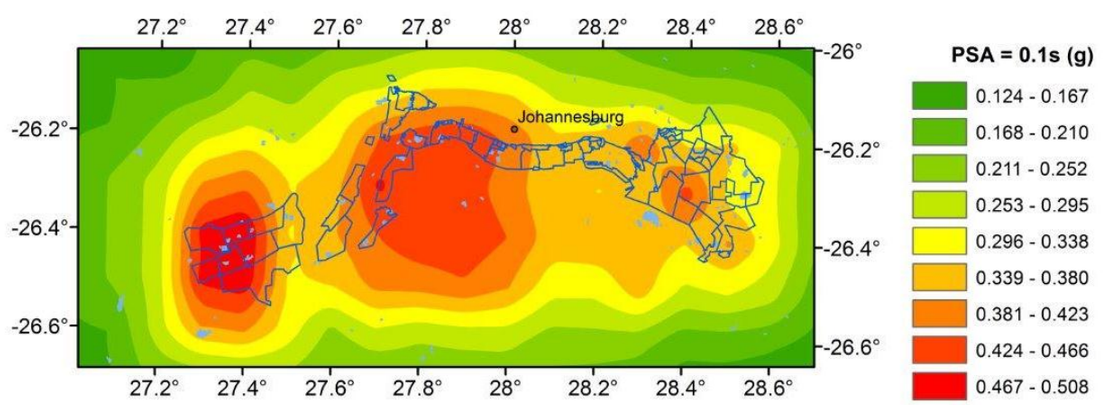

Figure 52 (b). Seismic hazard maps for Period A for the Gauteng gold mining regions of South Africa for spectral acceleration at period 0.1 s.

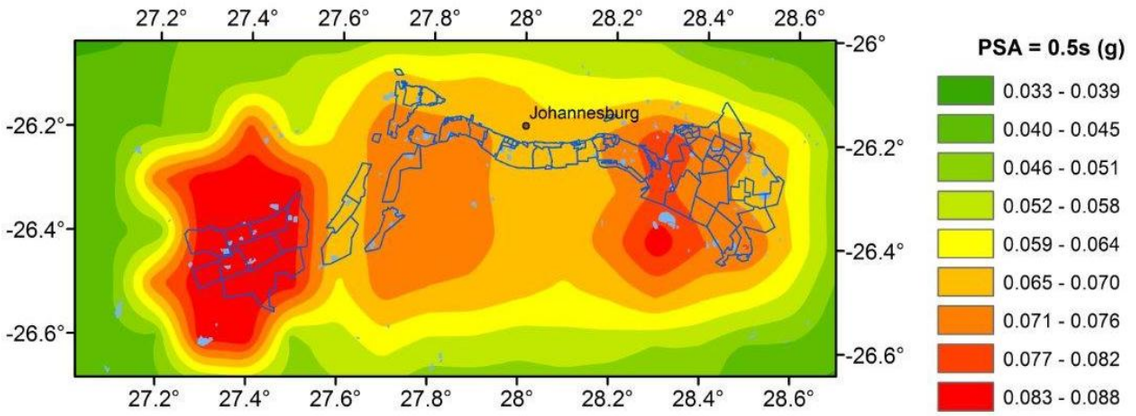

Figure 52 (c). Seismic hazard maps for Period A for the Gauteng gold mining regions of South Africa for spectral acceleration at period 0.5 s.

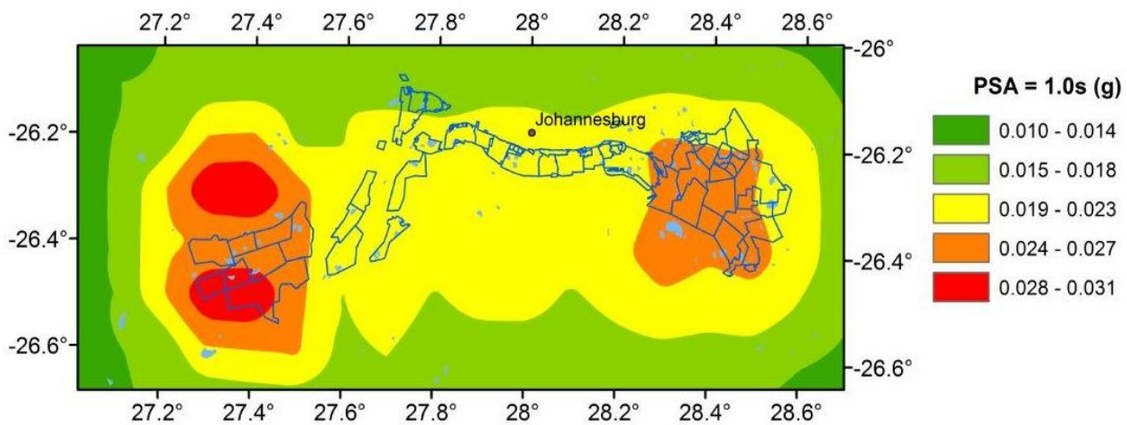

Figure 52 (d). Seismic hazard maps for Period A for the Gauteng gold mining regions of South Africa for spectral acceleration at period 1.0 s.

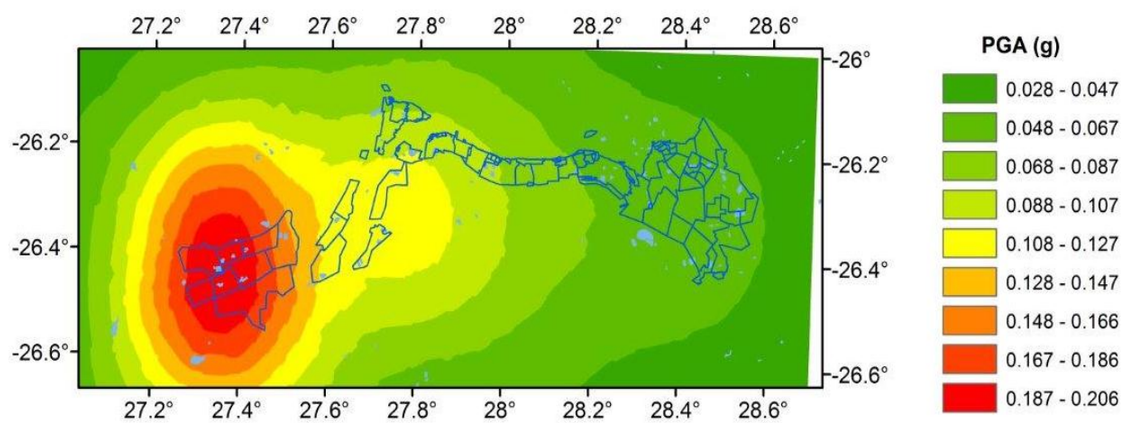

Figure 53 (a). Seismic hazard maps for Period B for the Gauteng gold mining regions of South Africa for PGA map.

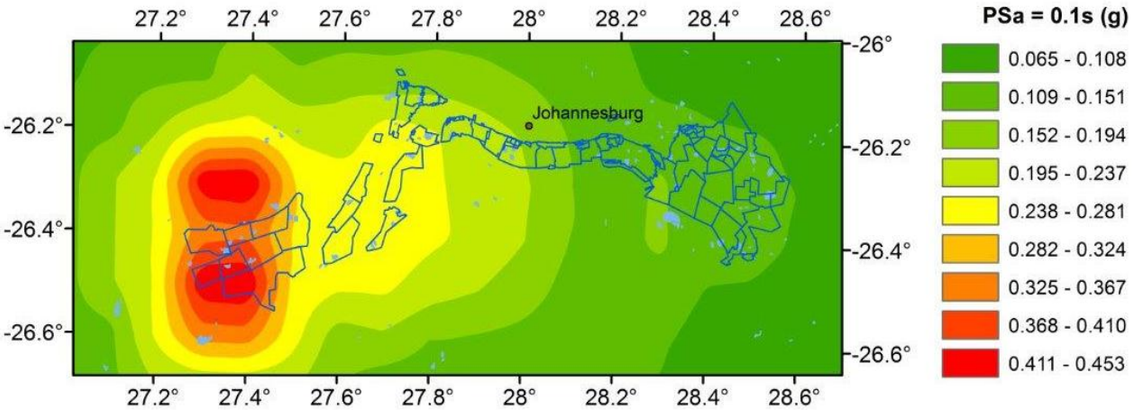

Figure 53 (b). Seismic hazard maps for Period B for the Gauteng gold mining regions of South Africa for spectral acceleration at period 0.1s.

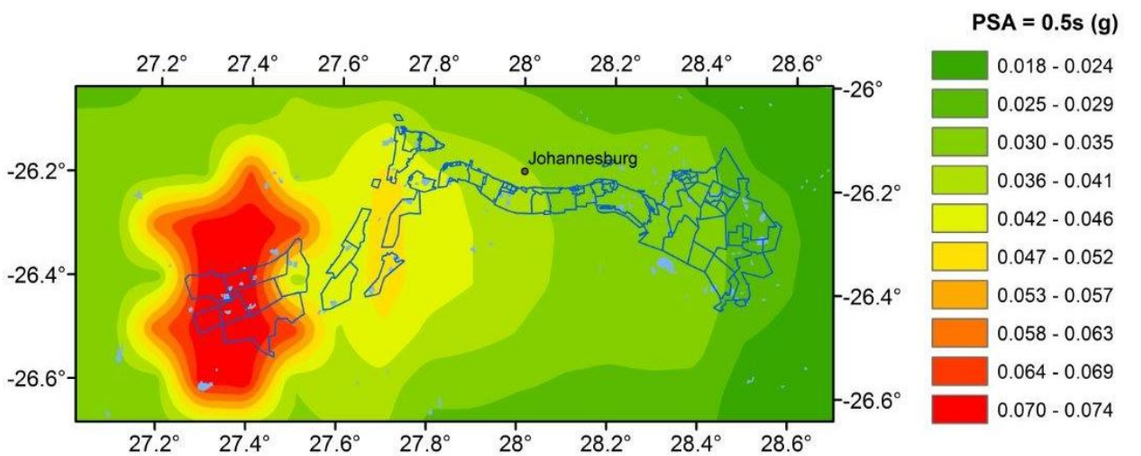

Figure 53 (c). Seismic hazard maps for Period B for the Gauteng gold mining regions of South Africa for spectral acceleration at period 0.5s.

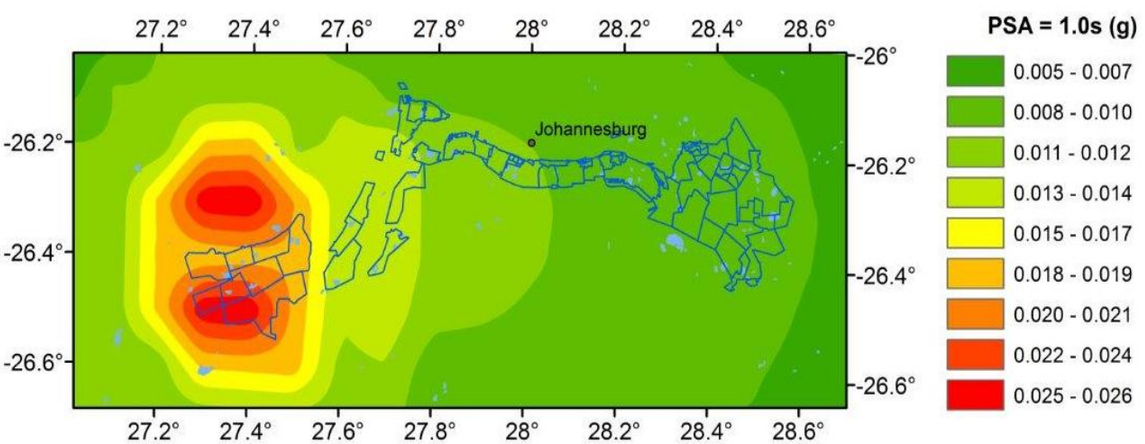

Figure 53 (d). Seismic hazard maps for Period B for the Gauteng gold mining regions of South Africa for spectral acceleration at period 0.5s.

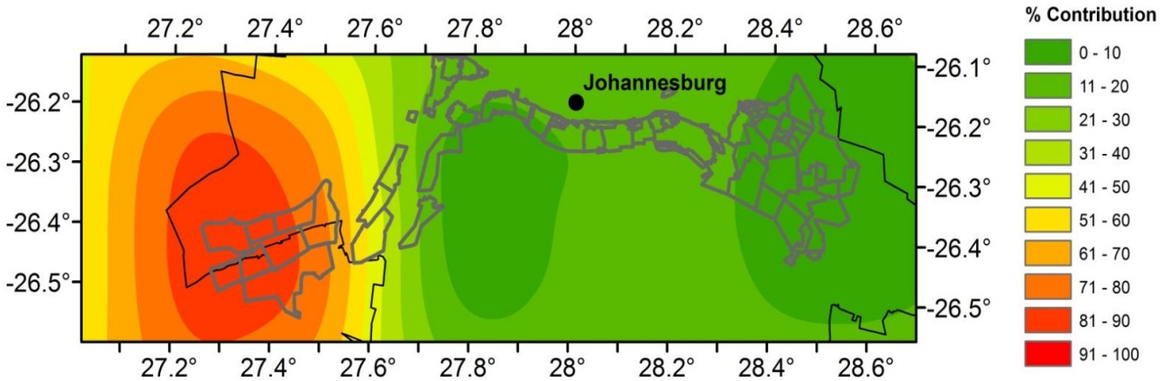

Figure 54 (a). Percentage hazard contribution of seismic zones in Period A for FWR seismic zone.

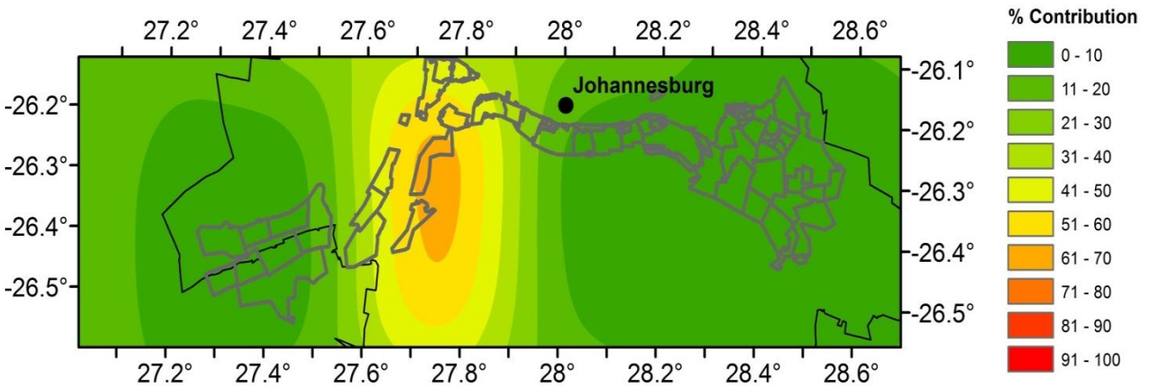

Figure 54 (b). Percentage hazard contribution of seismic zones in Period A for WR seismic zone.

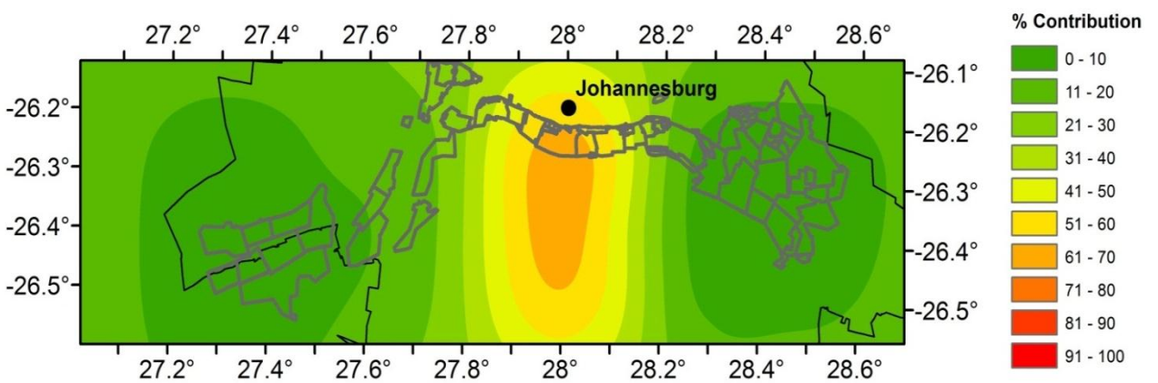

Figure 54 (c). Percentage hazard contribution of seismic zones in Period A for CR seismic zone.

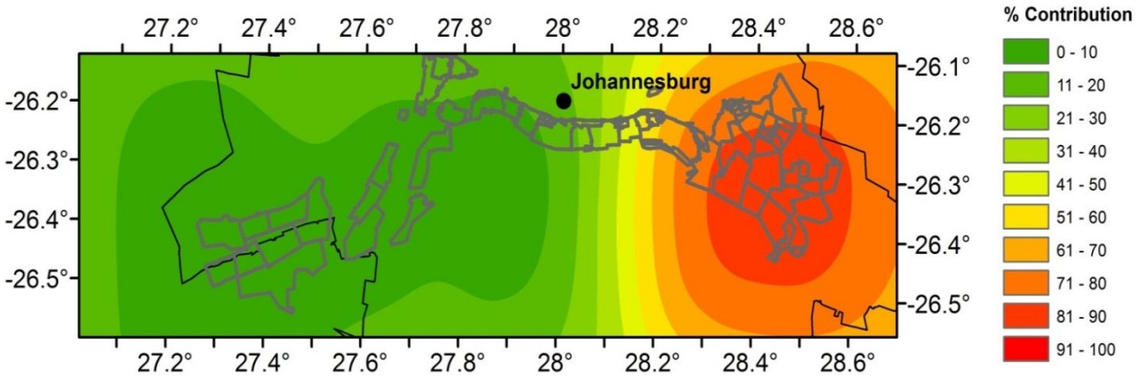

Figure 54 (d). Percentage hazard contribution of seismic zones in Period A for ER seismic zone.

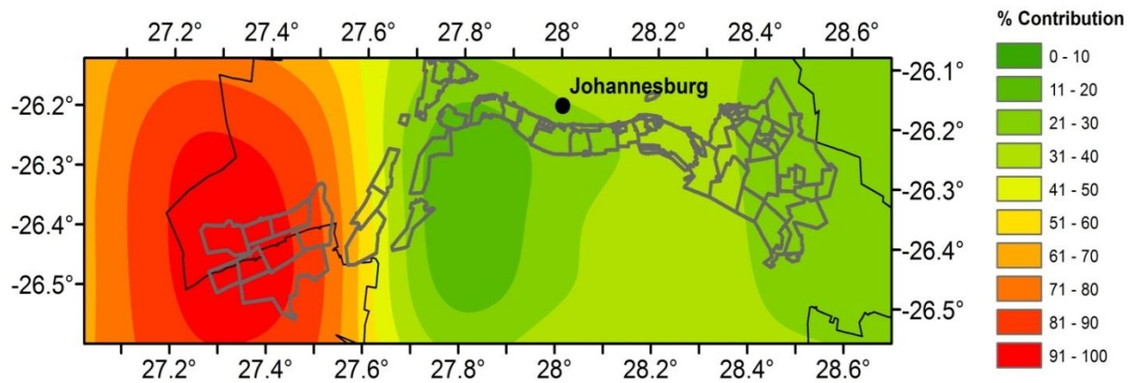

Figure 55 (a). Percentage hazard contribution of seismic zones in Period B for FWR seismic zone.

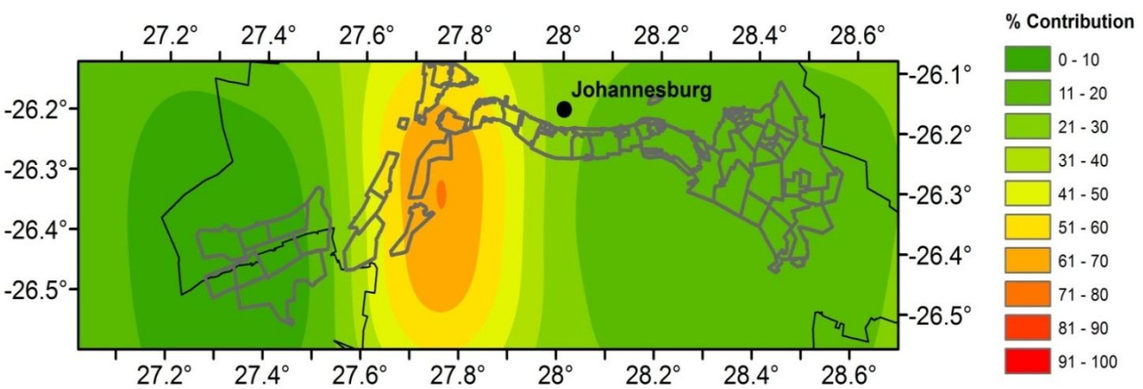

Figure 55 (b). Percentage hazard contribution of seismic zones in Period B for WR seismic zone.

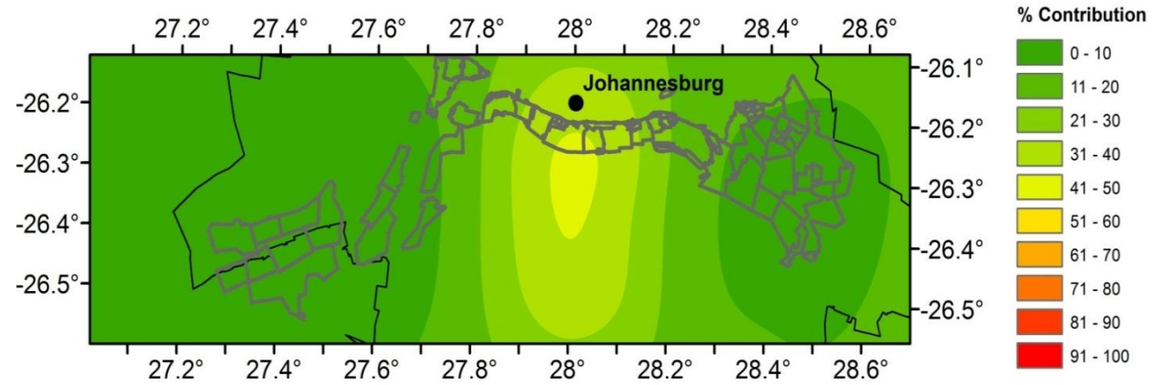

Figure 55 (c). Percentage hazard contribution of seismic zones in Period B for CR seismic zone.

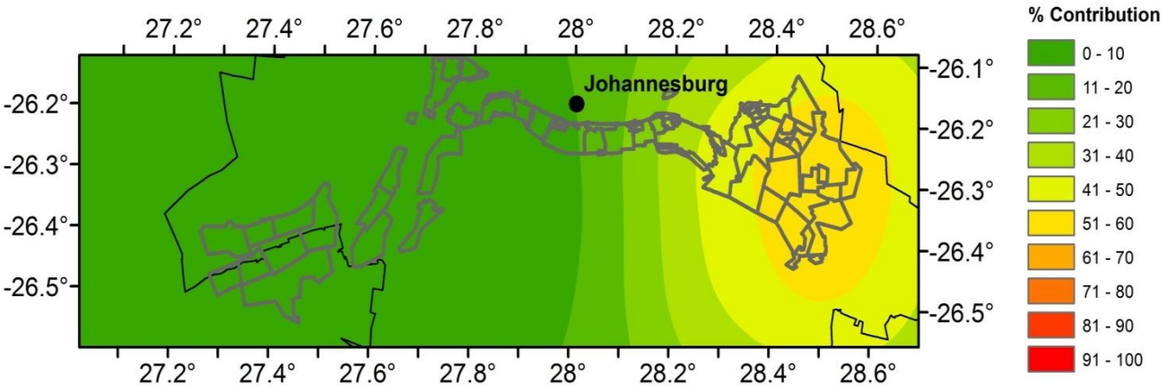

Figure 55 (d). Percentage hazard contribution of seismic zones in Period B for ER seismic zone.